E-SEM Characterization of *Escherichia coli* Biofilms Grown on Copper- and Silver-Alloyed Stainless Steels over a 48 – 96 Hour Time frame within a Drip Flow Bioreactor

Amelia M. McMullen

Thesis submitted to the faculty of the Virginia Polytechnic Institute and State University in partial fulfillment of the requirements for the degree of

Masters of Science

In

Material Science and Engineering

Mitsu Murayama

Sean G. Corcoran

Amy J. Pruden-Bagchi

April 27, 2018

Blacksburg, VA

Keywords: *E. coli* Biofilms, Antimicrobial Stainless Steels, Environmental Scanning Electron Microcopy, Drip Flow Bioreactor

E-SEM Characterization of *Escherichia coli* Biofilms Grown on Copper- and Silver-Alloyed Stainless Steels over a 48 – 96 Hour Time frame within a Drip Flow Bioreactor

Amelia M. McMullen

Abstract

The formation of bacterial biofilms on surfaces and their subsequent biofouling pose extensive safe and healthy concerns to a variety of industries. Biofilms are ubiquitous, and the biofilm state is considered the default mode of growth for the majority of the world's bacteria population. Once mature, biofilms are difficult to remove completely and have improved resistance against antibacterial agents. Given this, there has been significant interest to mitigate or at least manage biofilm formation on surfaces. One such method has been through the material design of surfaces, and to the interest of this study, through the development of antimicrobial stainless steels. Stainless steel is not an inherently antimicrobial material. Stainless steels alloyed with small amounts of either copper (Cu) or silver (Ag), both well-known natural antimicrobial agents, have been investigated since their initial development in the late 1990's onward. This class of materials have been proven to show significant antimicrobial effect over their traditional counterparts without compromising the characteristic mechanical properties of the stainless steels. However, most of the antimicrobial assessments for these materials documented within literature are conducted over a 24-hour timeframe and do not adequately account for the biofilm mode of growth. As so, this study aimed to assess how biofilms grow on this class of antimicrobial steels over a longer duration of growth and under growth conditions which more adequately modeled the biofilm mode of life.

The same strain of *Escherichia coli* commonly used in antimicrobial surface testing, ATCC 8739, was grown on submicron-polished coupons of a ferritic Cu-alloyed stainless steel (1.50 wt. % Cu), an austenitic Ag-alloyed stainless steel (0.042wt. % Ag), and a standard 304 series stainless steel, used as a baseline. Following ASTM-E2647-13, the *E. coli*/SS coupons were grown using a drip flow bioreactor under low shear conditions at either ambient temperature or 37 ± 3 °C with a batch phase of 6 hours and a continuous phase of 48 hours up to 96 hours. Directly after harvesting, the coupons were analyzed with an Environmental Scanning Electron Microscope (E-SEM) under low vacuum with a water vapor environment.

The effect of surface chemistry and alloy microstructure, surface roughness, rinsing the surfaces prior to inoculation and after harvesting, temperature, and growth duration on the resulting *E. coli* biofilms were all investigated in some capacity. Growth on the submicron finished surfaces indicated there were no significant differences between the biofilms grown on the three different steel compositions. Bacterial attachment appeared non-preferential to surface chemistry or alloy microstructure, suggesting that *E. coli* interacted with the surfaces effectively the same under the given growth conditions. To account for apparent randomness in bacterial attachment, it is hypothesized that the surface features of interest were on a size scale irrelevant to the size of single bacterial cells. To account for the lack of an observed biocidal effect from the Cu- and Ag-alloyed stainless steels, it is hypothesized that an organic conditioning film which developed on the surfaces from the fluid environment may have effectively inhibited the release of Cu and Ag ions from the steel surfaces.

E-SEM Characterization of *Escherichia coli* Biofilms Grown on Copper- and Silver-Alloyed Stainless Steels over a 48 – 96 Hour Time frame within a Drip Flow Bioreactor

Amelia M. McMullen

General Audience Abstract

Bacteria frequently self-organize into what are commonly called bacterial biofilms, or an aggregation of bacterial cells that attach to a surface and which are embedded within a self-generated matrix of polymeric substances, such as proteins and polysaccharides. The biofilm state offers a lot of survival advantages to bacteria, and once biofilms form on a surface they are very difficult to remove. The formation of bacterial biofilms on surfaces and their subsequent biofouling pose extensive safe and healthy concerns to a variety of industries. There has been significant interest to stop or at least manage biofilm formation on surfaces. One such method has been through the design of surfaces, and to the interest of this study, through the development of antimicrobial stainless steels. Stainless steel is not an inherently antimicrobial material. Stainless steels which include small amounts of either copper or silver have been proven to show a significant antimicrobial effect over their traditional stainless steel counterparts without compromising the other desirable properties of the steels. However, most of the documented antimicrobial assessments for these materials have been conducted over a 24-hour timeframe and do not adequately account for the biofilm mode of growth.

This study aimed to assess how biofilms grow on this class of steels over a longer duration of growth and under growth conditions which more adequately modeled the biofilm mode of life. This was done by growing a single strain of *E. coli* bacteria onto coupons of these stainless steel materials for either a 48-hour or a 96-hour timeframe within a low-flow, continuously-fed bioreactor. The coupons were visualized with an environmental scanning electron microscope to assess the effect of the material properties on the observed biofilms grown during this study.

Overall there were little differences observed between the *E. coli* biofilms grown on the copper-containing stainless steel, the silver-containing stainless steel, and the standard stainless steel used within this study. Mirror finish smooth surfaces were needed in order to adequately visualize the steel coupons. The bacteria appeared to attach randomly without any preference for steel surface chemistry or other surface features. This suggested that under the given growth conditions the bacteria interacted with the smooth steel surfaces the same. To account for this randomness, it is hypothesized that the relevant surface features were significantly smaller than the size of single bacterial cells. *E. coli* cells are between 1 – 2 micrometers long and 0.5 – 1 micrometers in diameter. There was also no antimicrobial effect observed on the copper-containing and silver-containing stainless steels. To account for the lack of an observed antimicrobial effect, it is hypothesized that a conditioning film of carbon-based molecules formed on the surface of the steels from the liquid growth medium environment, preventing bacterial cells from being damaged by the copper and silver within the steel surfaces.

Acknowledgements

I would like to thank Mitsu Murayama for the opportunity and support to work on this project, for his continued guidance in helping me learn and grow as a researcher, and for taking the time to review my thesis documentation.

I would also like to thank my other committee members Sean Corcoran and Amy Pruden for their valued input on this work and for taking the time to review my thesis documentation.

Additionally, I would like to thank Kasthuri Venkateswaran and the Biotechnology and Planetary Protection Group at NASA Jet Propulsion Lab for the week-long crash course on basic microbiology skills and for their input on the initial direction of the project.

I would also like to thank the staff scientists at the NCFL for their continued support and for teaching me how to use various equipment and instruments, particularly Steve McCartney, Chris Winkler, Ya Peng Yu, Deborah Berti, and Jay Tuggle.

Additionally, I have much gratitude toward the VTSuN lab and NanoEarth for allowing me to grow biofilms within their lab space. I would like specifically thank Weinan Leng for his continued help and guidance while operating within the VTSuN lab, and Virginia Riquelme Breazeal for her input on bacterial growth.

Of course, I would also like to thank my fellow labmates for their input and support during my time working on this project, Sayako Inoue, Joshua Stuckner, Chang Yu Hung, Katherine Frei, Jacob Haag, Sarah Ulrich, and Seth Guldin.

I would also like to thank Kimberly Grandstaff for all of her kindness, help, and guidance through my graduate experience.

Additionally, I would like to thank Cindy Perdue and Susette Sowers for all of their administrative support for pursuing day-to-day research.

Finally, I would also like to thank my fiancé, family, and friends for their continued love, support and encouragement during my graduate experience. I couldn’t have done it without your help.

With upmost sincerity, thank you all so much for helping me during this process of growth and for all you have taught me along the way. It is much appreciated, and I look forward to the opportunities this experience will help open in the future.

Table of Contents

List of Figures

List of Tables

Chapter 1 Introduction

1.1. Bacterial Biofilms Are Problematic

Colonizing bacteria and other single-cell microorganisms have the tendency to aggregate into what are commonly called biofilms. Within the past 20-30 years bacterial biofilm research has exploded and become increasingly relevant after microbiologists discovered bacteria express their genes differently, and subsequently intercellular communication and interaction differently, between the planktonic and colonizing states in order to optimize the conditions of life[1, 2]. The majority of the world's bacteria population are colonizing, and biofilm formation is now generally accepted as the default mechanism of bacterial growth. As so, it has become increasingly relevant and promising to solve bacterial contamination problems within the scope of bacterial biofilms rather than planktonic cultures of bacteria[2].

Biofilms are ubiquitous, colonizing almost any conceivable surface. The formation of biofilms and the subsequent biofouling of surfaces pose extensive environmental health and safety problems to a variety of human interests. All plants and animals are inhabited by biofilms as part of their natural microbiological flora, including humans[3]. This colonizing presence allows for the opportunity of frequent infections caused by biofilms of opportunistic pathogens[4]. Biofilms are responsible for many hospital acquired infections through the contamination of medical devices and biomedical implants[5]. According to Bryers et al. "(hospital acquired) infections are the fourth leading cause of death in the U.S. with 2 million cases annually (or ~10% of American hospital patients) leading to more than $5 billion in added medical cost per annum"[6]. Biofilms also can cause the biofouling and contamination of process water[7] and can render drinking water unhygienic[8]. Biofilms are also known to accelerate the surface corrosion of various metallic surfaces, such as within water and oil piping, a process frequently referred to as microbiologically influenced corrosion (MIC)[9]. According to NACE, a 2002 study conducted by the US Federal Highway Association estimated that "costs associated with metallic corrosion in a wide range of industries" has a "total annual estimated direct cost … of $276 billion in the United States – equivalent to 3.1% of the US gross domestic product"[10]. MIC is thought to be one of the leading causes of corrosion in the oil piping industry[11]. Biofilms can also contaminate food products within food processing plants, leading to spoilage and company loses as well as potential consumer food poisoning[12].

Given the extensive associated problems of biofilms within wide variety of industries, there has been much interest in ways to effectively eradicate, or at least effectively manage, biofilm growth on surfaces.

1.2. Definition of Biofilm and Stages of Biofilm Growth

It is generally accepted that a biofilm is an aggregate of microorganisms that adhere to each other and/or a surface, whether that surface is living or non-living, and in which the cells are surrounded within a self-generated matrix of extrapolymeric substances (EPS)[13]. Naturally occurring biofilms are generally comprised of multiple species of organisms, whereas laboratory grown biofilms can be controlled to contain a single organism, typically a single pure strain of bacteria. In naturally occurring biofilms, multiple species of bacteria will exist symbiotically,

often helping each other gain the resources each species needs to live. It has been well established that bacterial biofilms behave more like true multicellular organisms rather than a collection individual cells[2, 13, 14].

There are many benefits of the biofilm state over the planktonic state for bacteria survival. Biofilms are also dynamic in responding to their growth environment, adjusting through cell signaling to optimize survival. Some of the benefits of the biofilm state include an increased resistance to toxic compounds, the ability to grow in oligotrophic, or low nutrient, environments, the creation of a syntrophic metabolism, and the ability to more quickly communicate genetic information and cell signaling molecules. Bacteria express genes differently within the biofilm state which in turn creates emergent properties that offer bacteria increased protection from harmful conditions, the ability to more efficiently sequestrate nutrients, and the ability to utilize cooperative benefits[2, 13]. These benefits to survival are what makes mature biofilms so difficult to remove once formed.

Biofilm growth is usually defined as having five distinct phases: 1) the conditioning of a surface, 2) initial cell adhesion and reversible attachment, 3) irreversible attachment of cells to a surface and EPS production 4) maturation of the biofilm architecture, and 5) the detachment and spreading of cells to other locations[2]. Figure 1-1 helps illustrate this process.

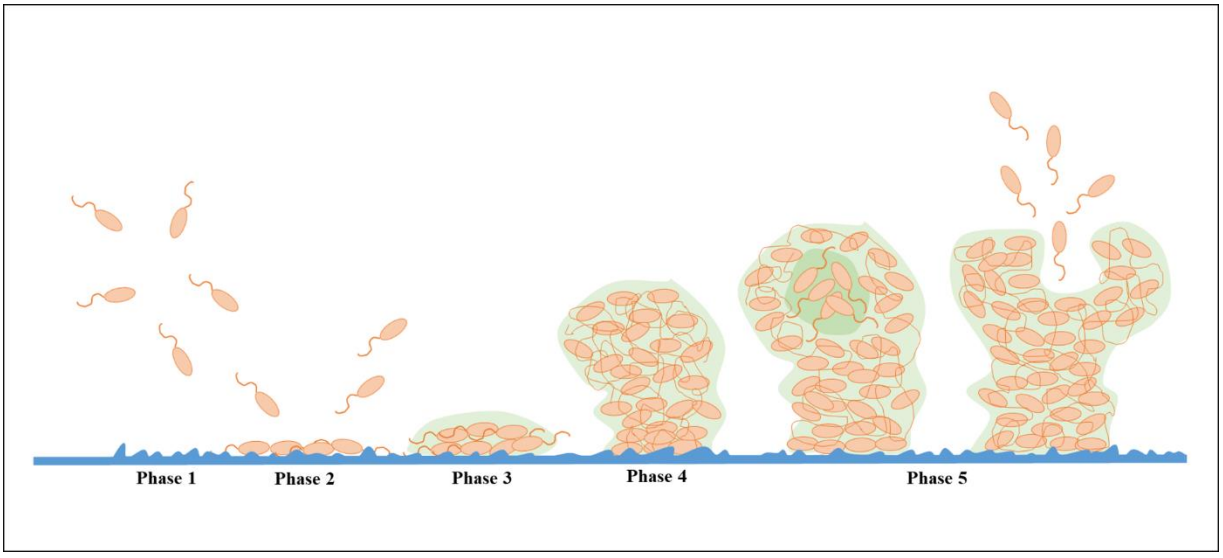

Figure 1-1 Diagram showing the five phases of biofilm growth. Phase 1) conditioning of surface of adsorbed organic molecules. Phase 2) initial reversible attachment of bacteria to the surface. Phase 3) production of EPS and more strongly attached irreversible attachment of bacteria to the surface. Phase 4.) maturation of the biofilm architecture. Phase 5) dispersion of cells, to start sequestration of other locations.[2]

A conditioning film forms on a given surface immediately after its submersion in a liquid environment. As soon as any clean and sterile surface is placed in a liquid medium, organic molecules will be adsorbed on its surface, such as proteins, polysaccharides, fatty acids, lipids and pollutants. Conditioning films form on any and all surfaces, regardless to hydrophobicity or hydrophilicity. The components within the conditioning film formed are directly related to the liquid medium it is formed in. It is thought that it is the adsorbed organic molecules of the

conditioning film are what bacteria will initially attach to on a given surface. As so, the formation of a conditioning film is regarded as the first phase of biofilm growth. Conditioning films have also been linked to modifying the physiochemical properties of a substrate surface, providing an additional food source for the initial bacteria attached[15].

After surface conditioning, bacteria will undergo initial attachment to the surface through both physical and physiochemical forces. Bacteria may initially find their way to a surface through hydrodynamic flow, gravity or Brownian motion, but initial adhesion to a surface is driven by electrostatic interactions between the bacterial cell and the surface. As so, attachment at this stage of growth is considered reversible since it is primarily driven by weak surface forces such as van der Waal interactions. Any factors which can affect the surface interactions between cells and a substrate will affect the reversible attachment phase of biofilm growth[2].

If the initial bacterial cells reversibly attached to a surface find the surface favorable, they will begin the third phase of attachment by excreting adhesins and other various EPS molecules. This bonds the cells more strongly to each other and to the surface, allowing for microcolony formation and the maturation of the biofilm structure[2]. EPS serves a wide variety of important function for biofilms but foremost it is the backbone to the complex structure of bacterial biofilms. EPS also provides a protective barrier and plays a role in the exchange of genetic information, the retention of enzymes, the sorption of ions and organic molecules, inter-biofilm redox reactions and much more[13].

After the irreversible attachment phase has started, the bacterial cells will continue to proliferate and develop a more complex EPS matrix and matured biofilm[2]. This will result in environmental gradients which prompt the development of cell task differentiation, or the administering of different roles to cells located at discrete regions of the biofilm. This differentiation allows bacteria to participate in cooperative interactions for survival[14]. Maturation of the biofilm results in the development of a complex heterogeneous structure and a rearrangement of bacteria away from the surface[2] .

Mature biofilms will undergo detachment, which refers to the release of individual cells or clusters of cells from the mature biofilm structure. Inactive detachment may occur through shear stresses in hydrodynamic flow, but active detachment has a physiological basis. For example, if a biofilm has exhausted the available nutrients from the region it attached to, it may detach in order to sequester a new, more nutrient rich area. Similarly, it may detach in response to any other number of unfavorable conditions. It is thought that the detached biofilm cells will then return to a planktonic state of growth; this thus completes the cycle for the five stages of biofilm formation[2].

1.3. Factors Known to Influence Biofilm Formation

Bacterial adhesion to a surface is ruled by the physicochemical properties of both the surface and the bacteria as well as the environmental conditions under which growth occurs. The reversible attachment phase of biofilm growth is the growth stage most susceptible to being influenced by the surface properties of the substrate. Once bacteria are established on a surface, biofilms quickly proliferate and the effect of the surface properties become less significant than

they were during initial reversible attachment, particularly to cells no longer close to the surface. As so, there has been much work associated with interrupting the reversible attachment phase of biofilm growth in hopes that it will help mitigate biofilm maturation on a given surface.

There are a variety of surface properties well known to have an effect on the initial stages of biofilm formation, however the principles which govern how different microbial cells interact and self-organize onto surfaces is still poorly understood at large[15]. Surface effects such as hydrophobicity and electrostatic forces typically do not influence cell adhesion until the cell has become extremely close to the surface, potentially less than 1nm[16].

In many ways planktonic bacteria suspended in aqueous media can be viewed as a colloidal suspension. As so, there has been much work associated with modeling bacterial adhesion to surfaces using the same thermodynamic principles that govern colloidal suspensions. In other words, researchers have attempted to model bacterial attachment to surfaces as the sum of the chemical and physical properties of both bacteria and the material surface[17, 18].

1.3.1. Wettability, Hydrophobicity, and Surface Energy

Wetting refers to the ability of a liquid, typically water, to sustain contact with and spread over a solid surface. The phenomenon results from a balance of the interfacial tension between the bulk surface of the solid, the surface of the liquid, and the relative environmental humidity or gaseous environment[19].

Wettability is usually measured through the contact angle of a sessile drop of the given liquid on the given surface. Contact angle is directly influenced by the surface tension of the liquid. The molecules in the bulk of a pure liquid are pulled in equal directions to have a net force of zero. However, at the interface of a liquid, the molecules lack neighbors with which to balance the forces and the bulk molecules exert a force pulling them inward in an attempt to maintain force equilibrium. This creates an internal pressure in the liquid causing it to contract inward to assume the lowest surface area to volume ratio possible, and thus the lowest surface free energy possible. Liquid droplets on surfaces are usually spherical because this is the lowest surface energy configuration possible. The intermolecular forces that cause the liquid to contract is known as surface tension. Surface tension is the force responsible for controlling the shape of liquid droplets, and thus the contact angle of the fluid with the surface[19].

Young's equation summarizes the relationship of the contact angle of a fluid as a force balance of the surface free energies of the three interfaces in a given system, solid, liquid and gas. Equation 1 shows Young's equation, where γ_{lv} is the interfacial tension of the liquid-vapor interface, γ_{sv} is the interfacial tension of the solid-vapor interface, γ_{sl} is the interfacial tension of the solid-liquid interface, and θ_Y is the contact angle of the liquid with the solid surface[19].

Equation 1. Young's Equation

$$\gamma_{lv}\cos\theta_Y = \gamma_{sv} + \gamma_{sl}$$

Figure 1-2 illustrates the relationship between the contact angle and the interfacial energies. Liquids with small contact angles on a surface correspond to high wettability of that

surface. Liquids with large contact angles on a surface correspond to low wettability of that surface. Surfaces that cause aqueous liquids to have contact angles less than 90° are considered hydrophilic, whereas surfaces that cause aqueous liquids to have contact angles greater than 90° are considered hydrophobic. Surfaces that cause aqueous liquids to have contact angles greater than 150° are considered super-hydrophobic[19]. Surfaces which have high wettability of water are frequently referred to as high energy surfaces, whereas surfaces that have low wettability of water are frequently referred to as low energy surfaces[15].

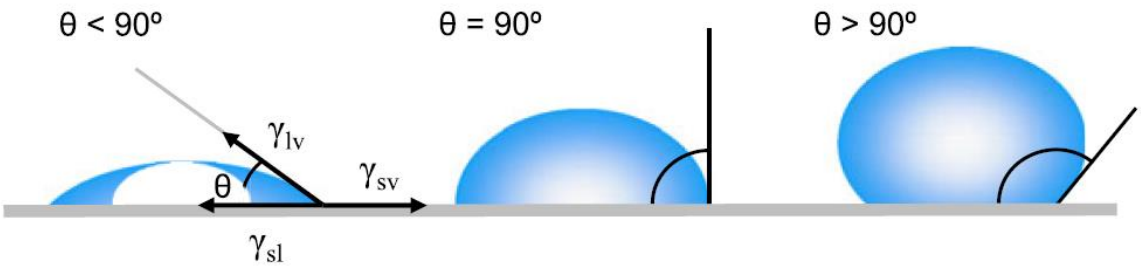

Figure 1-2. Relationship of contact angle, interfacial forces and wettability. Image directly borrowed from Yuan et al.[19]

In general, it has been found that bacteria adhere better to surfaces with moderate wettability in comparison to extremely hydrophobic or hydrophilic surfaces[20]. Within the scope of moderate wettability, it is also thought that bacteria tend to prefer hydrophobic surfaces to hydrophilic surfaces[17, 21]. Superhydrophobic surfaces are thought to be helpful for biofilm mitigation, as they can decrease the adhesion forces between bacteria and the surface which then allows for easy removal of bacteria before mature biofilms form[22]. Bacterial cells are largely hydrophilic but have small regions of hydrophobicity on their cell surfaces[15]. There currently is no good method to measure the hydrophobicity of bacterial cells, and there is much debate in regard to the effect on cell hydrophobicity on bacterial adhesion, so the effect has not been reviewed here.

As mentioned in 1.2, the first contact bacteria have with a surface is with the conditioning film formed on the substrate from contact with aqueous media. As so this conditioning film can have a significant effect on the surface energy and hydrophobicity of the substrate which in turn may either enhance or hinder initial bacterial attachment[16, 17].

In the scope of stainless steels, metals typically have a hydrophilic surface with a high surface energy and wettability and are frequently negatively charged in aqueous media. Metal oxides however tend to have a hydrophobic surface and are commonly positively charged in aqueous media[17]. All stainless steels have a passivation layer of chromium oxides and iron oxides which protect it against corrosion; within most neutral and slightly acidic medium the oxide layer is typically 2-5nm thick[23]. The composition of the oxide layer depends on the steel composition, the steel surface finish and the liquid media its immersed in[17, 23]. Hedburg et al. also found there to be no clear correlation between the oxide layer on stainless steel and the contact angle of water on its surface. Surface contamination of small molecule carbon had the primary effect for differences in the observed wettability of stainless steels in aqueous solutions

without chelating agents[23]. This notion further supports that the conditioning film formed on a surface during the first phase of biofilm formation can strongly influence the surface energy and wettability of that surface.

1.3.2. Zeta Potential, Surface Charge and Electrostatic Forces

Surfaces within liquid media can obtain charges on their surface through the ionization of surface groups, the adsorption of ions onto the surface, and the loss of ions from the surface. The development of a net charge on a surface causes a layer of counter ions to develop at the interface of the surface and the liquid media. This creates a double boundary layer of charge. The boundary layer within the liquid has two main regions. There is a strongly bonded layer which is closest to the surface, or the Stern layer, and there is a loosely bonded layer just outside of the Stern layer, called the slipping plane. The Zeta potential is a measure of the electric potential within the diffuse layer of the slipping plane and is used to assess the overall charge a surface or particle acquires while in a specific liquid media. pH strongly effects the zeta potential, as well as the ionic strength of the liquid media or the addition of any other additives to the media. The isoelectric point of a surface within liquid media is the pH in which the zeta potential carries no charge[24].

Most bacterial cells have been found to have a negative surface charge when within neutral pH [16, 18, 20]. Opposite charges attract; as so, surfaces which have an overall net positive charge while within neutral pH may be more susceptible to bacterial adhesion than surfaces which have an overall negative charge. Of course, these relationships could easily change with changing pH or other environmental factors which could affect surface charge, such as the ionic strength of a solution.

Stainless steels typically have a negative zeta potential when in neutral pH or slightly acidic media, with their isoelectric point ranging between pH 3-5[23]. This means that most stainless steel surfaces will have a positive zeta potential when within solutions that have approximately neutral pH, such as most freshwater and biological systems. Between this notion and the fact that metal oxides (thin passivation layer) are typically positively charged within aqueous media, it is likely that, in general, most stainless steel surfaces are favorable for bacterial attachment[17].

1.3.3. Surface Roughness

In general, it is thought that rougher surfaces are more susceptible to bacterial adhesion than smoother surfaces. The basis for this is that rougher surfaces have a larger surface area for bacteria to adhere to[25] and, if the grooves in the roughness are on the same order of the size of a given bacterial cell they can provide protection against the cell being swept away by shear forces[17, 25].

Interestingly, there have been surface roughness studies on stainless steels which suggest that when the grooves on a roughened surface have a width that is on the same order of size as the bacteria adhering to it, the bacteria will align longitudinally along the grooves. However, when the groove has a width that is much larger than the size of the bacteria or much smaller than the size of the bacteria, they tend to align much more randomly. Other studies with stainless

steel surfaces have shown that surface flaws on stainless steels, such as irregular topography, pitting, or scratches, only appear to influence bacterial attachment when the surface feature is on the same order of magnitude as the bacteria adhering to the surface.[17]

It is also likely that surface roughness may have an effect on the wettability and other surface forces of a material, however there was not much conclusive evidence for the results of this influence found in the literature. Also, it is likely very system specific.

1.3.4. Environmental Conditions

The environmental conditions under which a biofilm are grown can also strongly influence the observed growth.

For instance, a significant majority of bacteria are both mesophiles and nuetrophiles, meaning they can only survive within a moderate temperature range, approximately 20 – 45 °C, and a pH range which is close to neutral, approximately pH 6.5-7.5. *E. coli* can exist within a temperature range from 20 - 49°C, with its optimal growth temperature at 37°C. The optimal pH range for *E. coli* is between pH 6.0 and 8.0. However it can still grow, but at a slower rate, approximately between pH 5.0 -6.0 and pH 8.0 – 9.0 [26]. If the temperature and pH of an environment are outside an organism's optimal range, the growth rate of the bacteria will be slowed down and if it is too far out of its range it could kill the microorganism.

As mentioned above, pH also has a strong influence on surface charge of surfaces and subsequently the interactions associated with surface charge[24].

The hydrodynamic flow experienced by a biofilm during growth can also influence the rate of initial attachment of bacteria to a surface, as well as the resulting architecture of the matured biofilm. Biofilms which are grown under high shear flow tend to be shorter and denser than biofilms which are grown under low shear flow. This is explained as primarily being due to the laminar boundary layer being closer to the surface when under high shear flow, making the region where the biofilm can grow without being sheared off also shorter[25].

1.4. Biofilm Mitigation Through Material Design - Antimicrobial Stainless Steels

Given all the contamination problems, harmful infections, accelerated corrosion problems associated with biofilms, there has been much interest in ways to effectively eradicate, or at least effectively manage, biofilm growth on surfaces. One promising method is through material design and surface modification. If the reversible attachment phase of biofilm formation can be interrupted by a biologically resistant surface, this could help mitigate biofilm maturation on the given surface.

Biofilm mitigation through material design has largely consisted of either the creation of surfaces which release an antimicrobial agent or the creation of surfaces which reduce the adhesion forces between bacteria and the surface. Material design of surfaces which reduce the adhesion forces between bacteria and the surface have primarily been centered around the design of superhydrophobic surfaces. These materials resist biofilm formation by reducing the adhesion of bacteria to their surface. They do not import any biocidal effect and are best utilized with frequent cleaning of the surface[22]. The design of surfaces with antimicrobial agents have

largely been centered on antimicrobial surface coatings[27-29] or the integration of antimicrobial metals into the bulk of alloys[30, 31]. These materials aim to limit bacterial attachment and biofilm accumulation through the release of a biocidal compound from the material surface and commonly involve the incorporation of antimicrobial metals such as silver and copper. Depending on the application, antimicrobial surface coatings are less desirable than the integration of antimicrobial agents into a material's bulk due to the probability that the coatings will degrade over time due to system friction, regularly cleaning, and daily use of the components. When the antimicrobial agent is uniformly dispersed throughout a material's bulk rather than just the material's surface, the mechanism of bacterial inhibition will in theory remain the same even as a surface may be abraded or otherwise degraded through use.

Austenitic stainless steels, such as 304 and 316 varieties, are well known for being nonmagnetic, having high strength, high corrosion resistance, and superior workability and formability. Iron is stabilized in the austenite phase (typically via nickel) within austenitic stainless steels and the bulk of austenitic stainless steels have a face-centered cubic crystal structure. Ferritic stainless steels, such as 400 series steels, also have relatively high workability and corrosion resistance but in general have lower strength than austenitic stainless steels. Iron is stabilized within the ferrite phase within ferritic stainless steels and the bulk of ferritic stainless steels have a base-centered cubic crystal structure. Ferritic stainless steels are also magnetic. Austenitic and ferritic stainless steels are both used for a wide variety of industrial and commercial applications[32].

While being an excellent structural material which can be readily formed into many different types of components, stainless steels do not inherently resist bacterial adhesion and biofilm growth. Within the past 20 years there has been increased interest in developing stainless steels which can inhibit bacteria growth on their surfaces as a means to help mitigate microbe-related industrial problems. In the late 1990's and early 2000's it was found that small amounts of silver or copper alloyed into the bulk of stainless steels, with little modification to the original composition, can have an antimicrobial effect. Both ferritic and austenitic varieties of these materials have been developed. The first development of a copper-alloyed antimicrobial austenitic stainless steel was by the Japanese company Nisshin Steel in 1997[31] and the first development of a silver-alloyed stainless steel was by the Japanese company Kawasaki Steel Corporation in 2002, the company was later merged into JFE Steel[30].

Silver ions are well known antimicrobial agents, producing an antimicrobial effect by damaging cell membranes and by denaturing and subsequently inactivating bacterial cell proteins[33]. Copper ions are also well known antimicrobial agents and are thought to have a similar effect to bacterial cells to that of silver ions[34, 35]. It has also been found that bacterial DNA can lose its ability to effectively replicate due to the denaturing effects of cellular proteins from silver exposure[33]. Both metallic silver and copper have little to no health risk to humans in very small quantities, such as those quantities eluted off of copper- and silver-alloyed stainless steel [36, 37]. Stainless steels are also commonly used as potable water piping [38] as well as within biomedical applications [27].

The mechanism of this documented antimicrobial effect of copper- and silver-alloyed stainless steels has been linked to the elution of copper and silver ions from the alloy surface when in contact with aqueous media, along with the generation of active oxygen on the alloy surface. The exact mechanism of how this metal ion elution occurs is still unclear, however it is thought that the regions of the steel with copper- or silver-rich phases interrupt the protective chromium oxide layers on the surface of the steel, allowing for redox reactions which promote the release of copper or silver ions within aqueous media[30, 39, 40]. Yokota et al. demonstrated that an austenitic silver-alloyed stainless steel still had similar corrosion resistance properties to a standard austenitic steel despite this proposed breech in the passivation layers which allows for antimicrobial ion elution[30]. Zhang et al. recently suggested that this occurs in copper-alloyed austenitic stainless steel through the promotion of the formation of $Cr_{23}C_6$ by the copper-rich phases[40].

Since their initial development there has been a plethora of studies regarding the antimicrobial efficacy of copper- and silver-alloyed stainless steels[41-49]. These studies have all presented positive antimicrobial effects, however, the majority of these studies either only report on the antimicrobial effect of the materials over a 24-hour time frame (per standard antimicrobial testing method) or are otherwise assessed in ways which do not account for the biofilm mode of growth.

Many of the studies assessing the antimicrobial effect of copper- and silver-alloyed stainless steels followed the Japanese antimicrobial testing standard, JIS-Z-2801 (2010), or a modified version of it. This standard technique compares the quantity of live bacterial cells present on a test surface before and after their exposure to a given test surface material over a 24-hour timeframe; if the amount of surviving cells is low enough, the surface is deemed antimicrobial. In this test, bacterial cells are deposited in a homogenized, suspended state onto the test surface and are covered with a thin plastic film for 24 hours. The quantity of live cells is quantified through homogenization, serial dilution, and plating of cells washed from the test surface at initial inoculation of the surface and after the 24-hour exposure. The test requires the use of *Escherichia coli* (ATCC 8739) to represent all gram-negative bacteria and *Staphylococcus aureus* (ATCC 6538P) to represent all gram-positive bacteria[50].

It should also be noted that governments heavily regulate what products can be labeled and marketed as possessing an antimicrobial effect, and frequently different countries will have different standards in place. In many instances, it may be more appropriate to claim a material has “microbial resistant surface properties” rather than “antimicrobial surface properties,” unless it meets the current standards in place for antimicrobial testing in its given country of origin. In the USA, the EPA controls regulations on what products can be labeled antimicrobial. It should be noted that an industrial standard which assesses the antimicrobial effect of material surfaces in the scope of biofilms currently does not exist.

1.5. Scope of Study

The majority of the studies which previously assessed the antimicrobial properties of these copper- and silver-alloyed stainless steels were conducted over a 24-hour time frame with stagnant conditions. As so, it was of interest to investigate the biologically resistant surface

properties of these materials over a longer duration timeframe and with a growth protocol more representative of the biofilm mode of life. This was investigated by growing *Escherichia coli* biofilms on the surfaces of submicron polished coupons on a ferritic copper-alloyed stainless steel (1.50 wt. % Cu), an austenitic silver-alloyed stainless steel (0.042 wt. % Ag), and a standard 304 series stainless steel, used as a baseline. The biofilms were grown with a 6-hour batch phase and 48-hour continuous phase using a drip flow bioreactor at room temperature, the protocol of which followed ASTM E2647-13 with few modifications. The modifications are outlined within Chapter 3 on the document.

The majority of the tests were grown on coupons with a submicron surface finish, however the effect of surface roughness was also assessed with some tests ran on coupons with a 41 μm surface finish. The submicron surface finishes were intended to allow for the assessment of the alloys' surface chemistries and microstructural features on bacterial adherence, without the influence of roughness.

All tests were run with a 6-hour batch phase. The majority of the tests were run with 48-hour continuous phase at room temperature. A few tests were run with a 96-hour continuous phase at the elevated temperature of 37 ± 3 °C in an attempt to maximize bacterial growth and observe more mature biofilms.

All of the coupons were sterilized by soaking them in isopropanol. The effect of surface conditioning was also attempted to be assessed through the rinsing of some of the coupons with either sterile deionized water (DI H_2O) or sterile phosphate buffered saline (PBS) solution prior to their insertion in the bioreactor. Some of the coupons were also rinsed with either sterile DI H2O or PBS directly after harvesting the coupons before imaging in order to assess how well attached the observed cells were to the surface of a coupon.

The strain of E. coli used, ATCC 8739, was selected because it is used within the antimicrobial tests commonly conducted on this material class. Also, we were constrained by the biosafety level (BSL) of our lab space, which was BSL1. ATCC 8739 is a non-pathogenic BSL1 strain of *E coli*.

Drip flow bioreactors are flexible reactor systems which can be easily modified to allow for modeling a variety of conditions and research needs. The drip-flow bioreactor was designed by Darla Goeres et al at. Montana State University, first publishing on the design in 2009[51]. The reactor system was then later commercially produced by BioSurface Technologies Corporation in Bozeman, MT.

A drip flow bioreactor was chosen to grow the biofilms since it is a good choice for general biofilm studies, has previously been used in studies which assessed biologically resistant surface properties of surface coatings[52], and it was easy to modify the growth protocol for our specific research needs. The drip flow bioreactor grows biofilms under very low shear conditions with a continuous flow of nutrient medium at an air-liquid interface. Following ASTM E2647-13 with the bioreactor also provided a standard and reproducible way of growing the biofilms.

All of the biofilms grown were analyzed using an Environmental Scanning Electron Microscope (E-SEM) under low vacuum within a water vapor atmosphere. E-SEM allowed for non-destructive imaging of the biofilms without the need to perform time-consuming sample preparation used for biological samples within standard SEMs at high vacuum. This fixation, dehydration and coating process is also associated with the creation of artifacts, which was avoided with E-SEM. The only sample preparation required to image the biofilm samples in this study was to place each sample coupon on a metal specimen mount using double-sided carbon tape. However, E-SEM generally produces lower resolution images when operated in low vacuum (E-SEM) mode with water vapor environment compared to standard SEM operated at high vacuums. This is due to the fact that some of the high energy electrons of the incident electron beam will inevitably be scattered by water vapor molecules. This was the main drawback of using E-SEM over standard SEM.

Additionally, baseline assessment of the three stainless steel materials was conducted. The surface chemical compositions and alloy microstructures of the materials were assessed using SEM and energy dispersive x-ray spectroscopy (EDS). Quality control measurements were taken of the coupon surfaces with contact mode atomic force microscopy (AFM) to measure the roughness associated with each coupon finish.

It should also be noted that apart from standardizing growth parameters for biofilm growth within a drip flow reactor, the international standard, ASTM- E2647-13, offers a method of cell viability quantification of the biofilms grown within the reactor set-up on substrates[53]. This involves sacrificing the entire biofilm grown, homogenizing the cells within a buffer solution, and performing a serial dilution and plating to quantify the number of viable cells in the biofilm by the metric of $CFU/mL/cm^2$. This is useful as a means to assess biofilm resistant properties of materials by comparing the viability of cells within biofilms grown on a baseline material and the material with a microbiologically resistant surface modification. However, the *E. coli* biofilms grown in this study were not mature enough to conduct these type of cell viability comparisons in confidence, despite making efforts to maximize growth within the limitations of the bioreactor. Additionally, this type of cell viability assessment completely sacrifices the biofilm which would have limited the number of biofilms to be observed in the E-SEM. All observations of the biofilms were thus made using the E-SEM.

The methods used within this body of work had limitations, but also led to interesting observations, both of which will be addressed within Chapters 4 and 5 of this document.

Chapter 2 Experimental

2.1. Material Selection and Coupon Preparation

2.1.1. Material Selection

Copper- and silver-alloyed stainless steels were selected due to their versatile, corrosion resistant properties as well as their potential for biofilm resistant surface properties. A standard austenitic, 304-type stainless steel was selected as a reference material to the copper- and silver-alloyed stainless steels.

The austenitic silver-alloyed stainless was manufactured by JFE Steel, Japan, and was listed as having a 0.042 wt. % silver composition. The ferritic copper-alloyed stainless steel was manufactured by Nisshin Steel, Japan, and was listed as having a 1.50 wt. % copper composition. The baseline austenitic 304 type stainless steel was manufactured by Goodfellow. The remaining balance of the silver-alloyed stainless steel was typical to that of 304 series, low-carbon, austenitic stainless steels. The remaining balance of the copper-alloyed stainless steel was typical to an intermediate chromium, low-carbon ferritic stainless steel. The bulk of the austenitic stainless steels each had an assumed face-centered cubic crystal structure and the bulk of the ferritic stainless steel had an assumed body-centered cubic crystal structure. Table 2-1 summarizes the compositional information of the stainless steel materials.

Table 2-1. Compositions of Stainless Steels

Material Name	Manufacturer	Elemental Composition (wt. %, unless otherwise indicated)												
		C	Si	Mn	Ni	Cr	P	S	Cu	Ag	Mo	Nb	N	O	Fe
CuSS	Nisshin Steel	0.008	0.28	0.29	0.13	16.99	0.038	0.001	1.50	x	0.05	0.37	0.012	41 ppm	balance
AgSS	JFE Steel	0.05	0.30	1.00	8.10	18.20	0.03	x	x	0.042	x	x	x	x	balance
304SS	Goodfellow	< 800 ppm	x	< 2	8 - 11	17 - 20	x	x	x	x	x	x	x	x	balance

Table 2-1. Key	
CuSS	copper-containing austenitic stainless steel
AgSS	silver-containing austenitic stainless steel
304SS	304-type stainless steel
x	no data/not relevant
ppm	parts per million
balance	balances the remainder of the composition to 100 wt % (bulk)

2.1.2. Coupon Preparation

All of steel materials were purchased or otherwise received as thin sheets. The original CuSS sheet was approximately 110 mm × 150 mm and 1 mm thick. The AgSS sheet was approximately 110 mm × 150 mm and 0.75 mm thick. The original 304SS sheet was approximately 100 mm × 100 mm and 1.5 mm thick. The material sheets were waterjet cut into 8 × 8 mm^2 coupons by the Radford, VA machine shop, Materials Processing Inc. This was done as needed, which was twice. Each time approximately 20 coupons were cut from each sheet. Figure 2-1. shows an example of how the coupons looked as received once cut.

Figure 2-1. Coupons Cut out of Material Sheet

After being freed from the material sheet, the edges of each material coupon used were filed with a hand file to remove any barbs formed during waterjet cutting and to ensure the edges were planar to each other. During filing, each coupon was secured using a tabletop mount, exposing one side at a time for filing and rotating accordingly. After making the edges planar, the coupons were ready for further surface preparation.

For use in the bioreactor, one side of each material coupon used was mechanically grinded and polished to either a mirror finish (< 0.25 – 0.02 µm) or 320 grit (45 µm) finish. One trial involved two coupons with an 800 grit (7 µm) finish in comparison to two coupons of a 0.02 µm finish. Each coupon had to be individually polished to the desired finish. First, a coupon was adhered to a stainless steel or alumina cylindrical mount with Crystalbond 509 Clear. Crystalbond 509 Clear is a lab grade hot glue that melts at low temperatures and easily dissolves in acetone. The coupon was adhered to the mount by heating up the mount on a hot plate with Crystalbond 509 Clear on the mount surface. The coupon was then pushed into the glue so that it laid flat and parallel to the mount surface. Care was taken not to get any glue on the coupon surface. Mounts were periodically polished to ensure they were planar. Once the Crystalbond 509 Clear hardened, the coupon surface was first made planar using a 320 grit SiC paper and an EcoMet 3000 grinder/polisher. Afterward, the surface was polished at decreasing grits using 400 grit (26 µm), 600 grit (15 µm), 800 grit (7 µm), 1200 grit (3 µm) SiC papers, followed by 3µm, 1µm, and 0.25µm diamond paste and appropriate polishing cloths. Finally, the surface was polished with 0.02 µm colloidal silica and appropriate polishing cloth. Figure 2-2. summarizes the polishing regime used.

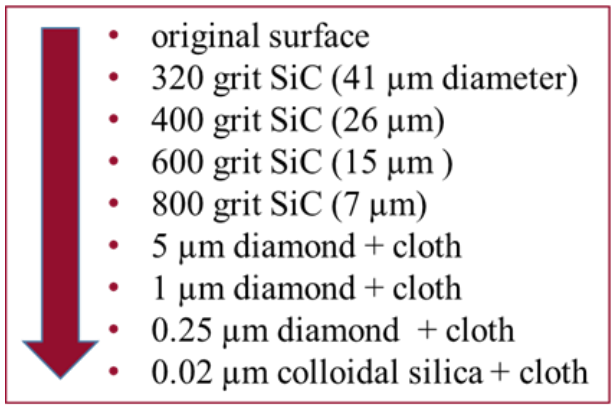

Figure 2-2. Polishing Regime Using EcoMet 3000

It should be noted that prior to switching polishing media sizes, the coupon surface was rinsed thoroughly with water and inspected under an optical microscope to help ensure uniformity in surface roughness. Moving between too large of a size difference in polishing media will result in non-uniform and poorly polished surfaces. Using an inappropriate polishing cloth and media type will also result in poor and non-uniform polished surfaced. Papers and cloths need to be changed when they become too worn to ensure uniform and effective polishing. It should also be noted that nitrile gloves were changed and disposed of between media sizes to minimize contamination, and obviously each polishing paste required separate cloths to minimize media size contamination. The EcoMet 3000 was also rinsed with water between switching media sizes. If media is contaminated, there is a large potential for scratches and lack of uniformity in the resulting surface finish.

To obtain any finish other than the 0.02µm finish, the polishing procedure was stopped at the desired surface roughness for a given coupon. The data gathered was on 0.25 µm surfaces, 0.02 µm surfaces, and 320 grit surfaces (and one trial with 800 grit surfaces).

After sufficient polishing, the coupon was removed from the crystal bond and cleaned. To do so, the mount was placed on a hot plate until the Crystalbond 509 Clear melted, the coupon was carefully removed with tweezers and placed into a small bath of acetone with filter paper at the bottom to protect the surface. The mount was wiped to remove molten glue and also cleaned with acetone. The coupon was then washed and rubbed with a clean cotton swab with both acetone and ethanol until all glue was removed. It was then washed repetitively with a DI water and dish soap solution inside a 2mL polypropylene centrifuge tube and sonicated in such a solution for a minimum of 1 hour. Finally, it was given a final wash with ethanol and a clean cotton swab. After being cleaned, the coupon was then analyzed for baseline measurements or placed into a sterilized, 2mL polypropylene centrifuge tube with 99% isopropanol for sterilization. Coupons were sterilized via the isopropanol bath for a minimum of 6 hours before being placed in the bioreactor.

Figure 2-3. shows an example of a cleaned coupon prepared with a mirror finish.

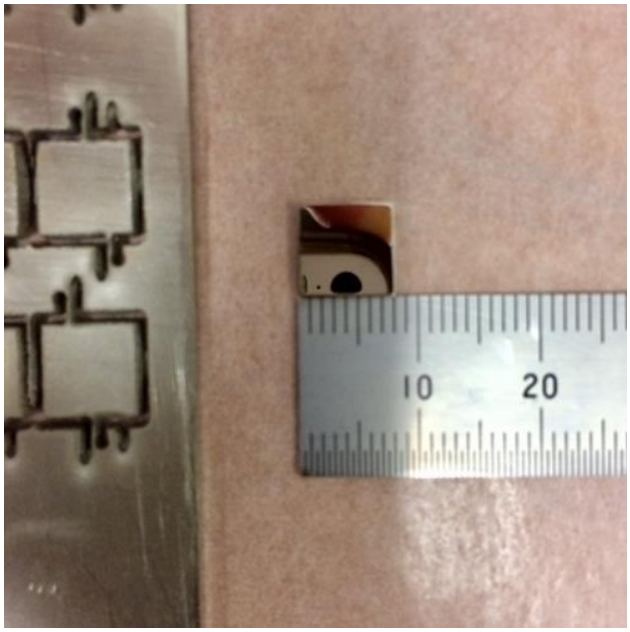

Figure 2-3. Cleaned Coupon with Mirror Finish

AFM surface roughness measurements were used to perform quality control measurements of the surfaces, using approximately three points on every few coupon surfaces as representative of all coupons polished to a specified surface finish.

Please see section Chapter 3.2 for baseline E-SEM/EDS data and AFM surface roughness measurements on the bare stainless steel coupons.

2.2. Drip Flow Bioreactor Set-up

The drip-flow bioreactor system was designed to grow laboratory biofilms at room temperature in a systematic, repeatable way under low shear conditions at an air-liquid interface. As mentioned, this type of reactor system was chosen since it provided a more realistic model of the conditions bacterial biofilms face in real life scenarios and it has been previously documented for use in biologically resistant surface studies.

Within this study, the set-up and growth protocol used for within the drip flow bioreactor followed ASTM E2647-13 exactly except for the following modifications.1) *Escherichia coli* (ATCC 8739) was used instead of *Pseudomonas aeruginosa*. Due to our lab's constraints on biosafety level (BSL1 only), and the precedent of the selected bacteria in surface studies of Ag- and Cu-alloyed stainless steels, the *E. coli* strain ATCC 8739 and its associated growth media was used. 2) Scored glass slide coupon holders were used to hold the 8×8 mm^2 stainless steel coupons in place via gravity rather than using entire glass slides as the growth substrates (more details to follow). 3) The viable cell quantification step of the ASTM E2647-13 was not performed within this thesis work, as the resulting *E. coli* biofilms grown were deemed not mature enough to perform this serial dilution and plating technique with confidence in accuracy. This quantification technique also would have completely sacrificed the grown biofilms, which would have limited the E-SEM imaging of the biofilms grown. 4) The majority of the growth tests were run at room temperature with a 48-hour continuous phase, which followed ASTM

E2467-13. However, an incubation box surrounding the drip flow reactor was created in order to conduct some of the growth tests at the optimal growth temperature for *E. coli* (37 ± 3°C), rather than at the colder room temperature of the lab which typically was around 20°C. This was done in an attempt to grow more mature biofilms on the surfaces of the stainless steel coupons and the parameter was tested along with a longer continuous phase growth time of 96hr.

The sections which follow provide a detailed explanation of the drip flow bioreactor system set-up and all associated grown protocols used to grow the ATCC 8739 *E. coli* biofilms on the three types of stainless steel coupons.

2.2.1. System Components and Assembly

A four-channel, drip-flow bioreactor was purchased from Biosurface Technologies Corporation and the majority of all associated system equipment was purchased from Cole-Parmer. The set-up of the drip flow reactor system followed ASTM E2647-13 and the associated bioreactor manual provided by Biosurface Technologies Corp. Again the only modifications to these standards were the use of *E. coli* and its associated media, the use of scored glass slides to hold the coupons in place rather than using the entire glass slide as the growth substrates, and the use of an incubation chamber surrounding the bioreactor chamberμ for some of the growth tests.

Figure 2-4. outlines the schematic of the drip-flow reactor chamber. The drip flow bioreactor came preassembled from BioSurface Technologies Corp. It also came with an associated plastic stand with which to sit the reactor on so it consistently sits at a 10° angle while in continuous phase mode. There are four chambers within the bioreactor, which allows for four test coupons to be run at the same time, or three tests coupons and a control. There are two small pegs at the bottom of each chamber with which to hold a glass slide in place via gravity. There is also a small grove in the center of each chamber to allow for easy removal of the glass slides. At the top of each chamber there is a mininert valve with a rubber septum. This enables sealed access to the chamber for the insertion of a syringe needle connected to the influent tubing and tank. At the bottom of each chamber there is a bacterial air vent. This is just an autoclavable syringe filter (≤0.5 μm mesh) used to allow sufficient airflow into and out of the chamber without allowing potential contaminates to enter. Each chamber lid has an O-ring which makes an air tight seal between the chamber and the outside. The entire drip flow reactor is autoclavable, which allows for easy and complete sterilization before and after growth tests.

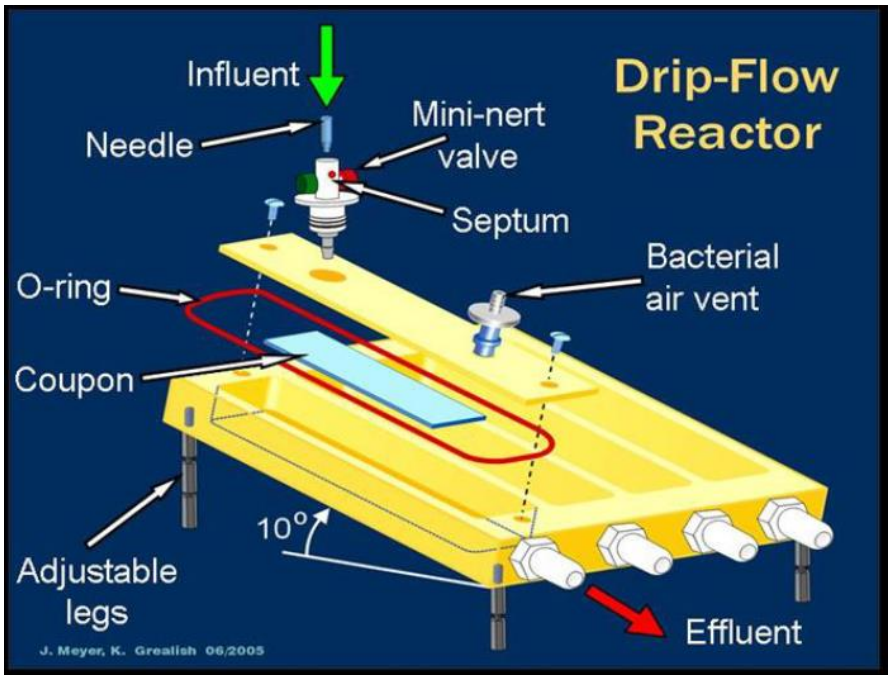

Figure 2-4. Drip-flow Bioreactor Chamber Schematic, image courtesy of ASTM E2647-13 [53]

Figure 2-5. outlines the overall reactor set up connected to the drip flow bioreactor. Left to the bioreactor, there was a 20 L influent carboy which had with two 1/4 in barbed bulkhead fittings in its lid. One of the fittings had nothing on the inside of the carboy and a stretch of 1/4 in tubing connected to a bacterial air vent. On the inside of the other fitting there was a stretch of 1/4 in tubing that touched the bottom of the carboy to draw fluid from the carboy. On the same fitting, there was 1/4 in tubing exiting the carboy to bring fluid to the pump and bioreactor. From the 1/4 in tubing exiting the carboy, it was connected to a glass flow break which interrupted the flow of the influent media so as to inhibit biofilms from growing up inside the influent carboy. There was a ring stand and clamp to hold the glass flow break upright at all times. After passing the glass flow break, the 1/4 in tubing was connected to a 1/4 in to 1/8 in reducer and 1/8 in tubing. The 1/8 in tubing was further broken into 4 separate lines with two 1/8 in T-shaped connectors. The four lines of 1/8 in tubing was then connected to four 1/8 in to 1/16 in reducers and 1/16 in tubing. The 1/16 in tubing was used to pass through the peristaltic pump and was the tubing diameter used to calibrate the pump flow rate. The 1/16 in tubing was then connected to syringe needles and subsequently each drip flow bioreactor chamber during the growth tests. The bioreactor was laid flat in batch phase and placed on the 10º angle stand during continuous phase.

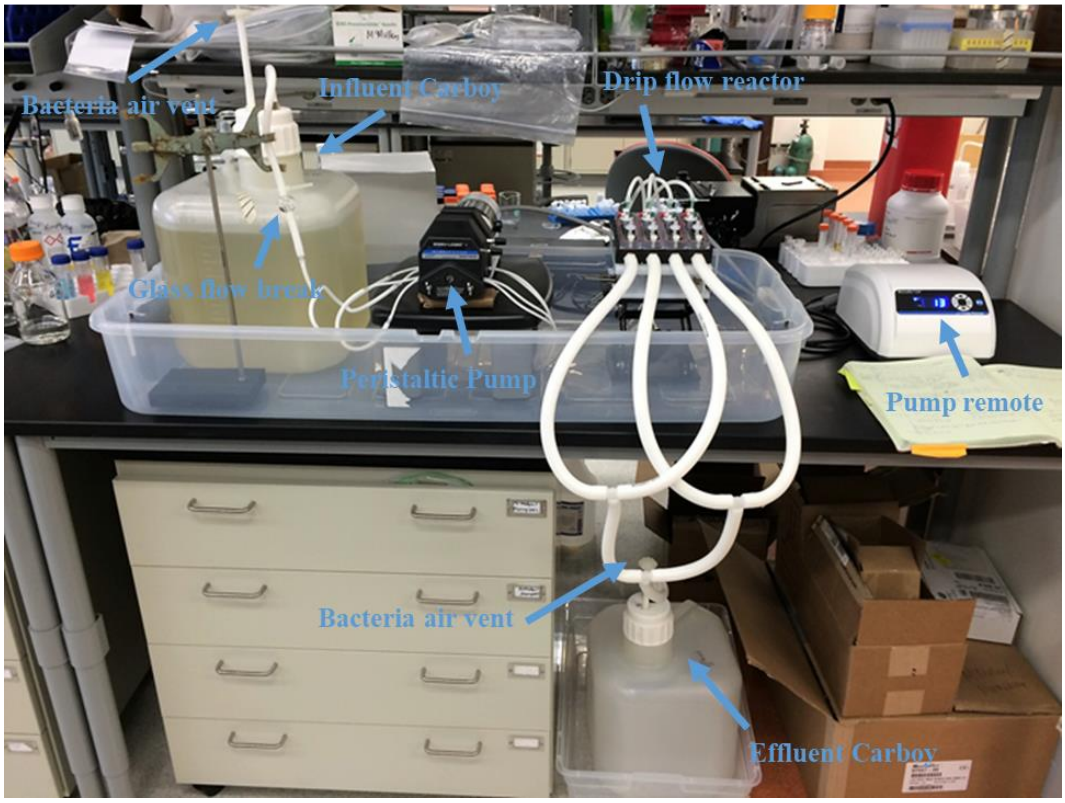

Figure 2-5. Drip-flow Bioreactor Set-up

On the right of the bioreactor, each effluent port was connected to 1/2 in tubing. The four lines of 1/2 in effluent tubing were then brought down to a single line using two 1/2 in T-shaped connectors. The single line of ½ in tubing was then connected to the 20 L effluent tank. The effluent carboy had the fittings same set up as the influent carboy. One of the barbed bulkhead fittings was 1/4 in, had nothing on the inside of the carboy, and had a stretch of 1/4 in tubing with a bacterial air vent. The other barbed bulkhead fitting was 1/2 in, and connected to the effluent tubing from the bioreactor on the outside of the carboy. On the inside of the carboy there was a stretch of 1/2 in tubing to help deliver the effluent fluid into the carboy. All components of the drip flow bioreactor system were able to be sterilized via autoclave except for the syringe needles, which were sterile and single-use for each growth test.

All components to the left of the bioreactor, as well as the bioreactor chamber and stand, were placed inside of a large polypropylene container on the benchtop, in case of any spills. The peristaltic pump head was placed on a plastic stand a few inches above the bottom of this container for similar concerns regarding spills and leaks. All components to the right of the bioreactor were placed inside of or above a second large polypropylene container, for the event of any spills. All of the tubing used within the bioreactor was Masterflex C-flex tubing, which combines the biocompatibility of silicone with the chemical resistance of Tygon tubing. It is important that the tubing used within the bioreactor was both biocompatible and able to be used within the peristaltic pump. The control panel to the peristaltic pump was placed outside of the

spill container nearby on the bench. It should also be noted that the screw top lids to each 20 L carboy had to have holes drilled though them to insert the barbed bulkhead fittings.

Figure 2-6. shows the dimensions of the scored glass slides used to hold the coupons in place via gravity. The distance which was selected held the bottom edge of the coupons 20 mm from the bottom of the reactor chambers. Thus, for each glass slide holder set, the bottom slide piece measured 20 mm long and the top slide piece measured 48.2 mm long. The distance between the two slide pieces was 0.8cm, the length of the stainless steel coupon squares.

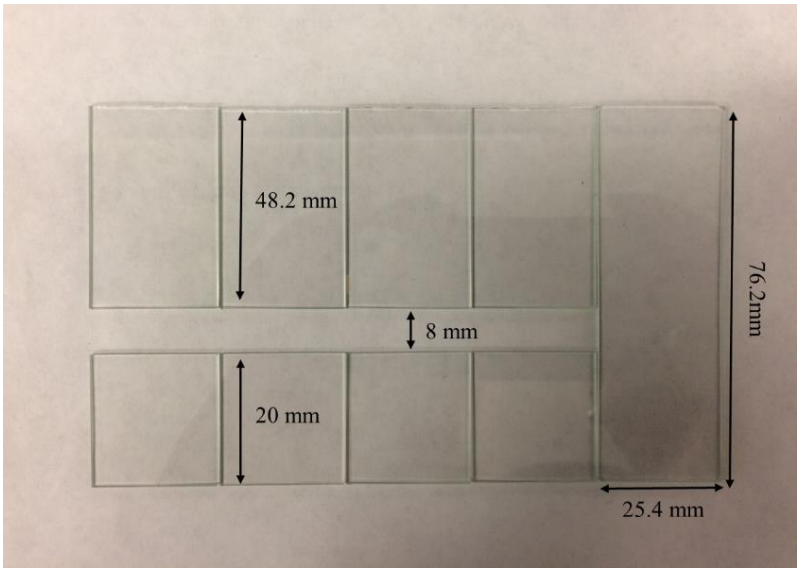

Figure 2-6. Glass Slide Gravity Coupon Holders

Multiple distances were tested with sample coupons to assess the best distance to hold the coupons from the dripping source. The distance which was selected (bottom edge of coupon rested 2 cm from the bottom, top edge of coupon rested 48.2 mm from top) had the greatest wetting from the influent broth while remaining outside of the higher shear forces within the "splash zone" at the area at the top of the glass slides. Some of these tested distances are shown in Figure 2-7. Figure 2-8. shows the finalized scored glass coupon holders in action.

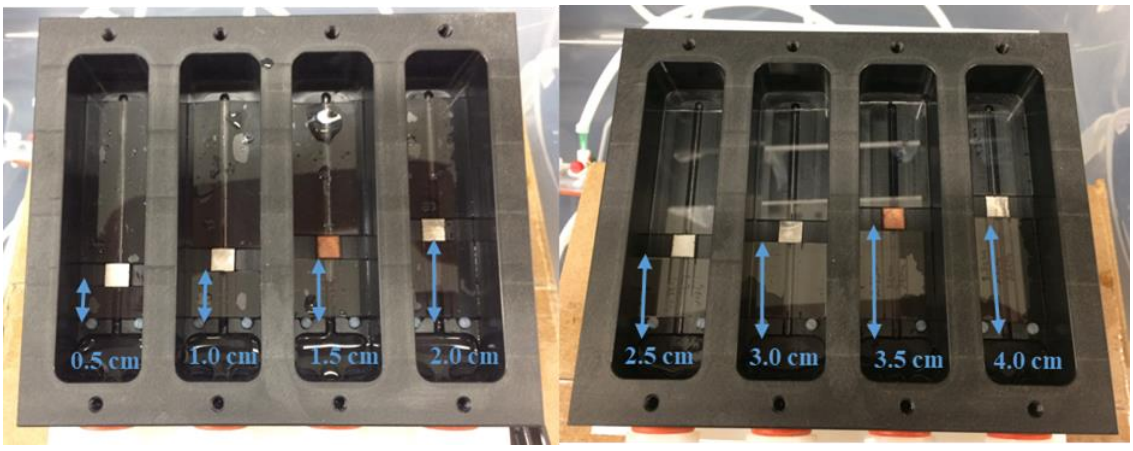

Figure 2-7. Various Coupon Holder Distances Assessed

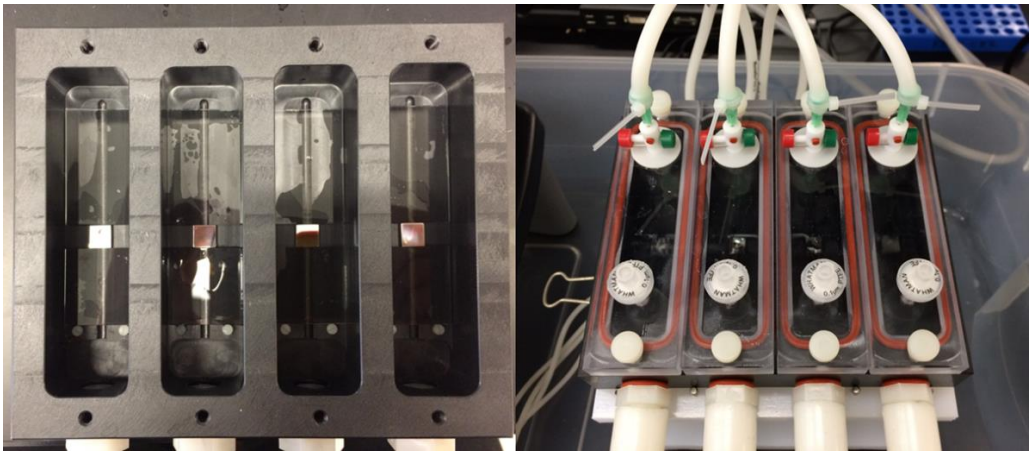

Figure 2-8. Glass Slide Coupon Holders Securing Coupons in Place in Drip-flow Reactor Chamber – 20 mm from Bottom

Generic lab grade borosilicate glass slides were used to make the scored glass coupon holders. The scored glass coupon holders were preparing by carefully measuring, scoring and breaking the glass slides to the desired measurements. A diamond score was used to make the scores along a flat metal ruler edge at the desired lengths. The scored and broken edges were then lightly grinded until smooth and planar using various grits of SiC paper. The dimensions of each top piece of scored glass slide and the dimensions of each bottom piece of scored glass slide were within less than 1mm from each other. The section cut out of each full slide was the width of each of the stainless steel sample coupons, 8 mm.

This method of securing the stainless steel coupons within the drip flow reactor chambers was considered with great care. The use of double-sided tape or other adhesives to secure the coupons on top of the glass slides was also considered. This would have created at least two problems. The use of any adhesives could have posed unknown toxicity problems to the bacteria or could have added an unknown additional food source to the bacteria other than the influent medium. Securing the coupons on top of the glass slides with an adhesive could have further interrupted flow over the surfaces in a way the reactor originally did not intend.

It was also a consideration to develop a flexible, autoclavable, reusable mold to place the coupons inside of within each channel. This would have been costly and time consuming to create. There was also the problem of finding a flexible, autoclavable plastic which would pose zero toxicity threats to the bacteria.

Additionally, it was a consideration to cut large coupon samples of the stainless steel material to the dimensions of a glass slide, eliminating the need to develop a way to secure the coupons in place. This would have caused two concerns as well. There was a very limited amount of sample material, and cutting only a few large coupon samples would have exhausted our available supply. It would have also been very difficult to create uniform surface finishes on coupons with maintaining a uniform level surface as large as the dimensions of a glass slide; this would have taken the control over coupon surface finish uniformity and repeatability out of the study.

Given this, the chosen design for the scored glass coupon holders eliminated these concerns. Borosilicate glass is fairly inert and is nontoxic. The scored glass coupons holders kept each stainless steel coupon in place via gravity alone, without posing any unknown toxicity or food source problems. Keeping the coupons flush or nearly flush to the glass slides also maintained similar flow over the surfaces as the reactor design originally intended. Glass slides are also a fairly inexpensive consumable and easy to replace if needed.

The scored glass slides were routinely checked for any degradation (chipping, deep scratches, etc.). However, the coupons holders were durable enough for the same set of glass coupon holders to be used throughout the entire duration of the study.

Figure 2-9 and Figure 2-10 show the incubated bioreactor chamber, which was developed and used to elevate the temperature of the bioreactor chamber from a colder room temperature (around 20°C) to the optimal growth temperature of approximately 37°C. The incubation chamber was made by cutting holes into a large styrofoam box to fit a hot plate cord, the influent tubing, and the effluent tubing. The holes were then filled in around the cord and tubing with removable foam insulator to help maintain the internal temperature. A hot plate was set inside of the box and set to a temperature of around 85 °C; this temperature was sufficient to heat the air in the box to 37 ± 3 °C. The hot plate was raised a few inches from the bottom of the box to avoid the cord from getting wet in the case of leaks or spills. It was also placed so it was not touching any surfaces within the box. A digital hygrometer was placed inside of the incubation box near the drip flow bioreactor chamber in order to monitor the temperature and humidity of the air inside the incubation box. The incubation chamber was allowed to reach approximately 37°C for at least 2-4 hours prior to batch phase with the reactor to maximize stability in the temperature of the incubation box. The incubation box surrounding the bioreactor chamber was developed in an attempt to maximize bacterial growth, and try to develop more mature *E. coli* biofilms on the surfaces of the stainless steel coupons.

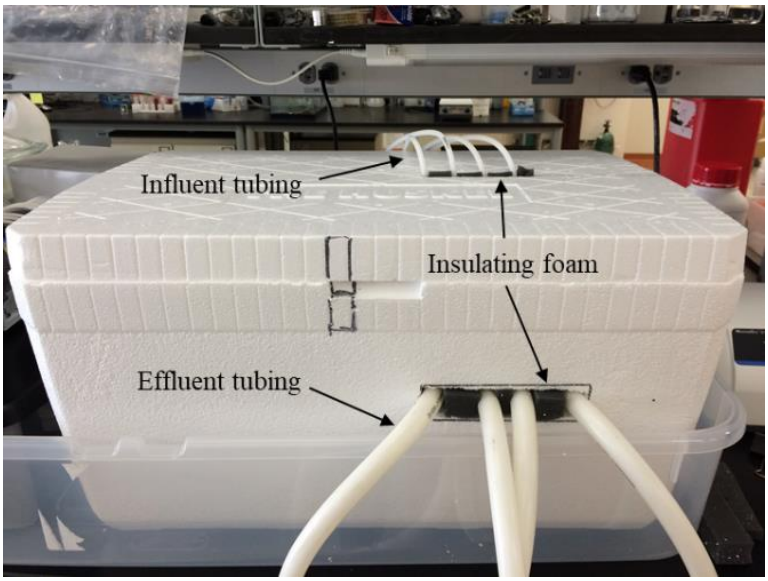

Figure 2-9. Incubated Drip-flow Bioreactor System

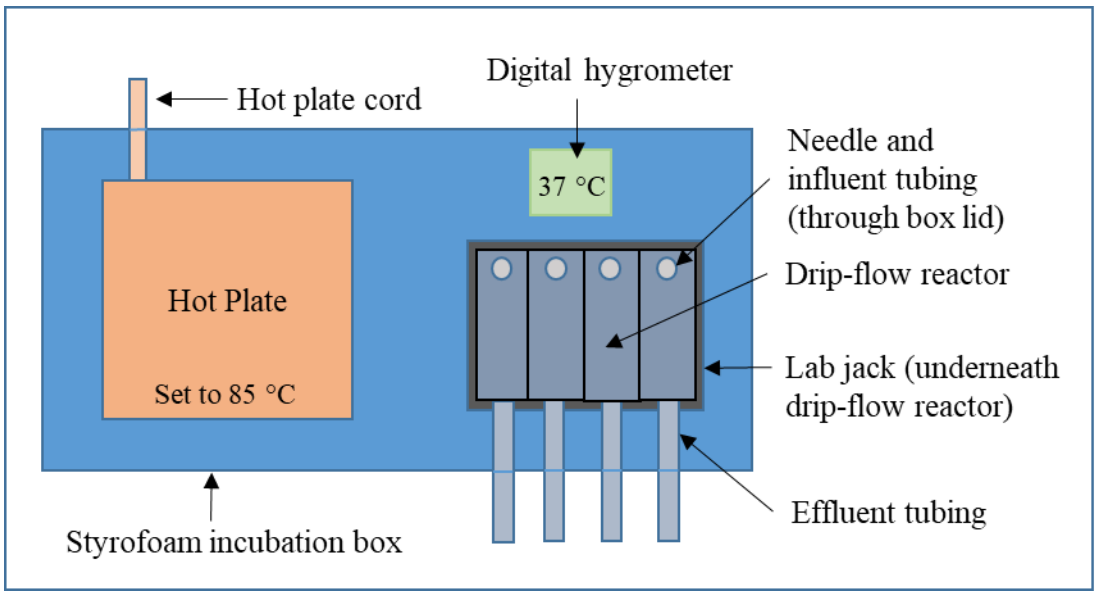

Figure 2-10. Schematic of Inside the Styrofoam Incubation Box

Below is a specific list of all the system components used within the drip flow bioreactor system. Each component with an item # was purchased from Cole Parmer. The list does not include the materials needed to create the styrofoam incubation chamber used in some of the growth tests. The materials needed to create the incubation chamber just included a large Styrofoam box, insulating packaging foam, a knife/saw to cut holes, a digital hygrometer, and a generic lab hotplate.

- 4-channel, drip flow bioreactor and 10° angle bioreactor stand (Biosurface Technologies Corp)
- Peristaltic pump and pump drive
  - Masterflex L/S Precision Modular Drive w/ Remote, Item # EW-07557-10
  - Two, Masterflex L/S two-channel Easy-Load II pump head, CRS rotor, Item # EW-77202-50
  - Masterflex Stainless steel mounting hardware; for two L/S Easy-Load II pump heads, Item # EW-77200-02
- Autoclavable tubing
  - 1/16in Masterflex C-Flex tubing (50 A), L/S 13, 25 ft; Item # EW-06424-13
  - 1/8in Masterflex C-Flex tubing (50 A), L/S 16, 25 ft; Item # EW-06424-16
  - 1/4in Masterflex C-Flex tubing, Opaque White, 25 ft; Item # EW-06424-72
  - 1/2in Masterflex C-Flex tubing (50 A), I/P 82, 25 ft; Item # EW-06424-82
- Autoclavable connectors/reducers
  - Masterflex Barbed Reducer, Polypropylene, 1/8" ID to L/S 13/14; Item # EW-40616-43
  - Cole-Parmer Reducing Connector, Polypropylene, 1/4" x 1/8"; Item # EW-41518-36
  - Cole-Parmer Barbed Tee Connector, Polypropylene, 1/8"; Item # EW-50623-66
  - Cole-Parmer Barbed fittings, T connector, Kynar, 1/2" ID; Item # EW-30703-78
- Autoclavable barbed bulkhead fittings

    - Thermo Scientific Nalgene 6149-0001 barbed bulkhead fitting kit, 1/2" tubing ID; Item # EW-06259-00
    - Two, Thermo Scientific Nalgene 6149-0002 barbed bulkhead fitting kit, 1/4" tubing ID; Item # EW-06259-10
- Two, autoclavable, 20L polypropylene carboys with screw-top lids; Item # EW-62507-20
- 1, autoclavable glass flow break (there were 4 supplied from BioSurface Technologies Corp)
- 6×6 in^2 lab jack with 10in max height
- Plastic stand to keep peristaltic pump head a few inches above spill container (monitor stand with a 50lb weight limit)
- 21 gauge, 1in, sterile, single-use syringe needles
- Syringe filters, < 0.5 µm (bacterial air vents)
- Ring stand and clamp to keep influent tubing/glass flow break in place
- 1mL and 15mL sterile, single-use syringes
- Small, 2-3in zip ties
- Metal clamps to clamp 1/2 in tubing
- Two large binder clips, or other clips, to secure bioreactor stand onto the lab jack
- Scored glass slide coupon holders, made from generic borosilicate glass slides with diamond score
- Material coupons

All components of the drip flow reactor system which came into direct contact with the growth medium and bacteria were able to be sterilized via autoclave, except for the sterile, single-use items, and the stainless steel material coupons. The stainless steel material coupons were not sterilized via autoclave, as there was concern for the autoclave water/steam to deposit unwanted contaminants onto the submicron finishes cleaned via sonication, which could potentially show up within the E-SEM and unintentionally influence the results. The material coupons were sterilized via an isopropanol bath.

2.2.2. Pump Calibration for 50mL/hr/line Flow Rate

Peristaltic pumps operate by creating suction through a wavelike series of contractions and relaxations within flexible tubing. Flexible tubing connected to a fluid reservoir is placed through a pump head and a rotor with various rollers compresses the tubing so it becomes pinched and then quickly relaxes, drawing fluid through the tubing.

The peristaltic pump used in this study was a Masterflex L/S Precision Modular Drive with a digital control and two, Masterflex L/S two-channel Easy-Load II pump heads. Each Easy-Load II pump head could only handle two lines of tubing at a time, so two of these stackable pump heads were purchased along with the necessary mounting hardware so that four lines of tubing could be handled simultaneously. The two pump heads were mounted into the modular drive, which had a remote control to turn the pump drive on/off and control the rotations per minute of the pump head rollers. The 1/16 in Masterflex tubing was then placed into the Easy Load II pump heads prior to turning on the pump to run fluid through the tubing.

The flowrate of fluid through a peristaltic pump is directly related to the diameter of the flexible tubing, the number of revolutions per minute (RPM) of the pump head rollers, the

overall flexibility of the tubing, and the viscosity of the fluid. ASTM E2647-13 outlined a flowrate of 50mL/hour/line to be used through the four-channel bioreactor, or a total of 200mL/hour. This flow rate used about 10 L of 270 mg/L influent media over 48 hours, and 20 L of 270 mg/L influent media over 96 hours. In order to achieve this specified flowrate with the specific pump drive, pump heads, and type of tubing used, a 1/16 in tubing diameter needed to be passed through the pump heads and the rollers needed to be run at 13 RPM.

The tubing diameter needed to achieve this flowrate with this pump system was assessed by first referring to the pump drive and pump head information provided by Cole Parmer. After getting in the ballpark of the desired flowrate with the necessary tubing size, the pump system needed to be calibrated with the 1/16 in tubing and influent media. Since the influent media was so dilute, it was similar enough to water so that the pump system could be calibrated using just DI H_2O. The pump system was calibrated by measuring the amount of water that would pass through the pump within a given time frame at a given rotor RPM. This was done using a beaker, graduated cylinders and a stopwatch, an example of which is visually given in Figure 2-11. For the data within Tables 2-4, the flowrate was assessed using the entire influent and tubing setup, including syringe needles, as seen in Figure 5, not just the tubing size passed through the pump head as in Figure 9. Before taking the calibration measurements, the pump was allowed to run for 10 minutes with water at the set flow rate, so as to prime the tubing and stabilize the flow rate.

Figure 2-11. Example of Pump Calibration Process

Table 2-2. summarizes all of the relevant calibration data taken in initially deciding on the RPM needed to achieve a 50mL/hr/line flowrate with the pump system. Care was taken to monitor the same tubing line through the same specific pump head channel. Line 1 refers to tubing always passed through the pump head channel closest to the drive within the first pump head. Line two refers to the tubing always passed through the pump head channel furthest from the drive within the first pump head. Line 3 refers to the tubing passed through the pump head channel closest to the first pump head (and drive) within the second pump head. Line four refers to the tubing passed through the pump head channel furthest away from the drive within the

second pump head. Average flow rate and standard deviation were calculated both for each individual pump line and the overall average between all four lines. It was determined that 13 RPM delivered the closest flowrate to the desired 50mL/hr/line, with an overall average of 49.46 ± 3.43 mL/hr between all four lines. 12 RPM was also quite close to achieving a 50 mL/hr/line with an average of 47.03 ± 1.58 mL/hr between all four lines. However, it was deemed that 12 RPM produced a flow rate slightly too low on average compared to 13 RPM. Tables 2-3 and 2-4 detail the average flow rate of fluid through the pump system at 13 RPM versus 12 RPM.

Table 2-2. Pump System Calibration Data

Prime Time (min)	Run Time (min)	RPM	Line 1			Line 2			Line 3			Line 4		
			mL	mL/min	mL/hr	mL	mL/min	mL/hr	mL	mL/min	mL/hr	mL	mL/min	mL/hr
5.00	10.00	13.00	9.00	0.90	54.00	9.00	0.90	54.00	7.00	0.70	42.00	9.00	0.90	54.00
	10.00	13.00	8.75	0.88	52.50	8.50	0.85	51.00	7.75	0.78	46.50	8.50	0.85	51.00
	10.00	13.00	8.50	0.85	51.00	8.50	0.85	51.00	8.00	0.80	48.00	9.50	0.95	57.00
	10.00	13.00	8.40	0.84	50.40	8.50	0.85	51.00	8.15	0.82	48.90	8.80	0.88	52.80
	10.00	13.00	8.40	0.84	50.40	8.50	0.85	51.00	7.80	0.78	46.80	8.90	0.89	53.40
	10.00	12.00	7.80	0.78	46.80	7.80	0.78	46.80	7.80	0.78	46.80	8.15	0.82	48.90
	11.00	12.00	8.60	0.78	46.91	8.60	0.78	46.91	8.30	0.75	45.27	9.00	0.82	49.09
	10.00	12.00	7.80	0.78	46.80	7.80	0.78	46.80	7.60	0.76	45.60	8.20	0.82	49.20
	10.00	12.00	7.90	0.79	47.40	7.80	0.78	46.80	7.20	0.72	43.20	8.20	0.82	49.20
5.00	10.00	13.00	6.60	0.66	39.60	8.80	0.88	52.80	8.90	0.89	53.40	8.20	0.82	49.20
	10.03	13.00	7.60	0.76	45.45	8.90	0.89	53.22	8.80	0.88	52.62	8.30	0.83	49.63
	10.00	13.00	7.50	0.75	45.00	8.80	0.88	52.80	8.80	0.88	52.80	8.30	0.83	49.80
	10.33	13.00	8.60	0.83	49.94	8.60	0.83	49.94	8.80	0.85	51.10	8.80	0.85	51.10
	10.00	13.00	8.50	0.85	51.00	8.10	0.81	48.60	8.40	0.84	50.40	8.30	0.83	49.80
	10.00	13.00	8.50	0.85	51.00	8.20	0.82	49.20	8.40	0.84	50.40	8.40	0.84	50.40
	10.00	13.00	8.60	0.86	51.60	8.30	0.83	49.80	8.40	0.84	50.40	8.40	0.84	50.40
	10.00	13.00	8.50	0.85	51.00	8.20	0.82	49.20	8.50	0.85	51.00	8.30	0.83	49.80
	10.00	13.00	8.70	0.87	52.20	8.20	0.82	49.20	8.50	0.85	51.00	8.30	0.83	49.80
15.00	10.00	13.00	8.50	0.85	51.00	8.70	0.87	52.20	8.50	0.85	51.00	9.00	0.90	54.00
	10.00	13.00	6.90	0.69	41.40	7.40	0.74	44.40	7.30	0.73	43.80	7.80	0.78	46.80
	10.25	13.00	8.40	0.82	49.17	8.50	0.83	49.76	x	x	x	x	x	x
	11.68	13.00	9.40	0.80	48.27	9.60	0.82	49.30	9.40	0.80	48.27	10.00	0.86	51.36
	10.00	13.00	7.60	0.76	45.60	8.00	0.80	48.00	7.20	0.72	43.20	8.60	0.86	51.60
	10.00	13.00	7.10	0.71	42.60	6.90	0.69	41.40	6.90	0.69	41.40	7.20	0.72	43.20
	10.00	13.00	7.80	0.78	46.80	8.30	0.83	49.80	7.90	0.79	47.40	8.80	0.88	52.80

Table 2-2 Key		
	=	taken on 7/11/2017
	=	taken on 7/25/2017
	=	taken on 10/17/2017
x	=	missing data point

Table 2-3. Mean Flow Rate and Associated Standard Deviation – 13 RPM

Line	Average Flow Rate (mL/hr)	Standard Deviation
1	48.57	3.92
2	49.89	2.87
3	48.52	3.61
4	50.89	2.87
All Lines	49.46	3.43

Table 2-4. Mean Flow Rate and Standard Deviation – 12 RPM

Line	Average Flow Rate (mL/hr)	Standard Deviation
1	46.98	0.29
2	46.83	0.05
3	45.22	1.50
4	49.10	0.14
All Lines	47.03	1.58

It should also be noted that peristaltic pump systems should be recalibrated periodically. The flexible tubing will eventually wear out over time and the pump RPM may need to be adjusted periodically to maintain the desired flowrate, before finally needing to replace the tubing. The pump head calibration was checked approximately once a month during this study.

2.3. Bacteria Storage and Media Preparation

As mentioned, the bacteria selected was ATCC 8739, a BSL1 strain of *E. coli*. This particular strain required nutrient broth (NB) and nutrient agar (NA) for growth media, both of which were prepared in-house from media powders manufactured by Becton Dickinson. Nutrient broth and agar contain a mix of beef extract, peptone and salts. This specific strain of *E. coli* will not grow well on tryptic soy media, though many other strains may. Nutrient broth and agar are considered a non-selective or nutritive media, meaning it can grow a wide variety of microorganisms.

The only other media prepared was phosphate buffered saline (PBS), which was used as a buffer wash solution as needed and was prepared from powder packets by Sigma Aldrich. Each PBS powder packet when dissolved in 1L DI H_2O yielded 0.01M PBS (0.138M NaCl; 0.0027M KCl) with a pH of 7.4.

For the initial bacteria propagation and storage after the bacteria arrived from the ATCC, the nutrient broth was prepared as specified in Figure 2-12. (8g/L).

Broth Medium Preparation
Nutrient broth……..……..8g
DI water……...1000mL
Autoclave at 121ºC

Agar Medium Preparation
Nutrient agar……..……..23g
DI water……...1000mL
Autoclave at 121ºC, pour plates, dry, refrigerate 4ºC

Nutrient agar composition
Beef Extract……3g
Peptone……...5g
Agar……..15g
Final pH 6.8 +/- 0.2
nutrient broth composition omits agar

Figure 2-12. Composition and Recipe for Nutrient Agar and Nutrient Broth

For the nutrient broth used to prepare the batch phase inoculum and continuous phase medium in the drip-flow bioreactor, 3g/L nutrient broth was prepared in order to follow the nutrient concentrations outlined within ASTM E2647-13. All prepared broth was stored at room temperature until used. 3g/L NB was used both to create overnight cultures for batch phase and 3g/L broth was diluted to make 270mg/L continuous phase broth. 900mL of 3g/L NB was diluted with DI H_2O to 10L total for 48hr continuous phase bioreactor runs. 1800mL of 3g/L NB was diluted with DI H_2O to 20L total for 96hr continuous phase bioreactor runs. ASTM E2647-13 suggests using purchased sterile, DI H_2O to make the influent broth dilutions. However, water which was deionized in-house was sterilized via autoclave instead due to budgetary constraints. All prepared broth was used within 2 weeks of being prepared. All broth was of course sterilized via autoclave prior to use.

The nutrient agar was always prepared as indicated in Figure 10, for both use in the initial propagation and storage of the bacteria as well as for use throughout all the growth tests. The plated NA was prepared as needed. 1L of prepared nutrient agar made about 50 sterile, poured agar plates. The plates were always poured directly after the NA was sterilized via autoclave and still in liquid form. The poured plates were allowed to dry in the biosafety cabinet overnight and afterward were covered in plastic and placed in a 4ºC fridge for storage until use. All plates were used within 1 month of being prepared.

Sterile nutrient agar plates and 8g/L nutrient broth were prepared in anticipation of receiving the lyophilized ATCC 8739 vial. The lyophilized bacteria pellet was propagated as specified by the ATCC to start the strain in our lab. The glass vial with the pellet was aseptically opened within a biosafety cabinet (BSC). 7mL of sterile nutrient broth was transferred into a sterile test tube. Approximately 0.5-1mL of the broth was aseptically withdrawn and transferred into the vial to hydrate the pellet. After the entire pellet was hydrated, the aliquot was aseptically transferred back into the broth tube. The tube was thoroughly mixed. 100 µL of the broth was used to make a T-streak on a nutrient agar plate. The tube and plate were incubated at 37ºC for 24hr. The tube was shaken at 200RPM with the cap loosened to allow airflow. The T-streak was inspected after 24hr to make sure there was no contamination. One isolated colony from the T-streak was aseptically transferred into 75mL of sterile 8g/L broth. Another isolated colony from the T-streak was aseptically transferred into 30mL of sterile 8g/L broth. The inoculated broths were incubated at 37°C and shaken at 200RPM for 24hr.

While the inoculated broth was being incubated, the storage vials and glycerol solution were prepared. 150, 2mL screw-top polypropylene vials (O-ring in cap) were placed into three polypropylene freezer storage containers. 100mL of a 30% volume glycerol in DI H_2O solution was prepared, and 500 µL of the solution was pipetted into each of the 2mL, screw-top vials. The cap on each vial was loosely screwed, and the lid on each freezer container was lightly closed. Autoclave tape was placed on the outside of the containers, and the vials/containers were autoclaved on liquid cycle for 10 minutes. After autoclaving, the cap of each vial was closed tightly while within the BSC. The lid to each freezer storage container was closed and it was allowed to sit in the BSC until the inoculated broth finished incubating.

After the two inoculated broths were incubated for 24hr, they were added to the 2mL screw top vials with sterile glycerol solution and the vials were frozen for long-term storage. Directly afterward, a serial dilution and plating of the broth was performed to calculate the viable cell concentration of the stored broth. To do so, 500 µL of inoculated broth was aseptically added into each 2mL screw top vial, which already contained 500 µL 30%vol glycerol. This brought the overall concentration of glycerol to a total of 15% volume glycerol. After the broth was added to a vial, the broth/glycerol mixture was thoroughly mixed by pipetting up and down several times with the micropipettor and pipette tip. Afterward, the sharp was disposed of and the vial was immediately closed tightly prior to placing it back into the storage box. After all 150 vials were prepared with 500 µL inoculated broth and 500 µL of 30% glycerol, the storage boxes with the vials were placed in the -4 °C freezer for 24hr. Afterward, they were placed into the -80 °C freezer for long-term storage. Taking two days to reach -80 °C allowed the freezing process to occur more gradually, which is generally considered to be less damaging to cells. The bacteria were then recovered as needed to perform the growth tests. Storing the bacteria like this ensured that all trials ran in the bioreactor used bacteria which had been manipulated in the same exact way from the initial ATCC pellet.

Figures 2-13a – 2-13e demonstrate the propagation process for storing the single strain ATCC 8739 bacteria which was described above.

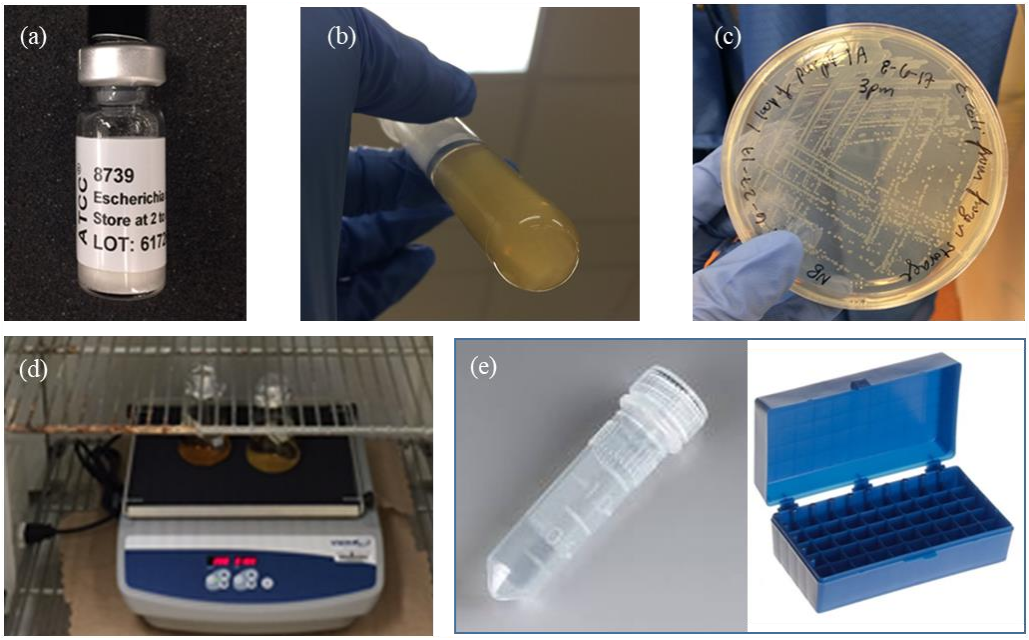

Figure 2-13a-e. Propagation Process for Storing Pure Strain ATCC 8739. (a) Glass vial of lyophilized ATCC 8739 pellet. (b) hydrated ATCC 8739 pellet. (c) T-streak of overnight broth of hydrated pellet. (d) overnight broth grown from isolated colonies on T-streak. (e) 2mL screw-top Eppendorf tubes with O-ring used to store ATCC 8739 strain inside of freezer storage boxes within -80ºC freezer

As mentioned, directly after the broth was transferred into the vials for storage, a serial dilution and plating was performed on each inoculated broth to determine the viable cell concentration of the stored broths, quantified in colony forming units (CFU) per milliliter. This

was done by performing a serial dilution of the broth, spreading known volumes of the dilutions on agar plates and incubating the plates for 18-24 hours. After incubation, the number of colonies formed on the plates were counted in order to calculate CFU/mL.

The 75mL, 24hr broth had an average bacteria concentration of 38.15 x 10^8 CFU/mL (blue and purple storage boxes) and the 30mL, 24hr broth had an average bacteria concentration of 40.7x10^8 CFU/mL (orange storage box). This was great, as it meant each broth had very similar viable cell concentrations. Keep in mind that within each frozen 2mL screw top vial stored, the concentration of frozen viable cells within each vial was approximately half of these concentrations since it was diluted with the same volume of glycerol solution.

2.4. Bacteria Recovery and Drip-Flow Bioreactor Growth Protocol

2.4.1. Stored Cell Recovery and Inoculum Preparation

Bacteria were recovered from the -80 °C freezer and prepared for inoculating the bioreactor as needed. Preparation of the *E. coli* inoculum took a minimum of 38 hours and a maximum of 48 hours before starting batch phase of the biofilm growth within the bioreactor. All manipulation of bacteria was performed within the BSC within the VTSuN lab in order to minimize contamination of the bacteria strain within the storage vials, inoculum, and bioreactor. Working within a BSC also minimized any potential health and safety concerns, which are already minimal with a BSL 1 organism.

To recover bacteria, a frozen vial of bacteria was removed from the -80°C freezer within a styrofoam centrifuge tube tray to minimize thawing. Very quickly, a stab was taken from the vial with a sterile inoculation loop and a T-streak was made on the agar plate. The vial was immediately replaced in the -80 °C freezer. The T-streaked plate, lid facing downward, was then placed in the 37 °C incubation cabinet and allowed to incubate for 18-24 hr.

After 18-24hr, the plate was inspected for any potential contamination. If it was determined there was only the single strain present, a single isolated colony was removed from the plate with a sterile inoculation loop and aseptically transferred into 100mL of sterile, 3g/mL nutrient broth. The broth was then placed on a shaker in the incubation cabinet and incubated at 37 °C, shaken at 200 RPM for 20-24 hr. The foil used to cover the 250mL Erlenmeyer flask with 100mL of the broth was loosely placed on the flask to ensure airflow into the flask during incubation.

The 20-24 hr broth was then used to inoculate the four bioreactor channels and start the batch phase of biofilm growth. Please refer to section 2.4.3. Batch Phase Growth for more information on how to inoculate the four bioreactor channels. Directly after inoculation of the bioreactor, the viable cell concentration of the broth was quantified in CFU/mL through a serial dilution and plating.

According to ASTM E6247-13, the inoculum cell concentration should rest on the order of 1 × 10^8 CFU/mL. All of the 20-24hr broths which were prepared to inoculate the bioreactor had an overall average viable cell concentration of 11.4 × 10^8 ± 3.3 x 10^8 CFU/mL. This was approximately one order of magnitude higher than the recommended viable cell concentration to

inoculate the reactor for *P. aeruginosa* biofilm growth. Table 2-5. tabulates the collected data associated with the viable cell concentration of each inoculum broth used. In the test descriptions used in Table 2-5., the hyphenated descriptions include the type of stainless steel, the surface finish in microns, the continuous phase growth duration in hours, and the temperature of both batch phase and continuous phase growth. Again, within this document, 304SS indicates the 304 type baseline austenitic stainless steel, AgSS indicates the silver-alloyed austenitic stainless steel, and CuSS indicates the copper-alloyed ferritic stainless steel. Some of the broths were plated more than once for a given dilution in order to add greater statistical relevance. Typically, the 10^7 diluted broth was plated in triplicate. The "x's" within Table 5 indicate a lack of data point for the multiple platings of that broth for a given dilution.

Table 2-5. Viable Cell Concentration of Inoculum Broths

Test Description		Broth	Concentration (10^8 CFU/mL)						Mean Concentration	Standard
SS-Finish-Time-Temp	Date	Incubation (hr)	10^6 Dilution		10^7 Dilution				(CFU/mL x 10^8)	Deviation
304SS-0.25-48-RT	8/10/2017	25	14.3	x	13	x	x	x	13.7	0.9
CuSS-0.25-48-RT	8/18/2017	24	12.2	x	11	8	11	x	10.6	1.8
AgSS-0.25-48-RT	8/25/2017	25	12	x	13	13	17	12	13.4	2.1
AgSS-0.02-48-RT	9/1/2017	24	10.1	x	10	13	17	x	12.5	3.3
CuSS-0.02-48-RT	9/7/2017	23	9.6	x	13	12	10	x	11.2	1.6
304SS-0.02/7-48-RT	9/22/2017	20	11.2	x	9	6	3	x	7.3	3.6
304SS-0.02/41-48-RT	9/28/2017	25	10.6	x	13	10	9	x	10.7	1.7
304SS-0.02/41-48-RT	10/10/2017	22	11.3	x	5	8	19	x	10.8	6.0
304SS-0.02/41-96-ET	10/23/2017	22	9.3	x	11	12	7	x	9.8	2.2
AgSS/CuSS-0.02-96-ET	10/30/2017	20	13	14	17	16	11	x	14.2	2.4
Average of All Inoculum Broths		**23**	**11.6**		**11.3**				**11.4**	**3.3**

2.4.2. Sterilization of Reactor System and Equipment

During the 38-48 hours required to prepare the bacteria for bioreactor inoculation, all other components of the bioreactor were sterilized or otherwise prepared. All components of the bioreactor system which come in direct contact with the growth medium and bacteria required sterilization before and after each growth test.

Prior to sterilization, all the components of the reactor system were cleaned with mild detergent and rinsed with DI water. The scored glass slide coupon holders were cleaned first by soaking in a 0.1M HCl solution, followed by sonication within a DI water and dish soap bath inside 50mL centrifuge tubes. The slides were sonicated in this bath for a minimum of 1 hour. They were then rinsed thoroughly with DI water and placed inside the cleaned drip-flow bioreactor channels until the whole bioreactor chamber was sterilized via autoclave.

The four material coupons used within each growth trial were prepared as outlined within section 2.1 Material Selection and Coupon Preparation. After cleaning, the coupons were soaked in 99% isopropanol inside of sterile, 2mL, snap-cap microcentrifuge tubes until the coupons were inserted into the sterilized bioreactor chambers. The cleaned coupons were soaked in isopropanol for a minimum of 6 hours and a maximum of 24 hours.

The cleaned, scored glass slide holders were sterilized along with the drip flow bioreactor chamber. The slides were inserted into the clean drip-flow bioreactor channels, if they were not

already inserted. The screws on the each of the four channels were loosened to minimize stress during autoclaving and to allow the inside of the channels to be steam sterilized effectively. The influent and effluent tubing were not connected to the reactor during sterilization to allow the reactor to be opened within the BSC to insert the sterile material coupons after sterilization. Also, it placed less stress on the reactor during sterilization to not have the tubing connected during sterilization. As so, the closed mininert valves and the effluent ports on the drip-flow bioreactor chamber were tightly covered with heavy-duty aluminum foil prior to sterilization. Autoclave indicator tape was placed over the top of the four bioreactor channels. Once prepared in this way, the bioreactor chamber was sterilized as close to the reactor inoculation time as possible. It was sterilized via autoclave on liquid cycle for 20 minutes. The bioreactor was immediately removed from the autoclave once the cycle was completed, and it was allowed to cool slightly within the warm secondary container. The channels were then screwed tightly shut. Allowing the reactor to cool like this minimized stress on the reactor which in turn minimized any warping of the plastic.

The material coupons were then inserted into each channel of the bioreactor inside a BSC while the reactor was still slightly warm. The coupons were either dried slightly from the alcohol they were soaking in, or rinsed with sterile PBS or sterile DI H_2O prior to insertion into the bioreactor chambers. Each coupon was handled with sterilized tweezers, and each coupon was inserted individually, opening each channel for the minimal amount of time to insert the coupon between the scored glass slide coupon holders in each channel. After coupon insertion, the bioreactor was carefully removed from the BSC and either set flat on a sterilized lab bench surface near the reactor set up or on top of the lab jack within the pre-warmed incubation box. It sat flat and undisturbed until inoculation. Figure 2-14. shows the sterilized bioreactor chamber with the material coupons inserted, ready to begin batch phase growth.

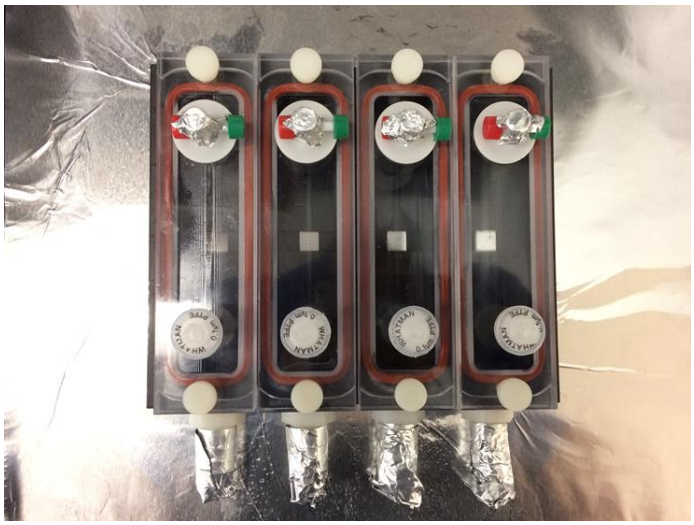

Figure 2-14. Sterilized Drip Flow Reactor Chamber with Inserted Coupons

Each of the 20L carboys were sterilized with the lids lightly screwed on, the bulkhead fittings in place, the tubing with the bacteria air vent in place, the tubing on the bottom half of the influent/effluent bulkhead in place, and heavy-duty aluminum foil covering the outside of the

influent/effluent bulkhead. Indicator tape was placed over the lightly screwed lids. After autoclaving, the lids were tightly screwed on the carboys. All of the influent tubing was connected to each other via connectors/reducers/glass flow break during autoclave sterilization except for the ends which connect to the influent tank, and the ends which connect to the sterile syringe needles. These disconnected tubing openings were wrapped with heavy-duty aluminum foil prior to sterilization. All of the effluent tubing was connected to each other via connectors during sterilization, except for the ends which connect to the effluent ports on the bioreactor and the end which connects to the effluent tank. These ends were covered with heavy duty aluminum foil prior to sterilization. All of the tubing and the carboys were sterilized via autoclave either on 20min liquid cycle or 20 min gravity cycle. These components were also sterilized as close as possible to the time of inoculation of the bioreactor. The influent carboy was frequently sterilized while sterilizing the water used to dilute the 3 g/L broth to 270 mg/L for the influent growth media.

Figure 2-15. shows an example image of all the foil-wrapped tubing prior to autoclave sterilization.

Figure 2-15. Foil-wrapped Reactor Tubing for Autoclave Sterilization

The 3g/L nutrient broth and the necessary DI H_2O were sterilized via autoclave in separate small containers prior to being aseptically poured into the sterilized influent carboy. The nutrient broth was sterilized in 300mL amounts in 500mL glass bottles. The broth volumes were measured using a 100mL graduated cylinder (± 0.6 mL). The DI H_2O was sterilized in 500-600mL amounts in 1L plastic/glass bottles. The DI H_2O volumes were measured out in a 2L volumetric flask (± 0.5 mL) and a 100mL graduated cylinder (± 0.6 mL) and distributed into the 500-600mL amounts in various containers. Placing the DI water and broth in many smaller containers for sterilization resulted in less evaporation, since smaller volumes require smaller autoclave times. This resulted in more accurate volume measurements while preparing the continuous phase media. It typically took 1 – 3, 40min liquid cycles to autoclave all of the

necessary DI water for the continuous phase media. Immediately after sterilization, the DI water and broth were aseptically poured into the influent carboy to prepare the 10-20 L of 270 mg/L sterile influent broth. The nutrient broth was prepared and sterilized at the more concentrated 3g/L, since 100mL of the 3g/L nutrient broth was required to grow the 20-40 hr broth used to inoculate the bioreactor.

Again, 900mL of sterile 3g/L nutrient broth was diluted with sterile DI water to a total of 10L for 48-hour continuous phase growth tests. 1800mL of 3g/L broth was diluted with DI water to a total of 20L for 96-hour continuous flow tests. As so, the overall concentration of the continuous phase media was 270mg/L of nutrient broth. This was the recommended broth concentration for tryptic soy broth continuous flow media for *P. aeruginosa* outlined within ASTM 32647-13. This suggested influent concentration was adapted for use with the *E. coli* and nutrient broth within this study. This low concentration is still quite high when compared to many oligotrophic water environments or scavenging situations.

After the influent carboy, tubing, and growth media were sterilized and prepared, the influent line was aseptically connected to the barbed bulkhead fitting on the influent carboy. This was done by quickly removing the foil on the end of the bulkhead fitting and tubing and aseptically inserting the tube on the fitting. The influent tubing was then supported by the ring stand clamp to keep the glass flow break upward and in place. The separate four influent lines were then inserted into the pump head, to be ready for connecting to the drip-flow reactor after starting batch phase. Please refer to section 2.4.3 Batch Phase Growth for more information on how both the influent tubing and the effluent tubing were aseptically connected to the bioreactor.

At this point, the entire system was ready to begin batch phase growth and subsequently continuous phase growth. After completion of the growth test, all equipment needed to be cleaned and sterilized as indicated in section 2.4.6. Sterilization and Disposal of Waste and Cleaning the Reactor System. Figure 2-16 illustrates what the benchtop and reactor system looked like after sterilization right before batch phase was started.

Figure 2-16. Sterilized Reactor System Ready for Batch Phase Growth

It should also be noted that all necessary micropipette tips, glassware, and microcentrifuge tubes were routinely sterilized via autoclave as needed.

2.4.3. Batch Phase Growth

After the reactor system was sterilized and the 20-24 hr broth inoculum was prepared, batch phase was started.

The area underneath the bioreactor was wiped down with 70% ethanol to help insure sterility in the surrounding bench area. While the reactor remained lying flat, the foil was removed from each effluent port and each effluent tube, and the effluent tubing was aseptically connected to the effluent ports of the bioreactor. This was done carefully so as not to disturb the coupons. The foil on each port and tube was removed one at a time to minimize the amount of time exposed to the open air.

Each effluent line was then clamped shut with tubing clamps. 15 mL of sterile 3g/L broth was aseptically transferred into each reactor channel with a sterile 21 gauge, 1 in syringe needle and a 15mL sterile syringe through the mininert valve. Then, 1mL of inoculum was inserted into each channel using a sterile 21 gauge, 1in syringe needle and 3mL sterile syringe. Next, each influent tubing line was aseptically connected to each needle, so that the needle rested in the opened mininert valve. From this point, batch phase officially started and the reactor was set flat in this position for 6 hours at either room temperature or within the incubation box at the elevated temperature of 37°C.

Figure 2-17a. shows the bioreactor setup operating in batch phase growth. The clamps in this image were make-shift. Appropriate 1/2 in tubing clamps were purchased after running the

first growth test and were used in all remaining growth tests. Figure 2-17b. shows the appropriate tubing clamps used in the majority of the growth tests.

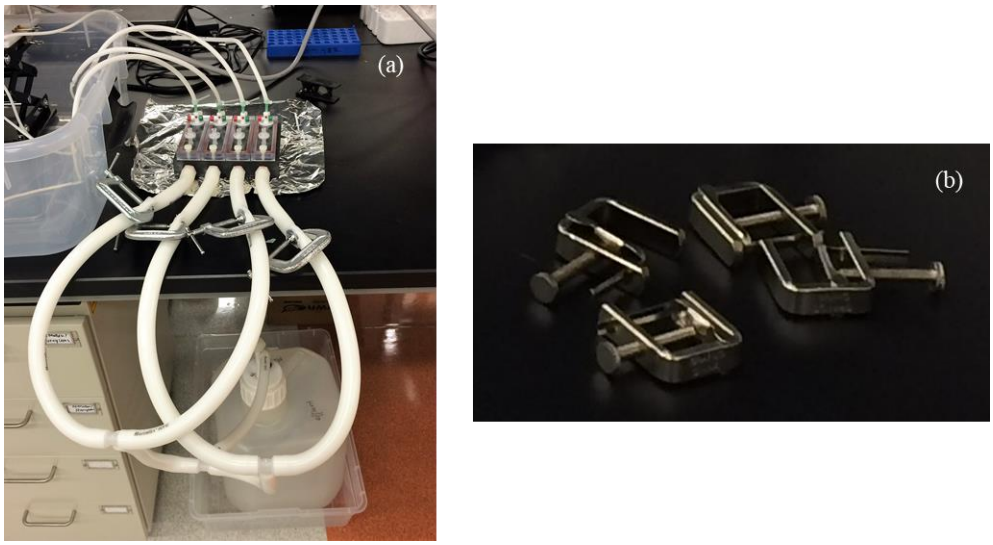

Figure 2-17a-b. Clamps Used on Inoculated Drip Flow Reactor Operating in Batch Phase Growth. (a) make-shift clamps until proper ones were bought. (b) proper ½ in tubing clamps used on all remaining tests

If the bioreactor was incubated at 37°C for the duration of all growth rather than at ambient room temperature, the drip-flow reactor was connected to the tubing within the incubation box so that the influent and effluent tubing were inserted through cuts holes in the box. Insulating foam was placed around the holes of the tubing to keep the box insulated. Additionally, the drip flow reactor was allowed to warm up within the box and the 15mL of growth broth within each channel prior to adding the inoculum and starting batch phase. Again, 85°C set on the hot plate within the incubation box allowed for long-term stability of approximately 37 ± 3°C within the incubation box. The temperature of the incubation box was monitored regularly with a digital hygrometer.

If the coupons were in any way slightly displaced from position during batch phase they were aseptically readjusted into positon by quickly opening and closing the channel chamber and repositioned with sterile tweezers. This was done directly before starting continuous phase after inverting the bioreactor.

Directly after batch phase was started, a serial dilution and plating was performed on the 20-24 hr inoculum broth for viable cell quantification of the broth. The plates were incubated for 18-24 hours at 37 °C and then promptly counted to calculate the CFU/mL concentration of the inoculum broth. Again, the average viable cell concentration of all the inoculums prepared was $11.4 \times 10^8 \pm 3.3 \times 10^8$ CFU/mL. After plating, the inoculum broth sterilized and disposed of.

2.4.4. Continuous Phase Growth

After allowing the reactor to operate in batch phase for 6 hours, continuous phase was started. It took a few minutes to get fluid flowing through the influent tubing, so first the peristaltic pump was started, set to flow rate at 13 RPM (approximately 50mL/hr/line or

200mL/hr total). Next the clamps on the effluent tubes were removed. Then bioreactor was carefully inverted and placed on the 10 angle stand on top of the lab jack. The stand was clamped to the lab jack with binder clips and the jack was adjusted into position to have the effluent tubing clear the secondary container and rest downward toward the effluent carboy. If the coupons were in any way slightly displaced from position during batch phase, they were aseptically readjusted into positon by quickly opening and closing the channel chamber and repositioned with sterile tweezers. By this point, fluid should have started dripping through the reactor channels and officially starting the continuous phase of growth. The bioreactor was allowed to operate in continuous phase for either 48 hours (2 days) or 96 hours (4 days). Continuous phase was the exact same for the incubated tests; the procedure was just carried out with the drip-flow reactor placed in the sytrofoam incubation box.

Figure 2-18. shows the bioreactor setup operating in continuous phase growth mode.

Figure 2-18. Drip Flow Bioreactor System Operating in Continuous Phase Growth

2.4.5. Harvesting Material Coupons

After continuous phase was over, the coupons were immediately harvested and transported to the Nanoscale Characterization and Fabrication Laboratory (NCFL) at the Virginia Tech Corporate Research Center for E-SEM analysis.

To end continuous phase, first the pump was turned off to stop flow through the reactor. The influent and effluent lines were then disconnected and the mininert ports and effluent ports were covered with aluminum foil. The bioreactor was then immediately taken into the BSC along with a sterile plastic multiwell plate, sterile tweezers, and a permanent marker.

Each channel of the reactor was opened to remove each coupon with sterile tweezers. One coupon and channel were handled at a time to minimize contamination of the coupons. After removal, the coupon was then either not washed, or rinsed with 1-15mL of either sterile PBS or

sterile DI H_2O, and immediately placed into a labeled well in the sterile multiwell plate. The lid of the well plate was closed in between handling coupons to minimize contamination of the coupons.

After each coupon was removed, the sterile well plate was wrapped back into its original packaging and placed into a small cardboard box for safe transportation to the NCFL. The drip-flow reactor channels were closed and placed back on the bench for later sterilization. The reactor system was labeled as contaminated until it could be sterilized and cleaned within the next 24 hours.

The coupon samples were then transported to the NCFL for E-SEM/AFM characterization, which was performed as soon as possible after coupon harvesting. The timing of the growth experiments was designed around availability of instrumentation time slots to minimize the amount of time between harvesting and characterization.

2.4.6. Sterilization and Disposal of Waste and Cleaning the Reactor System

After the coupons were characterized via E-SEM/AFM, the reactor system needed to be sterilized and cleaned. This was done within 24 hours after harvesting the material coupons for analysis.

The drip-flow reactor was again sterilized with the glass slides inside the chamber and the channel screws loosened via autoclave on a 20 min liquid cycle. The tubing, detached from the reactor, was also sterilized via autoclave either on 20 min liquid cycle or 20 min gravity cycle. There was no need to cover the ends of the tubing or the bioreactor ports with aluminum foil during cleanup sterilization.

At the end of continuous phase all of the influent media was transferred into the effluent tank and biologically contaminated. If the effluent tank contained 20L of waste, half of the waste was carefully redistributed into either the influent tank or other smaller containers and sterilized for 135 min liquid cycle (time required for sterilizing 10L of fluid). If the effluent tank only contained 10L of waste, the waste did not need to be redistributed for sterilization. The effluent tank was thus always sterilized while sterilizing the liquid waste. The influent tank may or may not have been sterilized while sterilizing waste media; if not, it was sterilized for 20min liquid cycle in the autoclave along with the tubing and drip-flow reactor. After all liquid waste media was sterilized, it was dumped down the lab sink drain, per BSL 1 liquid waste stream protocol.

All of the sterilized carboys, tubing and bioreactor were then cleaned with mild detergent and rinsed thoroughly with DI water. All components were then allowed to dry until needed for their next use. The tubing had clean DI water ran through the lines to maintain cleanliness. The glass slides were then either immediately thoroughly cleaned as mentioned in section 2.4.2, or were thoroughly cleaned closer to the time of the next growth trial.

Thus, it should be noted for each growth trial, all of the reactor components required sterilization directly prior to running a growth trial, as well as shortly after a growth trial prior to cleaning the components after use.

Chapter 3 Results

3.1.Baseline Analysis of Stainless Steels

A baseline surface analysis of each stainless steel material was conducted for later comparison to the material coupons after *E. coli* biofilms were grown on them. Scanning Electron Microscopy (SEM) and Energy Dispersive Spectroscopy (EDS) were used to gather surface microstructure and chemistry information. The SEM/EDS was performed under high vacuum within an Environmental Scanning Electron Microscope (E-SEM); the E-SEM was thus operated as a standard SEM. Contact mode Atomic Force Microscopy (AFM) was used to conduct quality control surface roughness measurements of the mirror finishes of the coupons.

3.1.1. SEM/EDS – Microstructure and Chemical Analysis

E-SEMs can be operated both in high-vacuum and low-vacuum modes. Low-vacuum E-SEM can be operated with the presence of a gaseous media such as water vapor[54]. For baseline analysis, mirror finish coupons of each material type were analyzed in the FEI Quanta E-SEM under high vacuum with a beam energy of 20 keV. The backscattered electron detector (BSD) was used to observe microstructure features by atomic mass differences (Z-contrast), and energy dispersive x-ray spectroscopy (EDS) was conducted to get estimates on the chemical compositions of observed microstructure features. The secondary electron detector (SED) was used minimally to analyze the bare metals, as the surface topography of mirror finish coupons is purposefully minimal apart from imperfections. EDS can only be performed within high-vacuum within the E-SEM, and based on the location of the EDS detector in this specific system, signal for EDS was optimized with a working distance of 12mm.

SEM micrographs present scaled information collected by rastoring the electron beam over a sample region. The resulting individual pixels in each image thus contain information about how the electron beam interacted with the sample material, portrayed through a grayscale with hundreds of different shades. For example, images with an 8-bit pixel format have 255 gray scale tones between black and white. The grayscale information portrayed in the micrograph is dependent on the type of detector used during the rastoring. In BSD images, theoretically pure black would indicate the lightest atomic element present (or vacuum), and pure white would indicate the heaviest element present. In SED images, theoretically pure black would indicate the lowest point of topography in the image and pure white would indicate the highest point of topography. Pure black and pure white are rarely ever present in micrographs. Additionally, there is often an overlap in electron signals between BSD and SED images, so sometimes Z-contrast images may have hints of topography information and topography-contrast images may have hints of Z-contrast information[54].

Figures 3-1 is a Z-contrast SEM image of submicron polished 304SS which shows a typical bulk microstructure for an austenitic stainless steel. Figure 3-1a shows a nice example of electron channeling through the steel, highlighting the various grains and instances of twinning inside the steel. Figure 3-2 shows an EDS area region taken on a 500× magnification of 304SS. Figure 3-3 shows the EDS spectrum associated with the area region on Figure 3-2. Table 3-1 shows the EDS chemical analysis of this region, which was representative of the average

composition of the bulk of the steel. The EDS data qualitatively confirms the manufacturer's compositional data for the material. The large carbon and silicon amounts supposedly present in the bulk may have been due to trace amounts of polishing media (SiC paper, diamond paste) on the coupon's surface. Carbon could have also been deposited through the cleaning process of the polished sample, from acetone and alcohols.

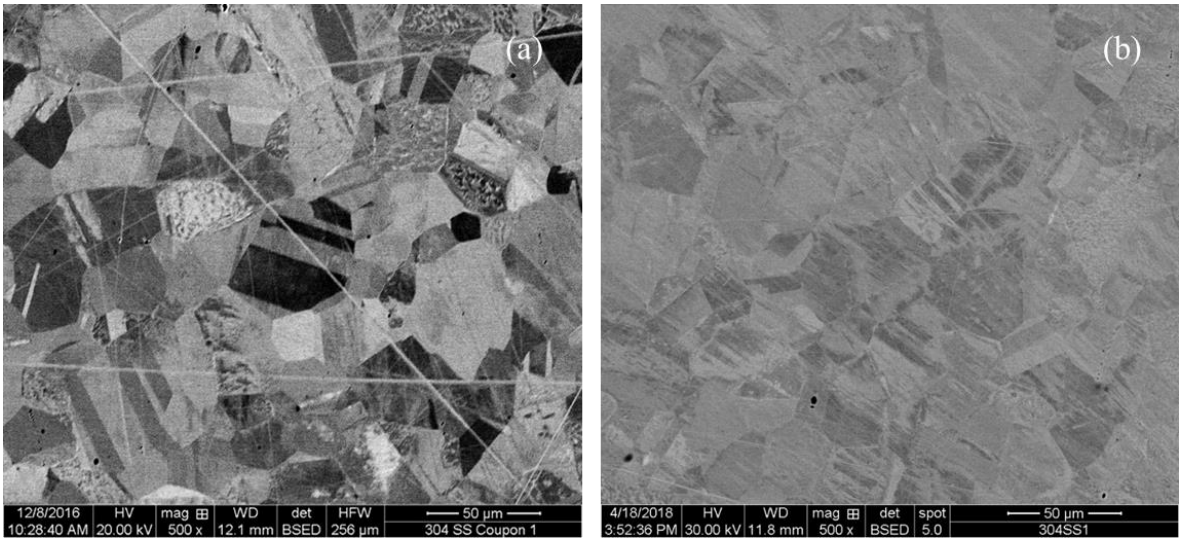

Figure 3-1 a-b. 500× BSD SEM Images of 304SS Samples (a). electron channeling through sample (0.25 µm finish) (b). sample without significant electron channeling (0.02 µm finish). Finish is unrelated to electron channeling.

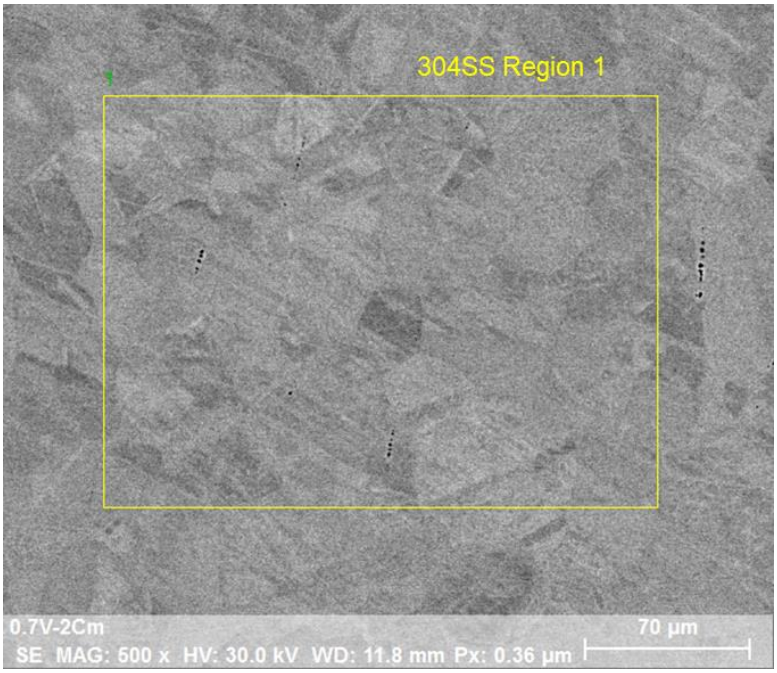

Figure 3-2. 500× EDS Bulk Area Region on 304SS, BSD

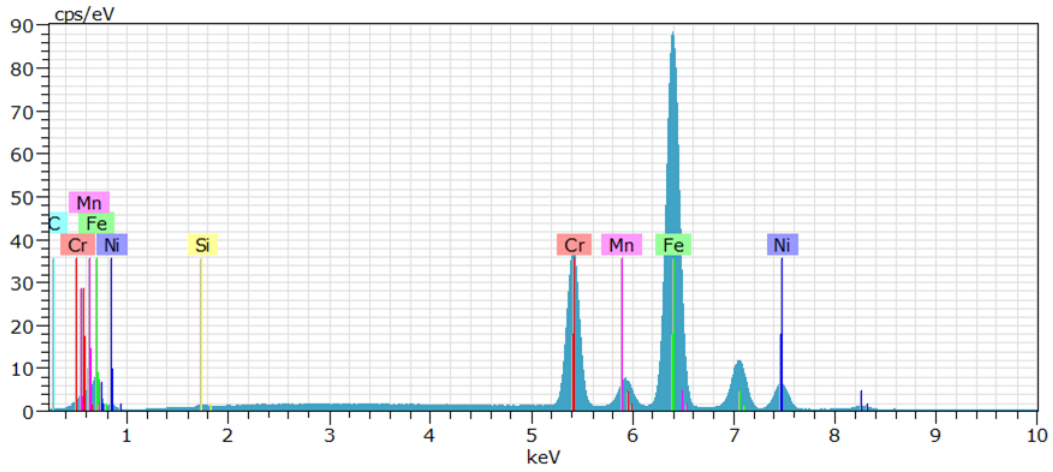

Figure 3-3. EDS Spectrum of 304SS, Region 1 on Figure 3-2.

Table 3-1. EDS Compositional Analysis Region 1 Figure 3-2.

Region	Composition (wt. %)					
	Fe	Cr	Ni	Mn	C	Si
Region 1	70.15	17.68	7.16	1.35	3.47	0.23

Figure 3-4 shows EDS spot regions taken on a 5000× magnification Z-contrast image of the 304SS steel. In this image, EDS was performed on various areas of an inclusion found within the steel, to compare the composition of the inclusion to that of the average composition of the bulk. The darker grayscale of the inclusion feature indicated it had slightly lower atomic mass elements than the bulk of the steel. Inclusions are chemical compounds, frequently with non-metal components, which form within steel as a product of various chemical reactions and contamination that occur during the melting pouring process of the steel. Figures 3-5 through 3-8 are the EDS spectrums associated with the four spot regions on Figure 3-4. Table 3-2 summarizes the EDS compositional analysis of the regions on the inclusion. The regions 1-3 had slightly lower amounts of iron, chromium, and nickel compared to the bulk of the steel, slightly higher amounts of manganese and silicon, and approximately the same amounts of carbon. The inclusions had approximately 1 – 2 wt.% magnesium, 5 – 10 wt.% aluminum, 0.4 – 1 wt. % calcium, and 0.25 – 0.5 wt.% titanium; these were not alloying elements found within the average composition of the bulk of the steel. Region 4, just outside of one part of the inclusion, had a similar composition to regions 1-3, except it had slightly smaller amounts of the magnesium, aluminum, calcium, and titanium.

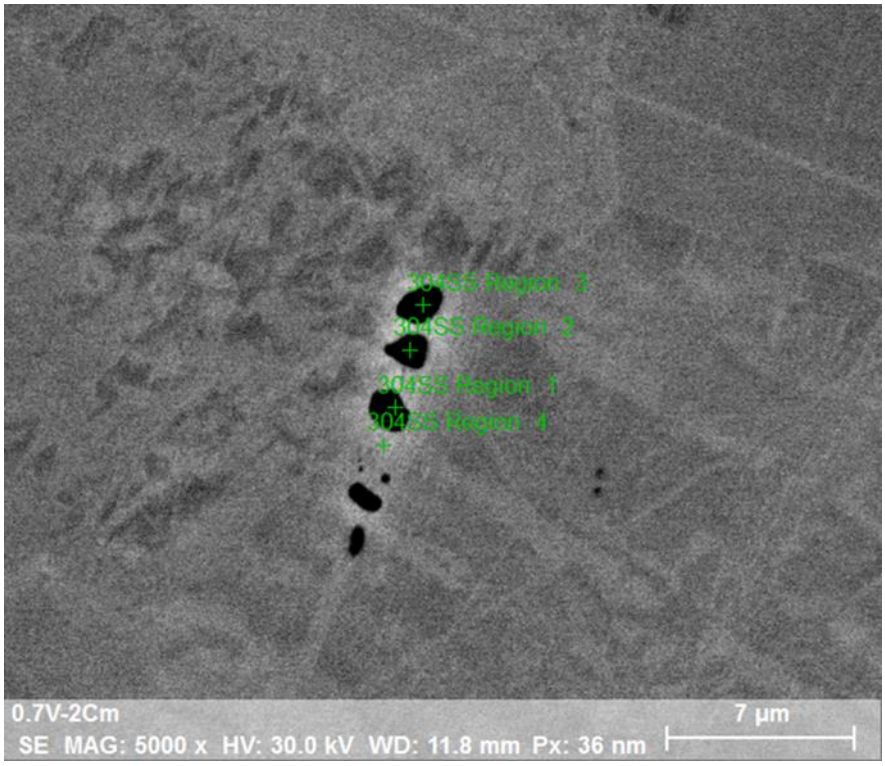

Figure 3-4. 5000x EDS Spot Regions on 304SS, BSD

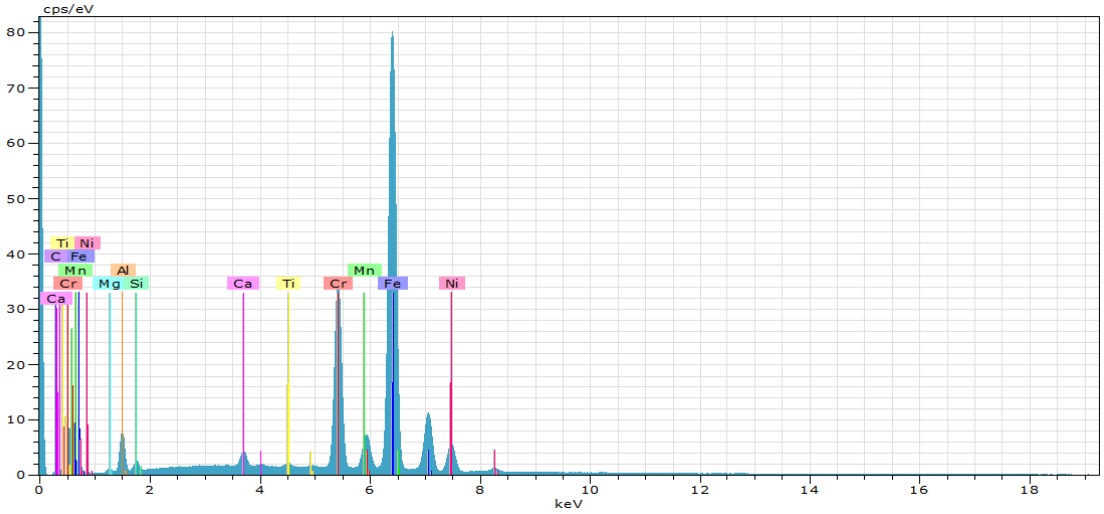

Figure 3-5. EDS Spectrum of 304SS, Region 1 on Figure 3-4.

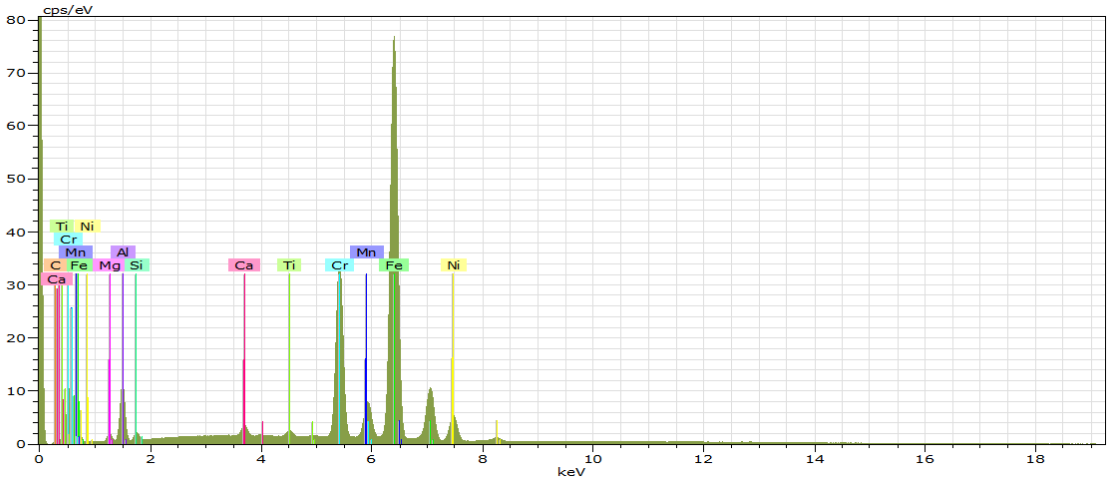

Figure 3-6. EDS Spectrum of 304SS, Region 2 on Figure 3-4.

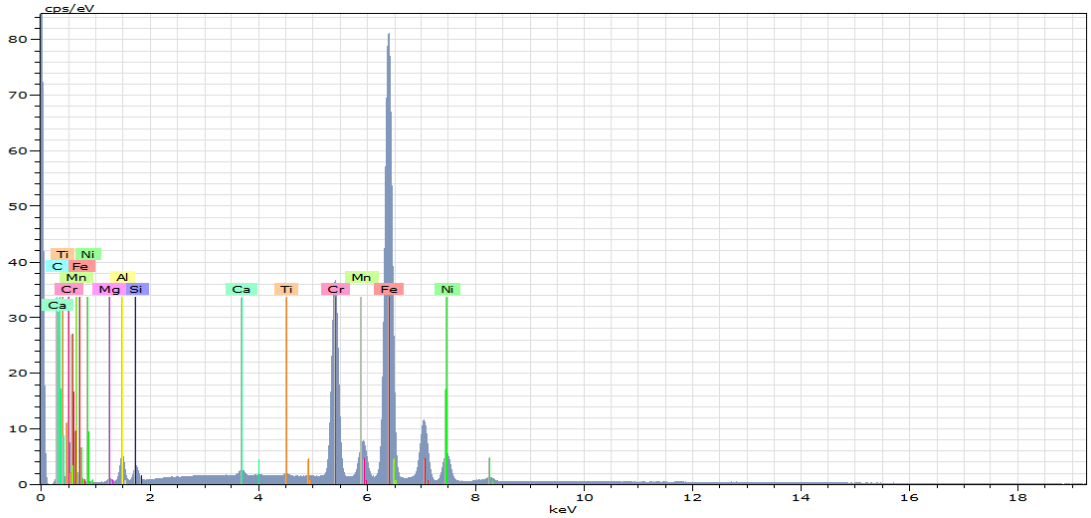

Figure 3-7. EDS Spectrum of 304SS, Region 3 on Figure 3-4.

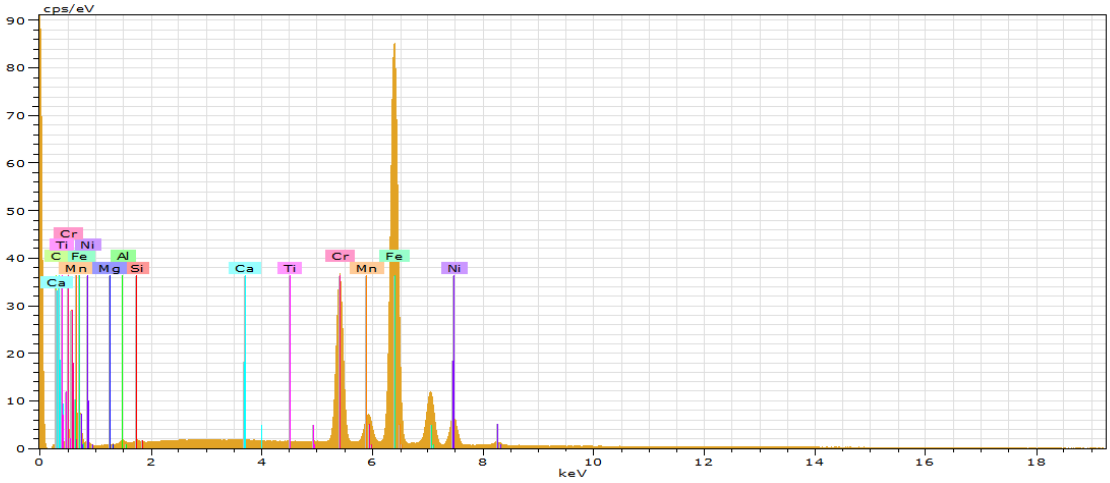

Figure 3-8. EDS Spectrum of 304SS, Region 4 on Figure 3-4.

Table 3-2. EDS Compositional Analysis Regions on Figure 3-4.

Region	Composition (wt. %)									
	Fe	Cr	Ni	Mn	C	Si	Mg	Al	Ca	Ti
Region 1	62.88	16.70	6.05	1.54	2.78	1.20	0.79	6.61	1.09	0.41
Region 2	69.40	16.27	5.50	1.98	2.56	1.05	2.17	10.22	0.76	0.57
Region 3	69.83	17.19	5.66	1.69	3.74	2.28	1.08	5.27	0.39	0.25
Region 4	69.90	16.34	80.60	1.34	2.78	0.38	0.26	0.83	0.09	0.02

Figures 3-9 is a Z-contrast SEM image of 0.02 µm polished CuSS which shows the typical bulk microstructure for this type of ferritic, copper-alloyed stainless steel. Figures 3-10 shows an EDS area region taken on a 500× magnification of CuSS. Figure 3-11 shows the EDS spectrum associated with the area region on Figure 3-10. Table 3-3 summarizes the EDS chemical analysis for this region, which was representative of the average composition of the bulk of the steel. The EDS data qualitatively confirms the manufacturer's compositional data provided for the material. The small amounts of carbon and silicon present in the bulk may have been due to trace amounts of polishing media (SiC paper, diamond paste) on the coupon's surface. Carbon could have also been deposited through the cleaning process of the polished sample, from acetone and alcohols.

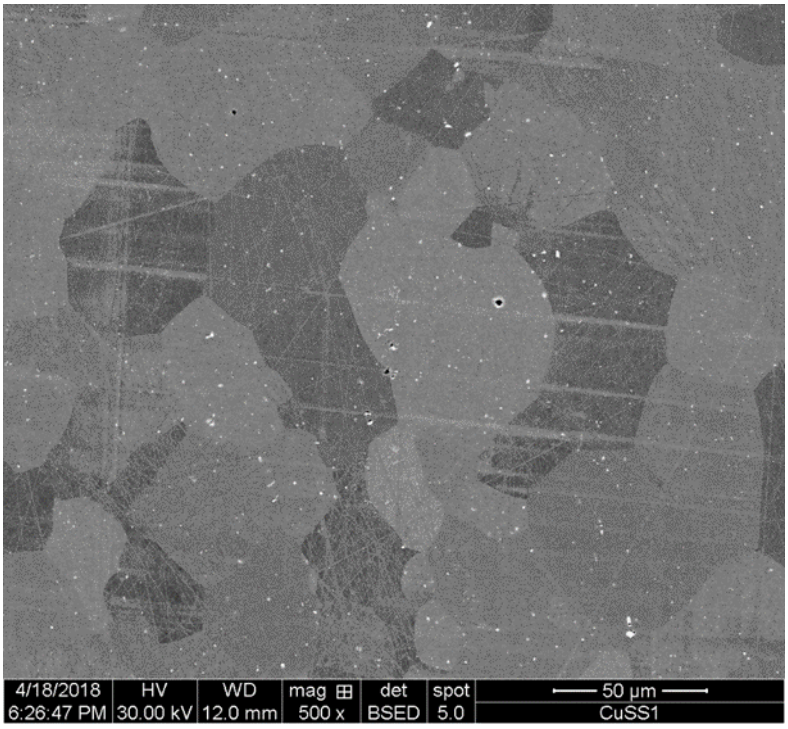

Figure 3-9. 2000× BSD SEM Image of CuSS

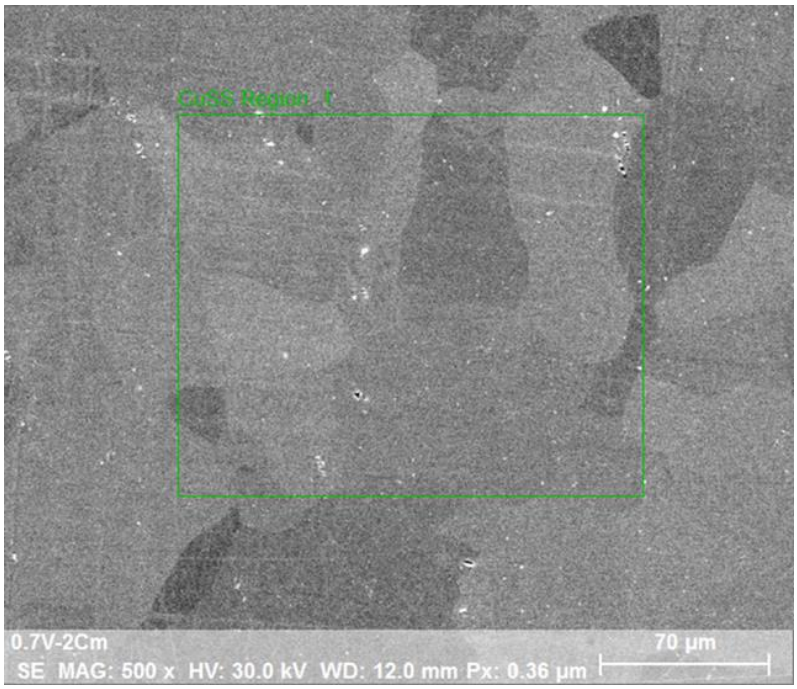

Figure 3-10. 500× EDS Region 1 on CuSS

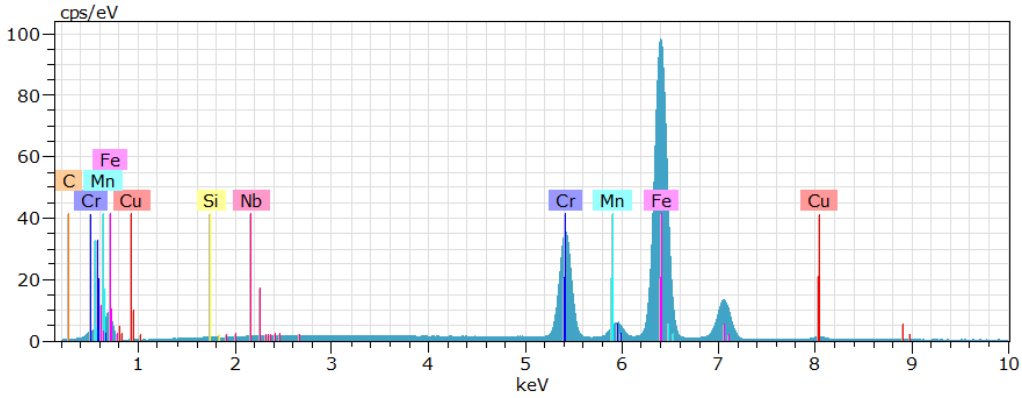

Figure 3-11. EDS Spectrum of Region 1 on Figure 3-10.

Table 3-3. EDS Compositional Analysis of Region 1 on Figure 3-10.

Region	Composition (wt. %)						
	Fe	Cr	Cu	C	Si	Mn	Nb
Region 1	77.94	16.57	1.49	3.25	0.17	0.36	0.22

Figure 3-12 shows three EDS spot regions and one EDS area region taken on a 5000× magnification Z-contrast image of the CuSS. This image shows the typical microstructural features found within the steel at higher magnifications. At higher magnifications, there were dark precipitates and light precipitates on the micron size scale. Again, regions significantly darker than the bulk are comprised of elements with lighter atomic mass than iron and regions

significantly lighter than the bulk are comprised of elements with heavier atomic mass than iron. Figures 3-13 through 3-16 show the EDS spectrums for regions 1 – 4 in Figure 3-12. Table 3-4 summarizes the EDS compositional data for each of the regions in Figure 3-12.

Region 1, the EDS spectrum of which is in Figure 3-13, was of the darker precipitate region. The EDS data indicated that the darker precipitates were regions with 1-2 wt.% lower amounts of iron and chromium than the bulk and which were rich in aluminum (8.27 wt.%) and magnesium (1.34 wt.%). These dark precipitates also had slightly lower amounts of copper compared to the bulk (0.1 wt. %, likely within the margin of error for EDS) and did not contain any niobium. The elemental analysis of these black regions was otherwise similar to that of the bulk. Regions 2 and 3, the EDS spectrums of which are in Figures 3-14 and 3-15, respectively, were of the lighter precipitate regions. The EDS analysis indicated that lighter precipitates were regions with 1-2 wt.% less iron and chromium than the bulk and which were very rich in niobium (14 – 19 wt.%). The elemental analysis of the white precipitates was otherwise similar to that of the bulk. Region 4, the EDS spectrum of which is in Figure 3-16, shows a higher magnification region of the bulk of the steel. The EDS data indicated that this region had an elemental composition very similar to the bulk, except that there was no niobium present. Given this, it is presumed that copper was uniformly distributed throughout the bulk of CuSS (even within the precipitate regions), that all of the niobium present existed only in the white precipitates, and that the black precipitates did not contain any niobium but were regions with large amounts of aluminum and magnesium.

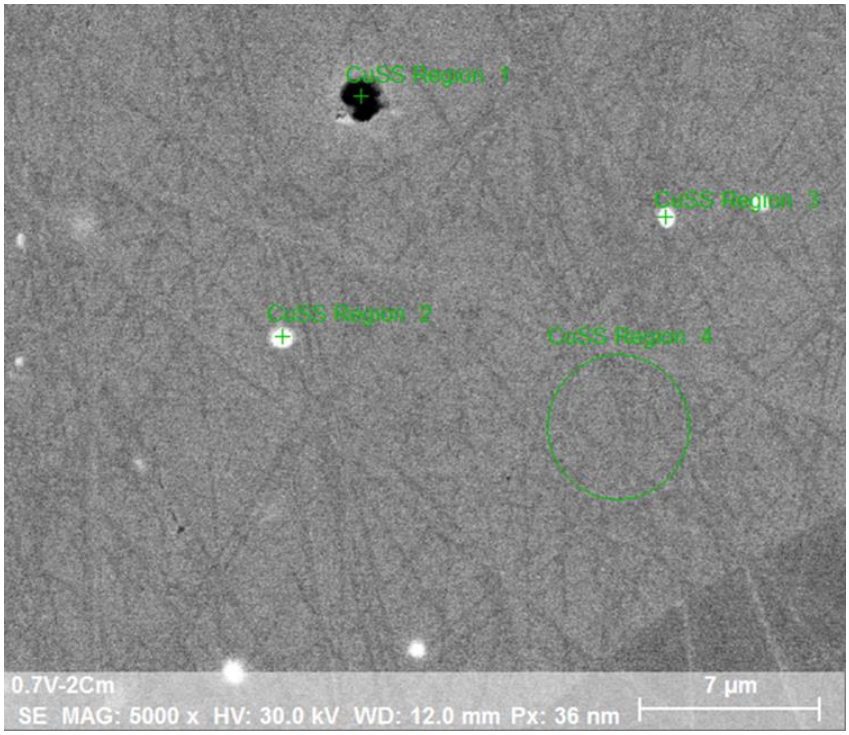

Figure 3-12. 5000× EDS Regions 1-4 on CuSS

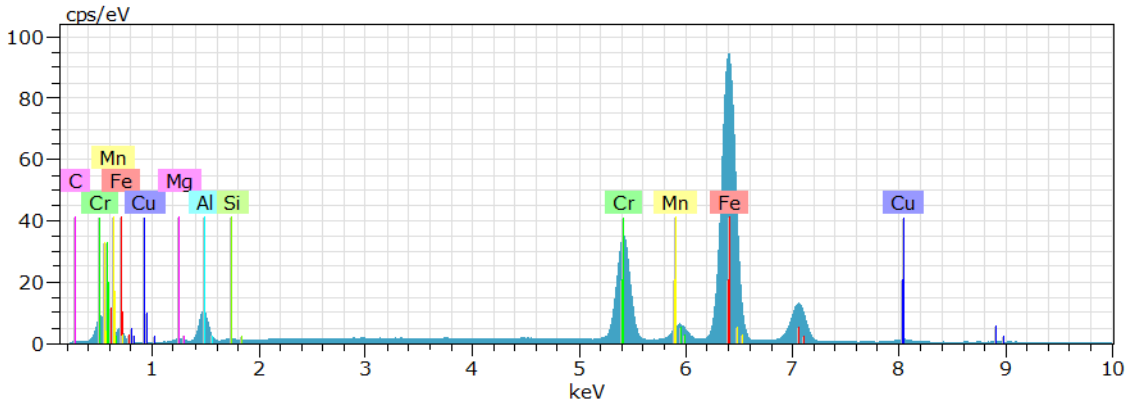

Figure 3-13. EDS Spectrum of Region 1 on Figure 3-12

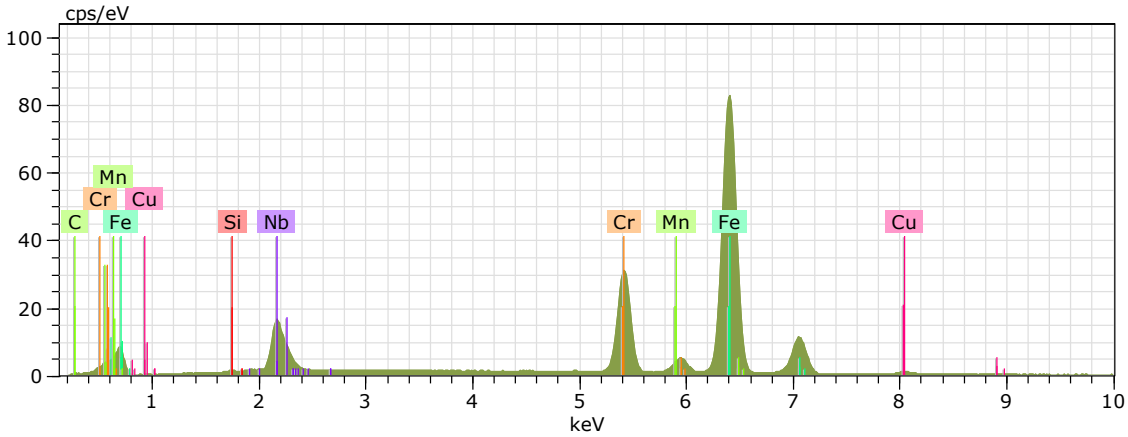

Figure 3-14. EDS Spectrum of Region 2 on Figure 3-12

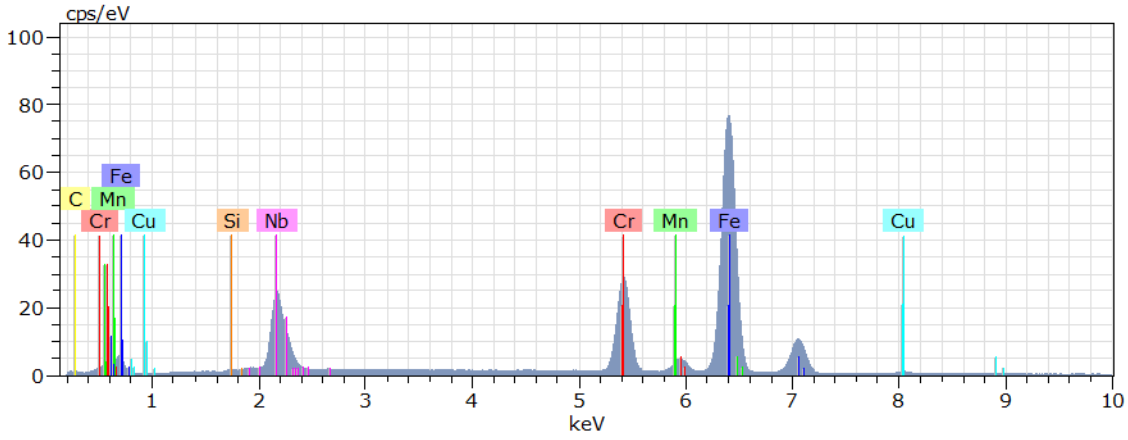

Figure 3-15. EDS Spectrum of Region 3 on Figure 3-12

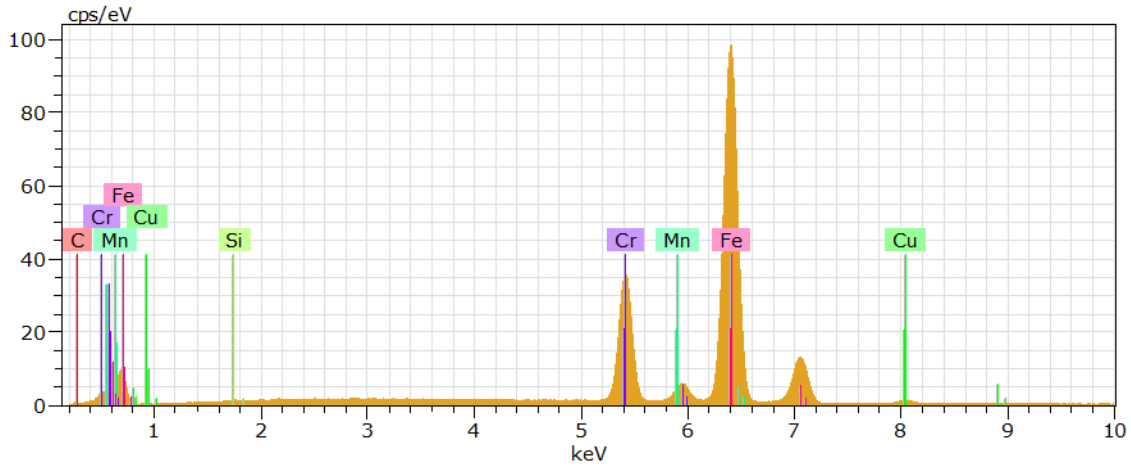

Figure 3-16. EDS Spectrum of Region 4 on Figure 3-12

Table 3-4. EDS Compositional Analysis of Region 1-4 on Figure 3-12.

Region	Composition (wt. %)								
	Fe	Cr	Cu	C	Si	Mn	Nb	Al	Mg
Region 1	70.57	14.31	1.3	3.49	0.29	0.42	x	8.27	1.34
Region 2	64.46	14.88	1.19	4.24	0.15	0.32	14.77	x	x
Region 3	58.52	13.46	0.96	6.83	0.05	0.26	19.92	x	x
Region 4	78.07	16.49	1.47	3.47	0.19	0.31	x	x	x

Figures 3-17 is a Z-contrast SEM image of 0.02 µm polished AgSS which shows the typical bulk microstructure for this type of austenitic, silver-alloyed stainless steel. Figure 3-18 shows an EDS area region taken on a 500× magnification of AgSS. Figure 3-19 shows the EDS spectrum associated with the area region on Figure 3-17. Table 3-5 summarizes the EDS chemical analysis for this region, which was representative of the average composition of the bulk of the steel. The EDS data qualitatively confirmed the manufacturer's compositional data provided for the material. The small amounts of carbon and silicon present in the bulk may have been due to trace amounts of polishing media (SiC paper, diamond paste) on the coupon's surface. Carbon could have also been deposited through the cleaning process of the polished sample, from acetone and alcohols.

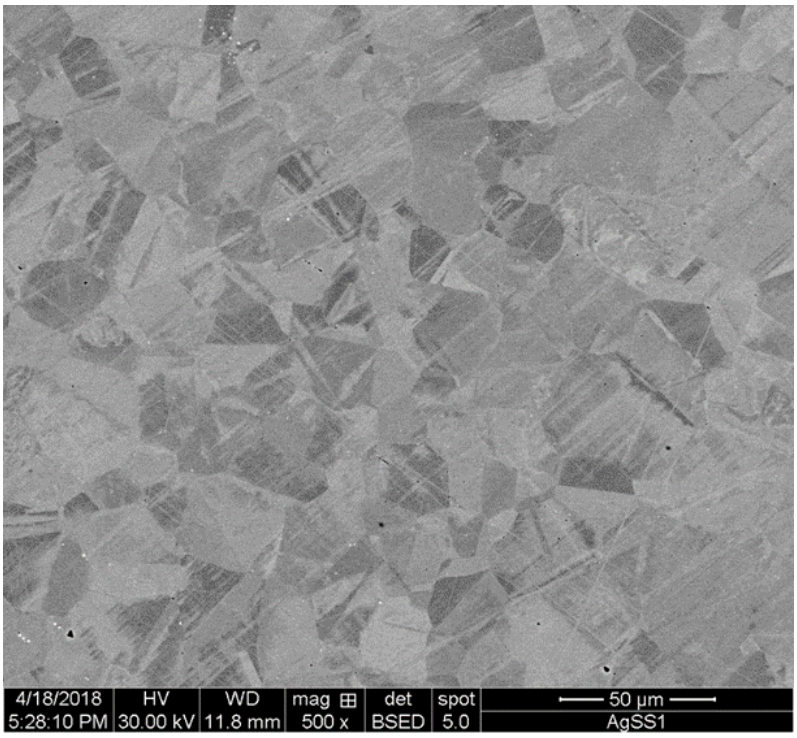

Figure 3-17. 500× BSD SEM Image of AgSS

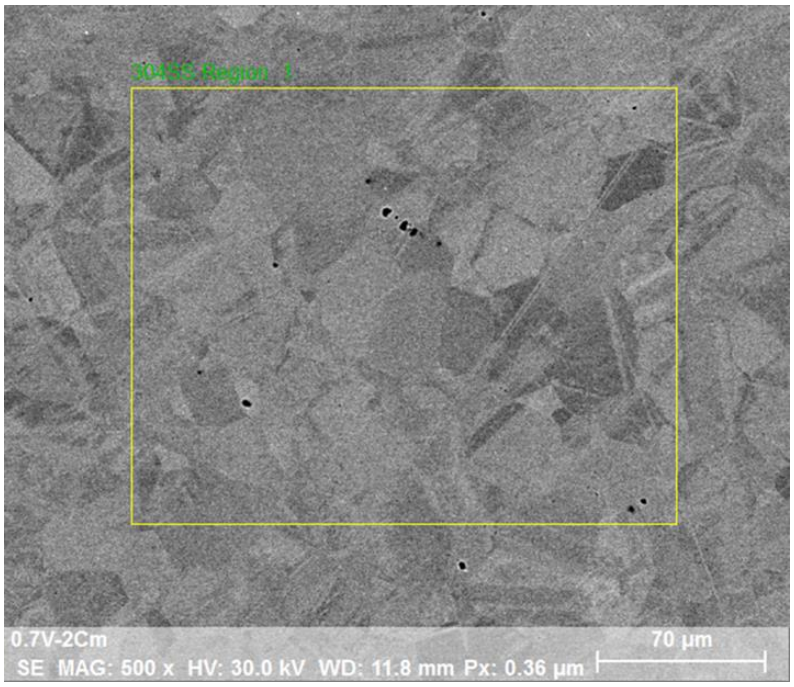

Figure 3-18. 500× EDS Region 1 on AgSS

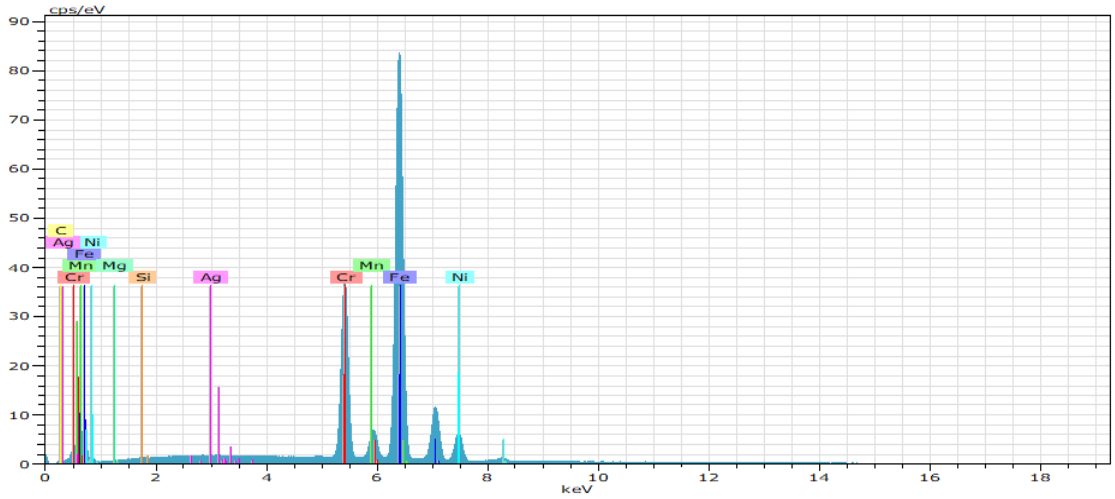

Figure 3-19 EDS Spectra of Region 1 on Figure 3-18

Table 3-5. EDS Compositional Analysis of Region 1 on Figure 3-18.

Region	Composition (wt. %)							
	Fe	Cr	Ni	C	Mn	Si	Ag	Mg
Region 1	70.85	18.58	7.49	1.68	1.12	0.20	0.07	0.01

Figure 3-20 shows five EDS spot regions taken on a 9000× magnification Z-contrast image of the AgSS. This image shows the typical microstructural features found within the steel at higher magnifications. At higher magnifications, there were dark precipitates and light precipitates on the submicron to micron size scale. Again, regions significantly darker than the bulk are comprised of elements with lighter atomic mass than iron and regions significantly lighter than the bulk are comprised of elements with heavier atomic mass than iron. Figures 3-21 through 3-25 show the EDS spectrums for regions 1 – 5 in Figure 3-20. Table 3-6 summarizes the EDS compositional data for each of the regions in Figure 3-12.

Regions 1-3, the EDS spectrums of which are in Figures 3-21 through 3-23, respectively, were of the darker precipitate regions. The EDS data indicated that the darker precipitates were regions with slightly lower amounts of iron and nickel than the bulk and which were rich in molybdenum. These dark precipitates also had higher amounts of silver compared to the bulk (0.36 -1.14 wt. % Ag) and potentially also had slightly higher amounts of manganese compared to the bulk. Regions 4 and 5, the EDS spectrums of which are in Figures 3-24 and 3-25, respectively, were of the lighter precipitate regions. The EDS analysis indicated that lighter precipitates were regions with slightly lower amounts of iron and nickle compared to the bulk, and which were the regions the richest in silver (2.49 – 3.82 wt. % Ag). Given this, it is presumed that the silver was less uniformly distributed throughout the bulk of this austenitic steel than the copper was in the ferritic copper-alloyed stainless steel. The silver alloyed into the steel was primarily located within the dark and light precipitates, with the greatest amounts of silver being located within the white precipitates.

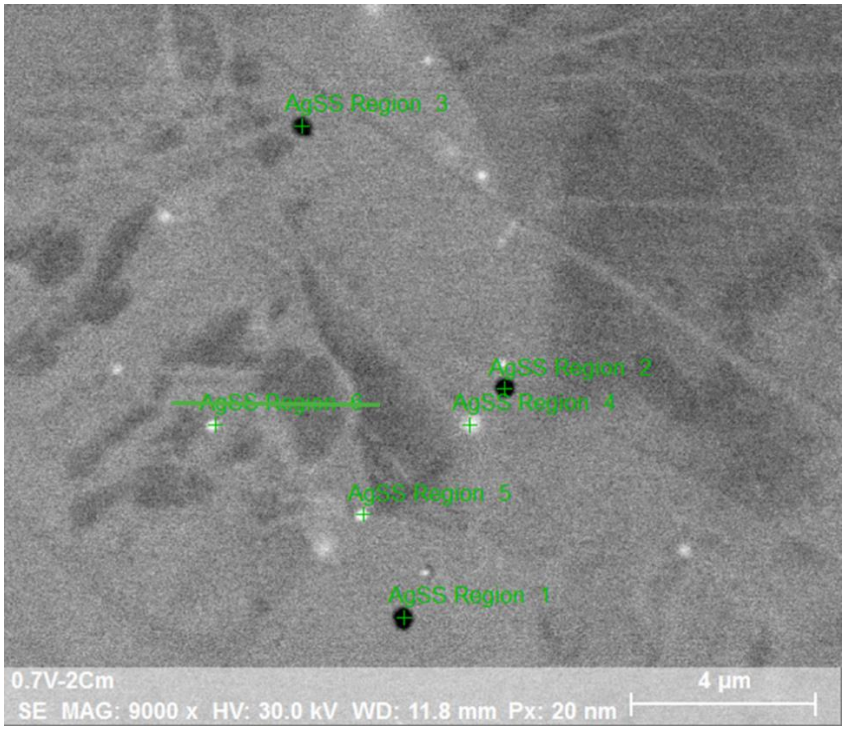

Figure 3-20. 9000× EDS Regions 1 -5 on AgSS

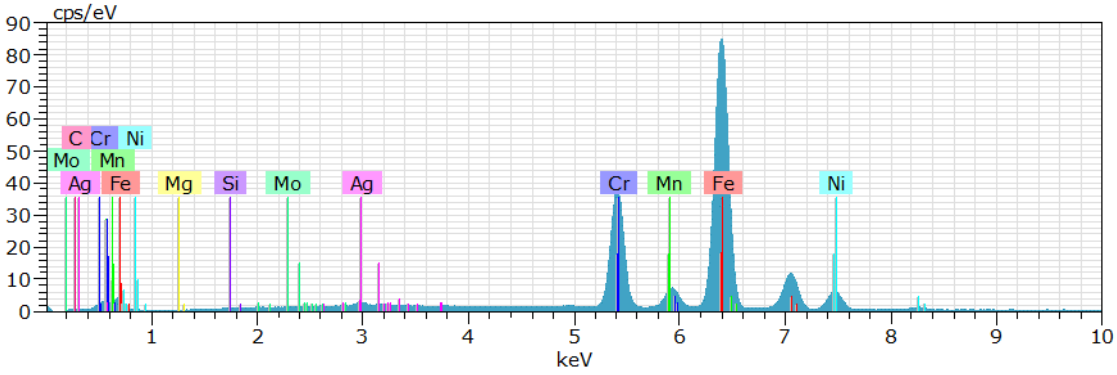

Figure 3-21. EDS Spectrum of Region 1 on Figure 3-20.

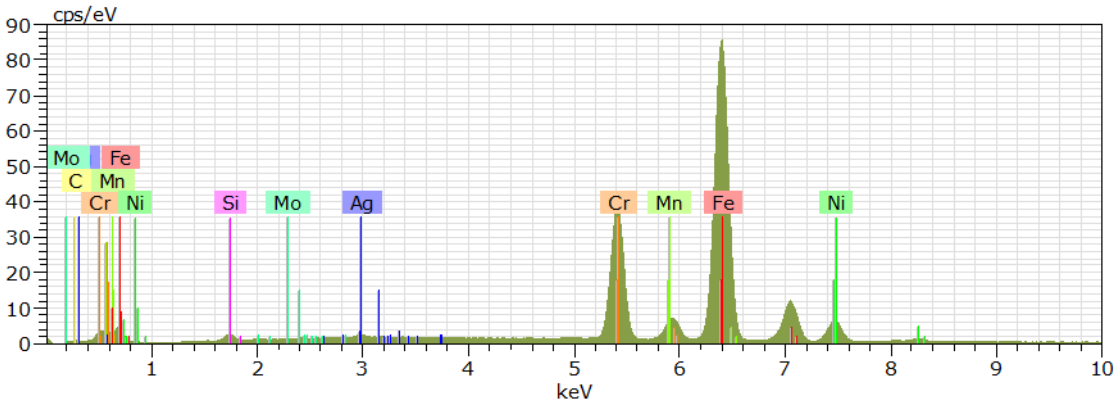

Figure 3-22. EDS Spectrum of Region 2 on Figure 3-20.

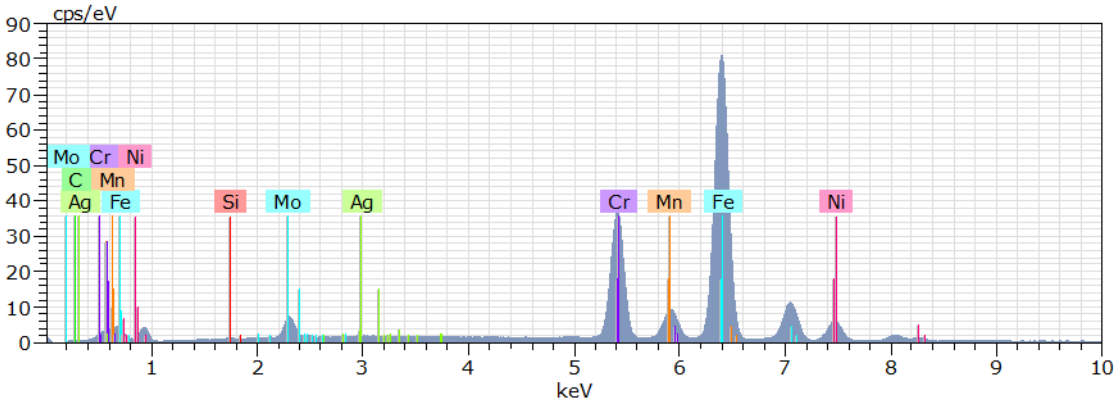

Figure 3-23. EDS Spectrum of Region 3 on Figure 3-20.

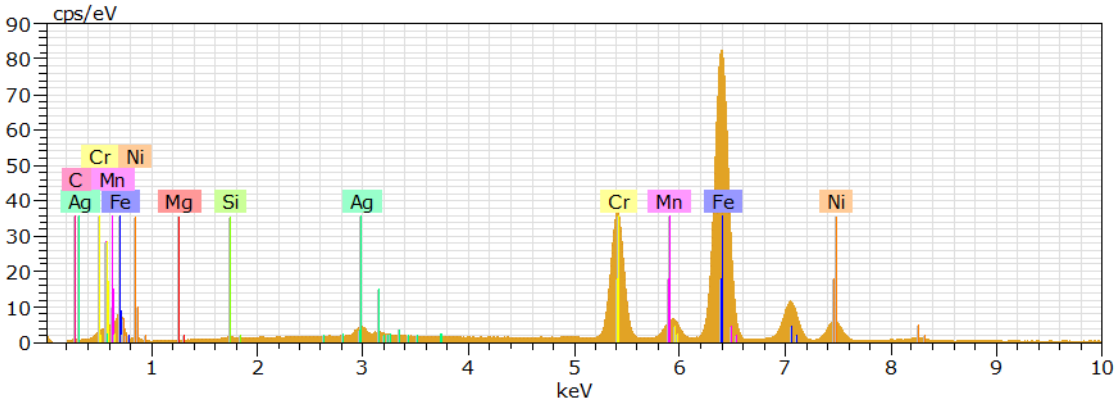

Figure 3-24. EDS Spectrum of Region 4 on 3-20.

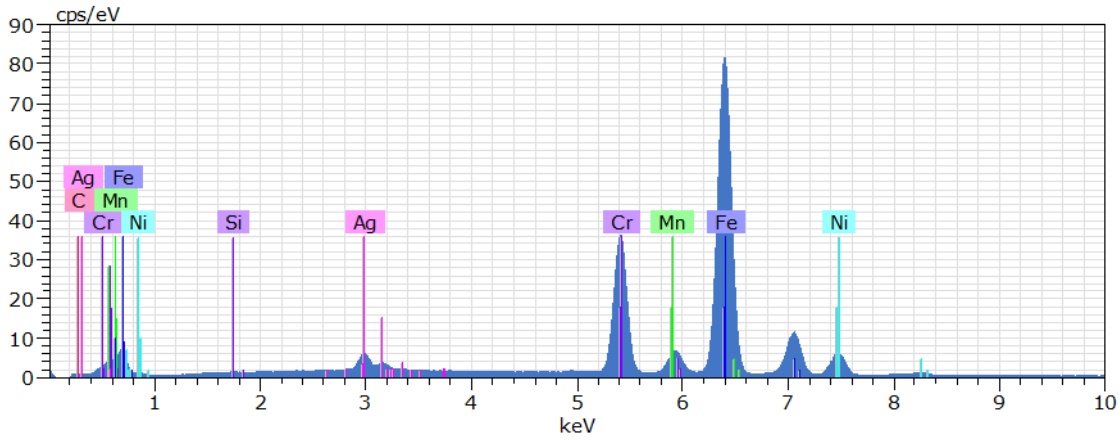

Figure 3-25. EDS Spectrum of Region 5 on Figure 3-20.

Table 3-6. EDS Compositional Analysis of Regions 1-5 on Figure 3-20.

Region	Composition (wt. %)								
	Fe	Cr	Ni	C	Mn	Si	Ag	Mg	Mo
Region 1	69.46	18.56	6.90	2.55	1.14	0.20	1.14	0.01	0.04
Region 2	68.56	18.19	7.10	2.93	1.06	1.35	0.75	x	0.07
Region 3	65.37	17.71	6.77	1.57	2.76	0.14	0.36	x	5.32
Region 4	68.33	18.37	7.01	2.57	1.02	0.19	2.49	0.02	x
Region 5	67.81	18.34	6.97	1.87	1.05	0.15	3.82	x	x

3.1.2. AFM – Surface Roughness Quality Control

Quality control surface roughness measurements were taken of the coupon surface finishes with a Veeco Multimode AFM. All surfaces were cleaned as outlined in section 2.1.2. All measurements were made in contact mode over a 15 -20 µm or 120 µm scan region with a silicon nitride (SiN) cantilever tip. Table 3-7 summarizes all of the surface roughness measurements made. Three regions were sampled from a single coupon surface with which to take an average. R_{max} refers to the single largest surface depth. R_q refers to the root mean square of the height deviation taken from the mean image plane. R_a refers to the arithmetic average of the absolute values of the surface height deviations from the mean image plane.

Table 3-7. AFM Surface Roughness Measurements, SiN Tip, Contact Mode

Sample	Finish (µm)	Region 1 Roughness (nm)			Region 2 Roughness (nm)			Region 3 Roughness (nm)			Average Roughness (nm)			Standard Dev Roughness (nm)		
		R_{max}	R_a	R_q	R_{max}	R_a	R_q	R_{max}	R_a	R_q	R_{max}	R_a	R_q	R_{max}	R_a	R_q
304SS	0.25	859.0	16.4	34.6	122.0	4.8	8.5	310.0	15.5	26.4	430.3	12.2	17.1	383.0	6.4	13.3
CuSS	0.25	183.0	5.3	8.6	351.0	6.9	15.1	1052.0	35.4	70.6	528.7	15.9	30.3	460.9	16.9	34.1
AgSS	0.25	114.0	5.7	8.2	74.1	6.0	8.0	152.0	4.0	5.7	113.4	5.2	6.5	39.0	1.1	1.4
304SS	0.02	64.4	1.2	2.3	23.0	0.8	1.3	21.4	0.7	1.0	36.3	0.9	1.1	24.4	0.3	0.7
CuSS	0.02	33.3	0.7	1.5	35.1	0.4	0.7	61.4	0.5	1.4	43.3	0.5	0.9	15.7	0.1	0.4
AgSS	0.02	71.8	1.0	2.8	22.2	0.7	0.9	18.8	0.6	0.8	37.6	0.8	0.9	29.7	0.2	1.1

The regions scanned on the 0.25 µm surface finished coupons had R_{max} values which were all between 113.4 ± 39.0 nm and 430.3 ± 383.0 nm. This indicated that for all of the

surfaces polished down to 0.25 μm surface finish, all of the largest scratches sampled were less than 0.5 μm. The average roughness from the image plane were even smoother, ranging closer to the actual polishing media size.

The regions scanned on the 0.02 μm surface finished coupons had R_{max} values which were all between 36.3 ± 0.7 and 43.3 ± 0.4 nm. This indicated that for all of the surfaces polished down to 0.02 μm surface finish, all of the largest scratches sampled were less than 0.05 μm, which was very close to the polishing media size. The average roughness from the image plane were even smoother, ranging 1-2 orders of magnitude smaller than the polishing media size (between 0.5 ± 0.1 – 1.1 ± 0.7 nm). This was likely due to an etching effect imparted on the surface from the colloidal silica polishing solution.

It should be noted that the average size of an *E. coli* cell is 1 – 2 μm long and 0.5 – 1 μm in diameter. The AFM data thus indicated that all of the surfaces polished to 0.25 μm or lower had surface roughness at least one order of magnitude smaller than the average size of an *E. coli* cell. This eliminated the effect of surface roughness when growing the *E. coli* on the submicron polished surfaces, and instead allowed the effect of the steels' surface chemistries and microstructures to be the primary influence on cell attachment on the submicron finished surfaces.

3.2.E-SEM Characterization of *E. coli* Grown on Stainless Steel Coupons Using Drip Flow Bioreactor

All of the stainless steel coupons with *E. coli* grown on their surfaces within the drip flow bioreactor were characterized with the FEI Quanta E-SEM under low vacuum with a water vapor environment. Operating the E-SEM in this mode allowed for imaging the samples while they were fully hydrated with minimal sample preparation prior to imaging.

Since SEMs use a highly focused electron beam for imaging and chemical analysis (EDS), typical SEM samples must be observed under vacuum and must be dry. E-SEMs, however, allow for maintaining a high humidity environment under low vacuum. This minimizes the dehydration of biological samples, and allows them to be imaged without the potentially damaging and time-consuming fixation, dehydration, and coating technique required to observe biological samples under high vacuum within a standard SEM. The only sample preparation required to image the biofilm samples in this study was to place each sample coupon on a metal specimen mount using double-sided carbon tape. The *E. coli*/stainless steel samples were imaged as soon as possible after being harvested from the bioreactor. In fact, the start time of each growth test was based on the time slot availability of the E-SEM.

The mean-free path of a high-energy electron is very short when it passes through liquid water or water vapor, and the inevitable scattering of some of the electrons with water molecules lowers image quality. Despite its advantages for imaging biological samples, low vacuum E-SEM operation with water vapor thus generally has a much lower imaging resolution than standard SEM conducted in high vacuum. As so, the working distance to analyze all the samples was kept at a minimum (<10 mm, usually between 7-9 mm) in order to increase signal. The beam was typically kept at a larger spot size (4-5) and a 20 kV acceleration voltage. The

chamber pressure was typically kept around 1 Torr. These operating parameters all helped optimize signal and consequently image quality while characterizing the *E. coli*/stainless steel samples.

Both the secondary electron detector (SED, topography-contrast) and backscattered electron detector (BSD, Z-contrast) were used in analyzing the *E. coli*/stainless steel samples. Bacteria and bacterial biofilms are primarily composed of organic elements with relatively light atomic number. The influent broth was also primarily composed of lighter, organic elements. Stainless steels are composed primarily of metallic, heavier elements. As so, it was fairly easy to identify the location of biofilm and other organics on the stainless steel surfaces with the BSD. When analyzing samples, the BSD was typically used to first assess where bacteria and other organics were located on the coupon surfaces, and the SED was typically used to collect images of the bacteria-steel interactions with higher resolution and detail.

Table 3-8. summarizes all of the *E. coli* growth tests run with the drip-flow bioreactor on the three types of stainless steel surfaces. Within Table 3-8, the "test #" is the number associated with each growth test within the remainder of this document. "Date characterized" refers to the date the *E. coli*/SS coupons were characterized within the E-SEM. The "bioreactor channel" refers to which channel each coupon was placed in. For each test, coupon 1 or A was grown in channel 1 (leftmost channel from top view), coupon 2 or B was grown in channel 2, coupon 3 or C was grown in channel 3, coupon 4 or D was grown in channel 4 (rightmost channel from top view). "Material" refers to the material type of the substrate coupons, where 304SS is the baseline 304 stainless steel, CuSS is the copper-alloyed stainless steel, and AgSS is the silver-alloyed stainless steel. The asterisk next to the surface material types indicates that the coupon was polished to the same mirror finish on both sides. An "R" next to the material type indicates that the particular coupon was resurfaced after a previous trial, rather than being polished from the raw surface finish of the material. Pre-wash refers to whether or not the cleaned and sterilized coupon was rinsed with either sterile buffer solution (PBS) or sterile DI water prior to being inserted into the bioreactor channel before growth. Post-wash refers to whether or not the material coupon was rinsed with either sterile buffer solution or sterile DI water directly after being harvested prior to E-SEM analysis.

Table 3-8. Complete Summary of Growth Tests

Test #	Date Characterized	Bioreactor Channel	Material	Finish (µm)	Growth (hr)	Pre-Wash	Post-Wash
1	8/10/2017	1	304SS-1*	0.25	48	none	none
1	8/10/2017	2	304SS-2*	0.25	48	none	none
1	8/10/2017	3	304SS-3*	0.25	48	none	none
1	8/10/2017	4	304SS-4*	0.25	48	none	none
2	8/18/2017	1	CuSS-1*	0.25	48.42	PBS	1-2mL PBS
2	8/18/2017	2	CuSS-2*	0.25	48.42	PBS	none
2	8/18/2017	3	CuSS-3*	0.25	48.42	PBS	1-2 mL PBS
2	8/18/2017	4	CuSS-4*	0.25	48.42	PBS	none
3	8/25/2017	1	AgSS-1*	0.25	48	PBS	none
3	8/25/2017	2	AgSS-2*	0.25	48	PBS	5mL PBS
3	8/25/2017	3	AgSS-3*	0.25	48	PBS	10mL PBS
3	8/25/2017	4	AgSS-4*	0.25	48	PBS	15mL PBS
3	8/25/2017	n/a	AgSS-5*	0.25	0, dried broth	PBS	none
4	9/1/2017	1	AgSS-A	0.02	45	PBS	none
4	9/1/2017	2	AgSS-B	0.02	45	PBS	5mL PBS
4	9/1/2017	3	AgSS-C	0.02	45	PBS	10mL PBS
4	9/1/2017	4	AgSS-D	0.02	45	PBS	15mL PBS
4	9/1/2017	n/a	AgSS-E	0.02	0, dried broth	PBS	none
5	9/7/2017	1	CuSS-A	0.02	45	PBS	5mL DI H_2O
5	9/7/2017	2	CuSS-B	0.02	45	PBS	5mL DI H_2O
5	9/7/2017	3	CuSS-C	0.02	45	PBS	5mL DI H_2O
5	9/7/2017	4	CuSS-D	0.02	45	PBS	5mL DI H_2O
6	9/22/2017	1	304SS-A	0.02	46	DI H_2O	3mL DI H_2O
6	9/22/2017	2	304SS-B	7	46	DI H_2O	3mL DI H_2O
6	9/22/2017	3	304SS-C	0.02	46	DI H_2O	3mL DI H_2O
6	9/22/2017	4	304SS-D	7	46	DI H_2O	3mL DI H_2O
7	9/28/2017	1	304SS-RA	0.02	45.75	PBS	none
7	9/28/2017	2	304SS-RB	41	45.75	PBS	none
7	9/28/2017	3	304SS-RC	0.02	45.75	PBS	none
7	9/28/2017	4	304SS-RD	41	45.75	PBS	none
8	10/23/2017	1	304SS-RA	0.02	96.33	none	none
8	10/23/2017	2	304SS-RB	41	96.33	none	none
8	10/23/2017	3	304SS-RC	0.02	96.33	none	none
8	10/23/2017	4	304SS-RD	41	96.33	none	none
9	10/30/2017	1	CuSS-2	0.02	94.66	none	none
9	10/30/2017	2	AgSS-D	0.02	94.66	none	none
9	10/30/2017	3	CuSS-4	0.02	94.66	none	none
9	10/30/2017	4	AgSS-E	0.02	94.66	none	none

Key to Table 3-5
Wash of "none" = coupon unrinsed before insertion, after isopropanol sterilization
* = double-sided coupons
R = resurfaced coupon
Pre-wash = rinse before coupon insertion, after isopropanol sterilization
Post-wash = rinse after coupon harvesting, before characterization

There was also one coupon in Test 3 and Test 4 which were not grown within the bioreactor. These coupons were cleaned, sterilized via isopropanol, and then sterile influent broth was allowed to dry on their surface directly before E-SEM imaging (after the other coupons in the test were harvested). These were used as reference for what the influent broth looked like within the E-SEM independent of bacteria. Figure 3-26a-b shows one of these two dried broth coupons imaged within the E-SEM. Both images were analyzed on the same day as Test # 3.

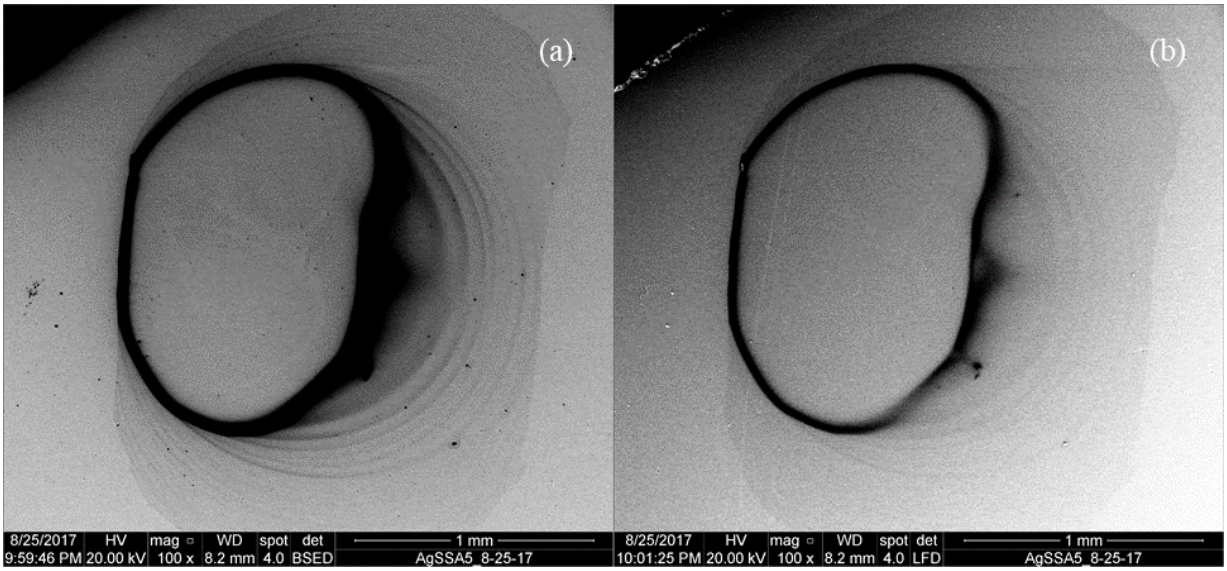

Figure 3-26. E-SEM Images of Dried, Sterile Influent Broth on AgSS Surface (0.25 µm finish). (a) 100× BSD E-SEM Image. (b) 100× SED E-SEM Image

Most of the growth tests run had overlapping experimental parameters. For instance, tests run with coupons of the same substrate material and growth temperature may have had more than one different surface roughness, different pre-washes or post-washes, or different growth durations. Similarly, the longer duration growth tests of 96 hours were also the only tests run at elevated temperature. This was done to maximize *E. coli* growth in an attempt to obtain more mature and thicker biofilms, since the 48-hour, room temperature growth tests did not produce mature biofilms.

Tables 3-9 through 3-13 in sections 3.3.1 – 3.3.4 break down this complete summation of tests outlined in Table 3-8 by the experimental parameters of substrate material, substrate surface roughness, *E. coli* growth duration, the washing of the substrate surfaces before growth, the washing of the coupons after growth, and the bioreactor temperature during growth. The results of this experimental study will be discussed in this manner. However, the potential overlap of experimental parameters must be kept in mind when considering the entirety of the work.

3.2.1. Influence of Stainless Steel Substrate Material on *E. coli* Growth

Material type had little effect on the biofilms observed. By E-SEM analysis alone, there was no observed correlation between a material's surface chemistry and alloy microstructure and bacterial attachment. Bacteria attachment appeared to be completely random and based entirely on where the coupon surfaces were consistently wetted during growth. All of the observed

biofilms existed in droplet shapes on the coupon surfaces, typically with the majority of cells along the droplet edges and cells either collected in the center of the droplet or scattered throughout the center of the droplet. Multiple biofilm droplets were frequently observed on a single coupon surface. There were no significant distinguishing features between the observed biofilms grown on the different types of stainless steels. There was no direct way to assess biofilm resistant properties of the copper- and silver-alloyed stainless steels using E-SEM analysis alone.

Table 3-9 organizes all of the *E. coli* growth tests by material substrate types. Under the column "Coupons," this describes which coupons within the reactor channel were of the given material type for a given test. "All" indicates that all four coupons, one in each reactor channel, were all of the labeled material type for the test number. The numbers 1-4 indicate which reactor channels had coupons of the labeled material type for the test number, 1 indicating channel 1, 2 indicating channel 2, etc. "X"'s indicate that the coupon in a given reactor channel was not of the labeled material type for a test number.

Table 3-9. Growth Tests with the Same Substrate Material

Same Materials		
Material	**Test #**	**Coupons**
304SS	1	All
304SS	6	All
304SS	7	All
304SS	8	All
AgSS	3	All
AgSS	4	All
AgSS	9	x 2 x 4
CuSS	2	All
CuSS	5	All
CuSS	9	1 x 3 x

Color Key (Material Types) for Tables 3-6 to 3-10	
	= 304SS
	= AgSSA
	= CuSSA
	= test ran both AgSS and CuSS coupons, in separate channels

Figures 3-27 through 3-37 demonstrate the apparent randomness and similarities in the shapes of the biofilms formed on the three stainless steel types. Figures 3-27 through 3-31 are of biofilms grown on 304SS. Figures 3-16 through 3-34 are of biofilms grown in CuSS. Figures 3-35 through 3-37 are of biofilms grown on AgSS. On a 1-2 micron level, there were three main shapes that the biofilms formed, seemingly independent to the material type. On a submicron level, the biofilms had many similarities in how the cells were arranged, also seemingly independent of material type. Section 3.3.1 primarily reviews the shapes of the biofilms on the 1-2 micron level. Sections 3.3.2 – 3.3.4 will help demonstrate that the biofilms were of similar structures on the submicron level as well.

The first biofilm shape observed was a large, circular or ovular droplet, often with a collection of cells growing in the center and with the majority of cells collecting around the edges of the droplet. This type of droplet shape was large, approximately 1-2mm in diameter and length. This shape type will be referred to as Shape 1. This type of droplet was most frequently observed on coupon surfaces which were unwashed, but unwashed coupons sometimes did not

form large droplets. Figures 3-27, 3-32, and 3-36 illustrate this first type of biofilm droplet shape observed.

The second type of biofilm droplet shape observed was the presence of many medium sized, circular or ovular droplets on the coupon surfaces. These droplets were about 0.5mm to 1mm in diameter and were often associated with even smaller droplets, anywhere less than 0.5mm in diameter. This shape type will be referred to as Shape 2. Again, with this type of droplet shape the majority of the cells appeared reside along the edges of the droplet and often had some cells scattered throughout their centers. This type of droplet shape was most frequently observed on coupons that had a pre-wash but not a post-wash. Again, though, this was not always true. Sometimes this droplet shape was observed with no pre-wash and/or on coupons that had a post-wash. Figures 3-28, 3-29, 3-30, 3-33, and 3-35 demonstrate this second type of biofilm droplet shape.

The third type of droplet shaped observed was the presence of irregularly shaped clusters of cells on the coupon surfaces. These biofilms were not primarily ovular or circular, but were any number of irregularly shaped, roughly oblong collections of cells. This shape type will be referred to as Shape 3. Shape 3 biofilms still had similar structures as Shape1 and Shape 2. However, in the Shape 3 type biofilms the occurrence of a larger collection of cells in the center rather than the edge of the droplet occurred more frequently than with the Shape 1 and Shape 2 type biofilms. Figures 3-31, 3-34, and 3-37 demonstrate this third type of biofilm droplet shape.

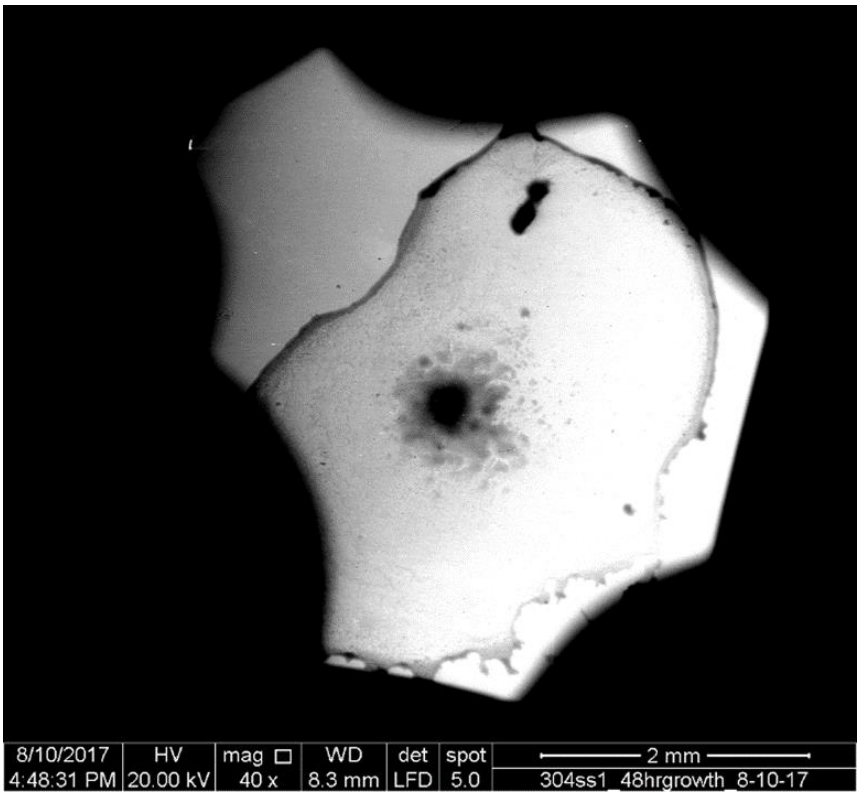

Figure 3-27. 40× SED E-SEM Image of Biofilm on 304SS, Coupon 1 in Test #1

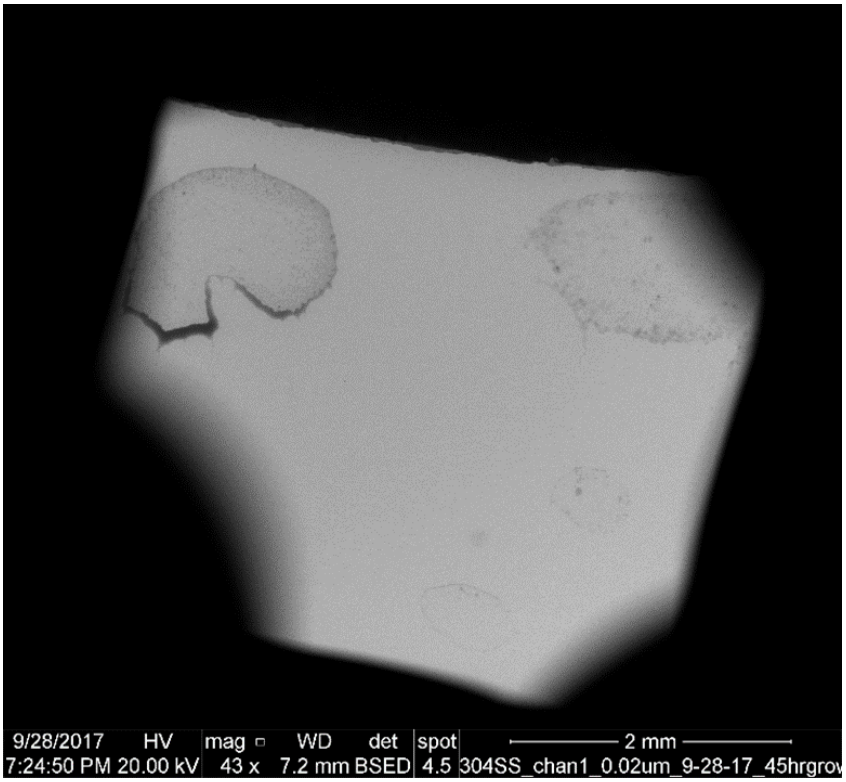

Figure 3-28. 43× BSD E-SEM Image of Biofilm on 304SS, Coupon 1 in Test #7

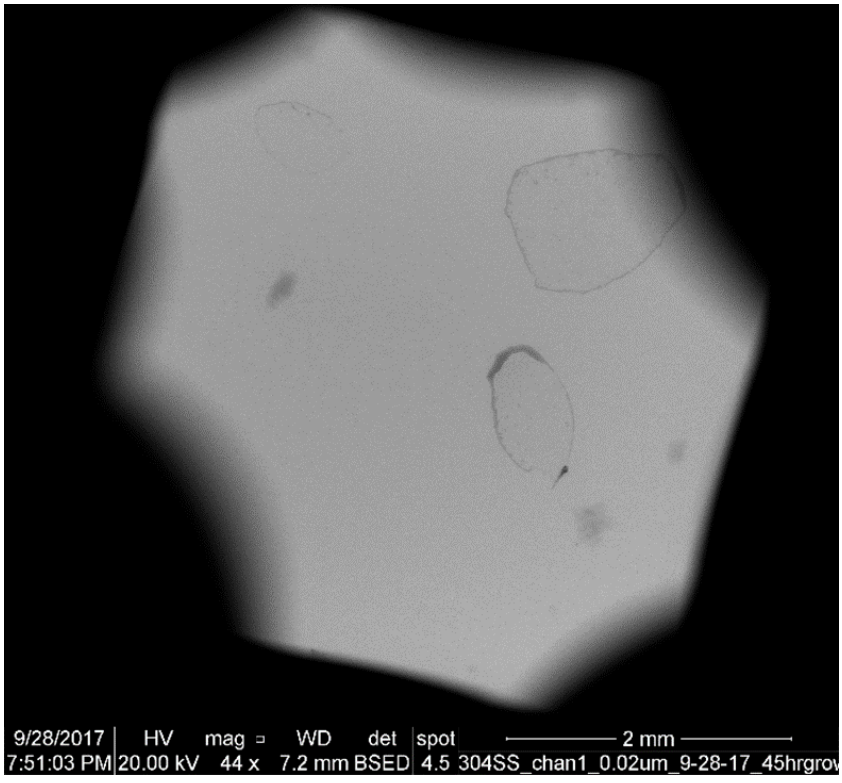

Figure 3-29. 44× BSD E-SEM Image of Biofilm on 304SS, Coupon 1 in Test #7

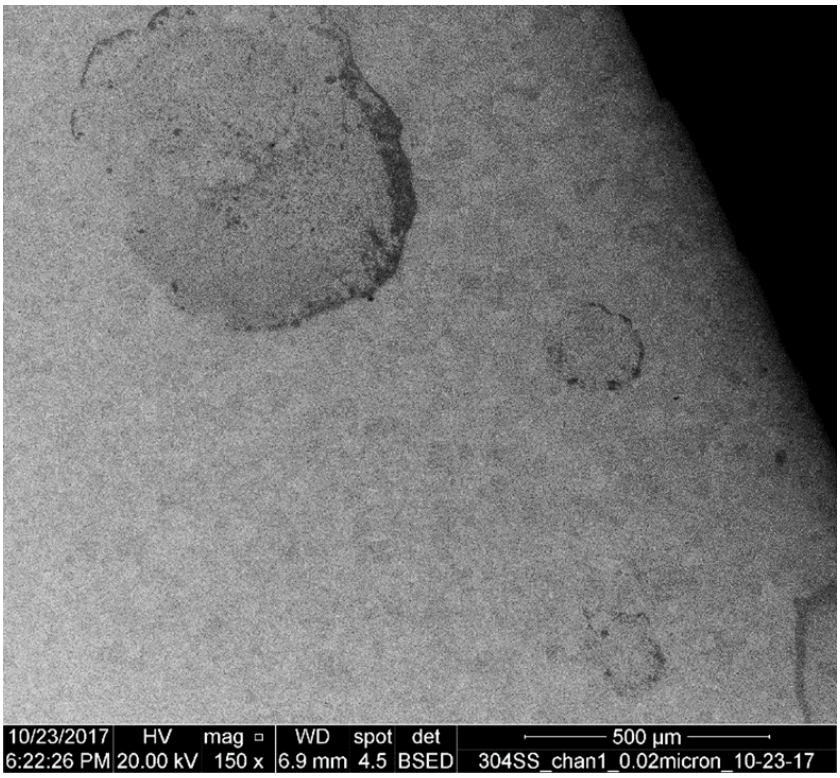

Figure 3-30. 150× BSD E-SEM Image of Biofilm on 304SS, Coupon 1 in Test #8

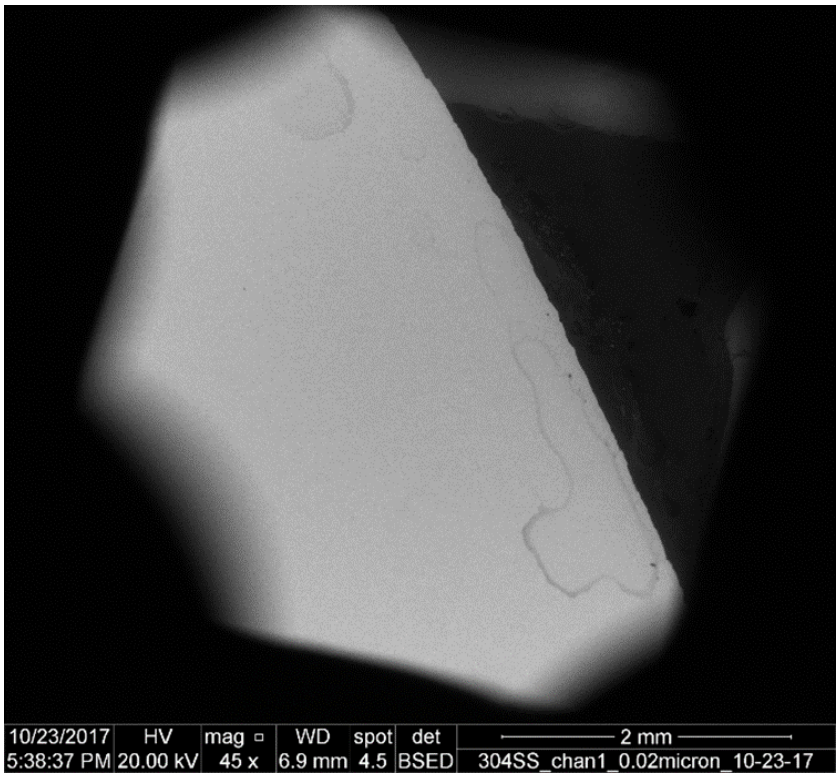

Figure 3-31. 45× BSD E-SEM Image of Biofilm on 304SS, Coupon 1 in Test #8

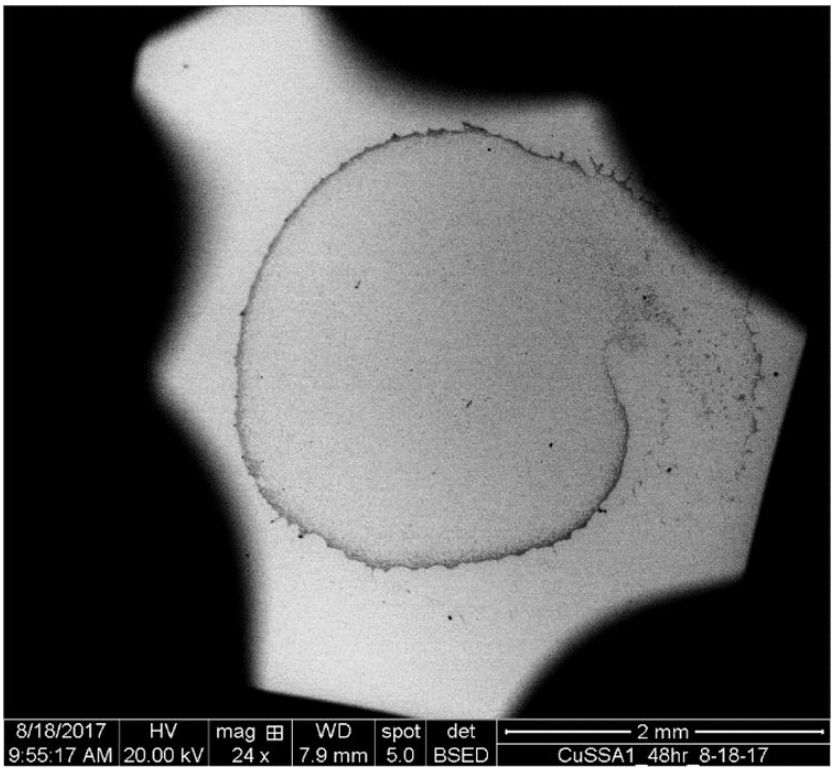

Figure 3-32. 24× BSD E-SEM Image of Biofilm on CuSS, Coupon 1 in Test #2

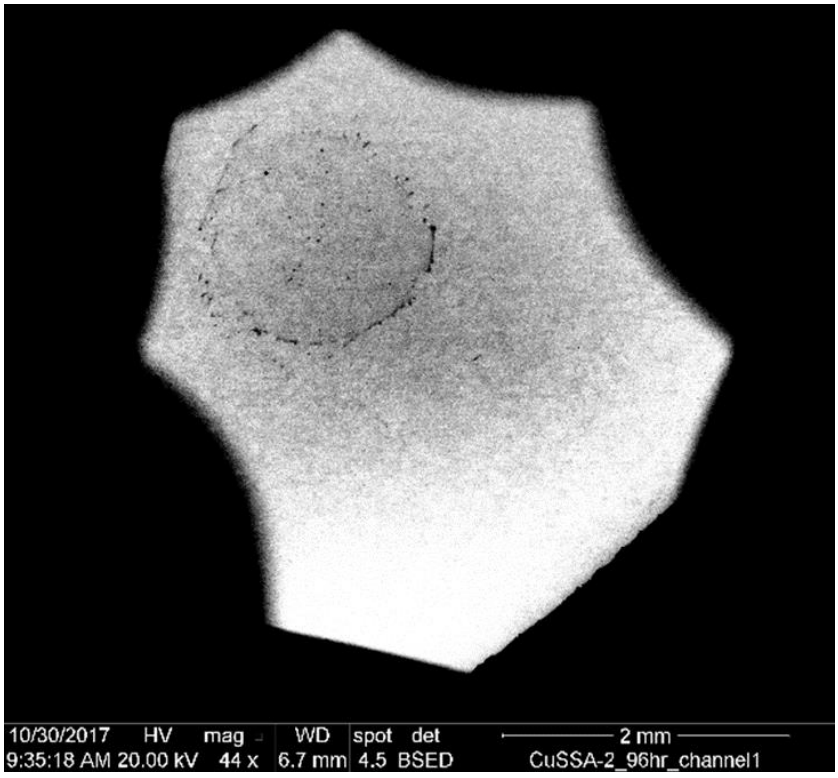

Figure 3-33. 24× BSD E-SEM Image of Biofilm on CuSS, Coupon 1 in Test #9

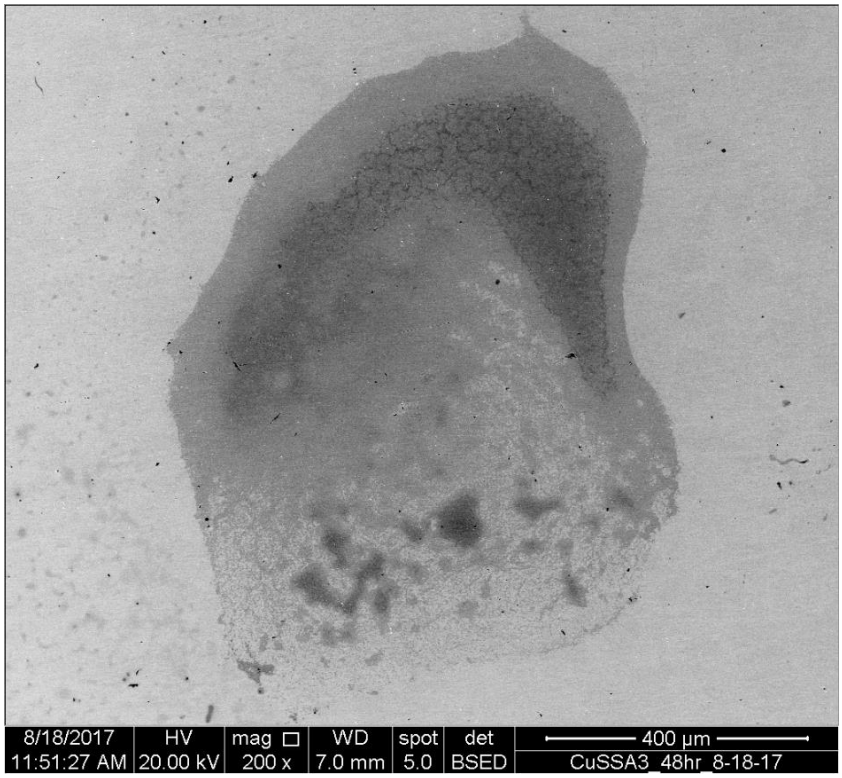

Figure 3-34. 200× BSD E-SEM Image of Biofilm on CuSS, Coupon 3 in Test #2

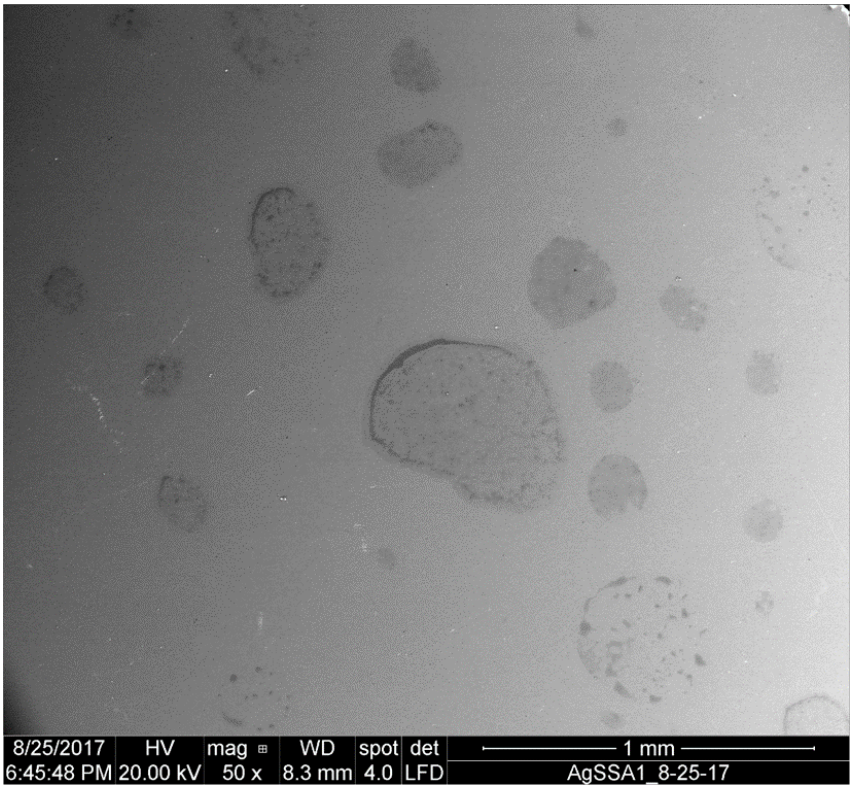

Figure 3-35. 50× SED E-SEM Image of Biofilm on AgSS, Coupon 1 in Test #3

Figure 3-36. 65× SED E-SEM Image of Biofilm on AgSS, Coupon 1 in Test #9

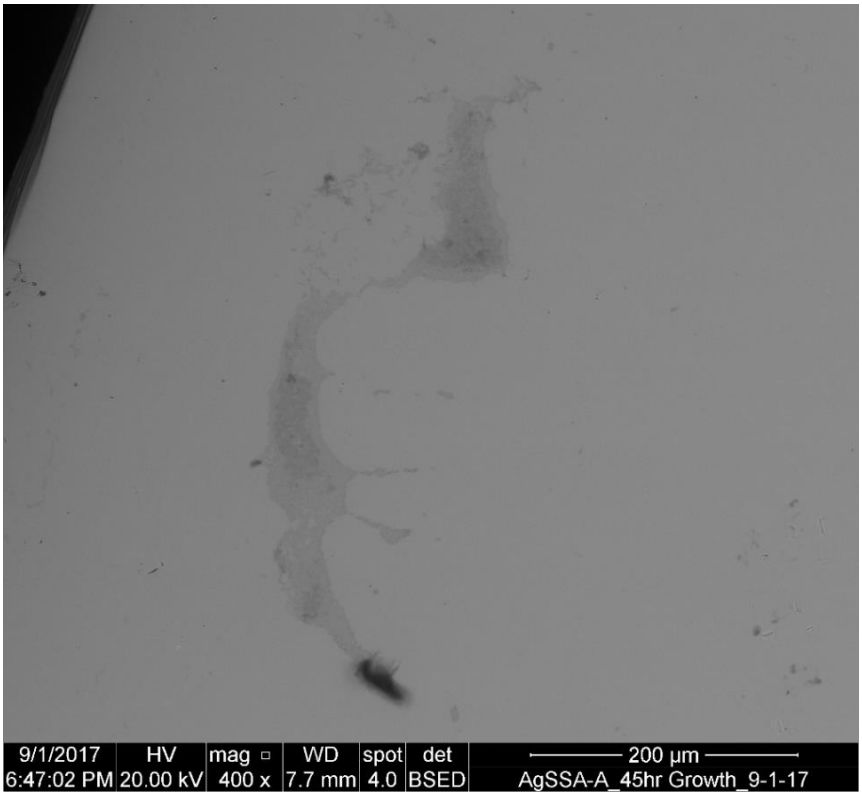

Figure 3-37. 400× BSD E-SEM Image of Biofilm on AgSS, Coupon 1 in Test #4

Figures 3-38 through 3-40 further demonstrate the apparent randomness of bacterial attachment to the various surface chemistry features of the submicron polished stainless steels. Bacteria appeared to attach randomly to the surfaces, regardless to grain structure as seen in Figure 3-38, regardless to the surface scratch and white niobium-containing precipitates as seen in Figure 3-39, and regardless to the white silver-containing precipitates, as seen in Figure 3-40.

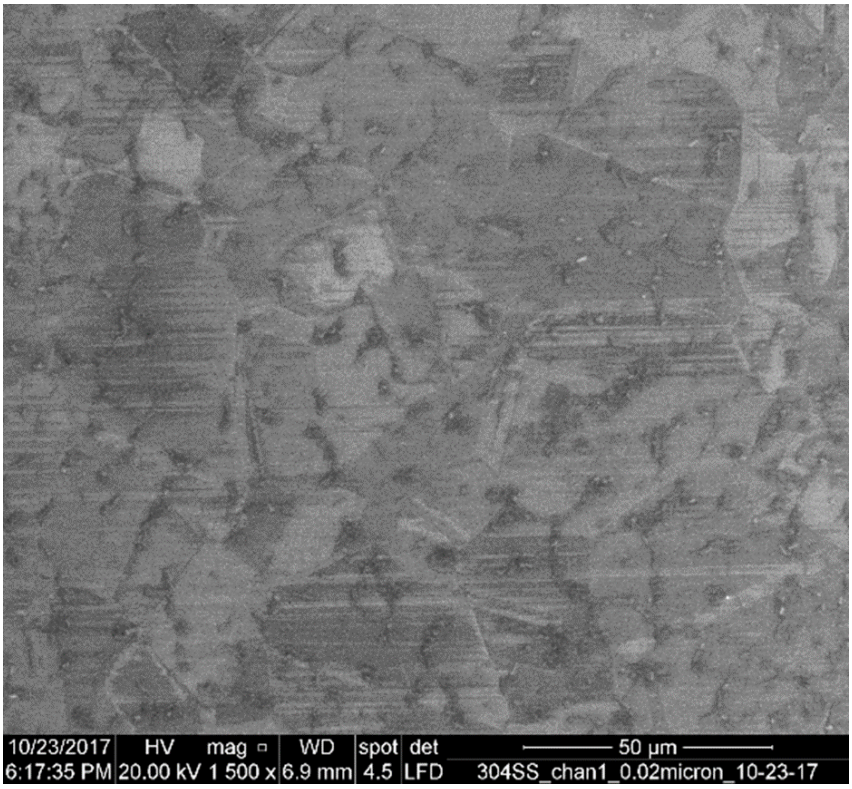

Figure 3-38. 1500× SED E-SEM Image of Biofilm on 304SS, Coupon 1 in Test #8

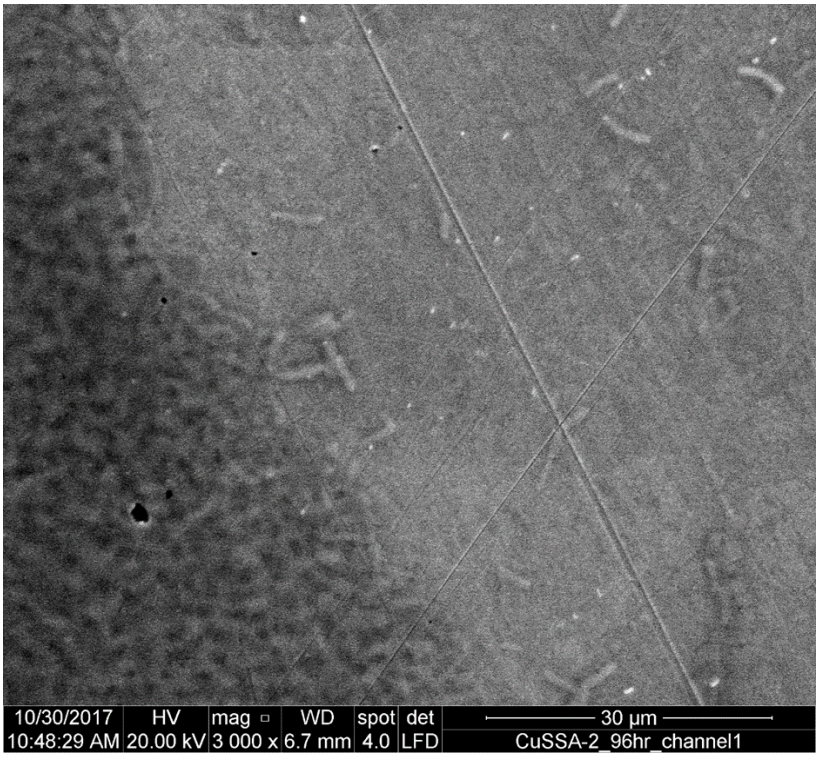

Figure 3-39. 3000× SED E-SEM Image of Biofilm on CuSS, Coupon 2 in Test #9. White spots are niobium-containing precipitates; some overlap in BSD signal was present in the SED imaging.

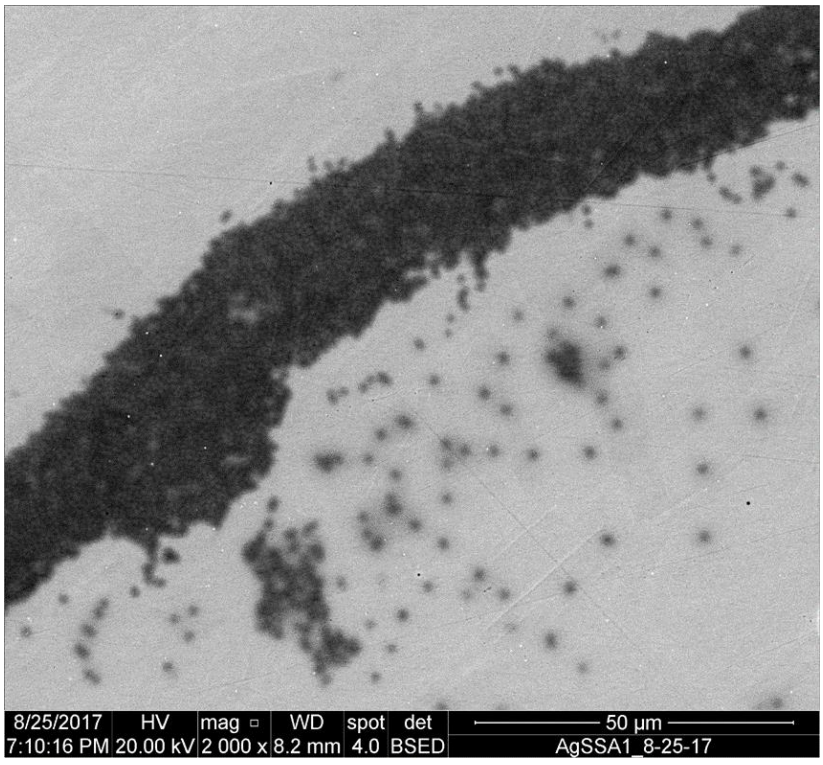

Figure 3-40. 2000× BSD E-SEM Image of Biofilm on AgSS, Coupon 1 in Test #3. White spots are silver-containing precipitates. Dark spots (smaller than bacteria) are molybdenum-containing precipitates.

3.2.2. Influence of Surface Roughness on *E. coli* Growth

There was little to no discernable difference between the biofilms grown on the 0.02 µm, 0.25 µm and 7 µm surface finished coupons, as already demonstrated in Figures 3-27 through 3-40. This suggests that reasonably smooth surfaces likely have similar surface interactions with the *E. coli* cells. The 41 µm finished surfaces were too rough to adequately analyze within the E-SEM, as they caused too much contrast in the background to be able to observe the presence of bacterial cells. However, low magnification BSD images of the 41 µm polished surfaces showed similar low atomic mass droplet-like regions. This suggests that bacterial growth on these surfaces did occur; it was just not possible to directly observe via E-SEM. These droplet-like features on the 41 µm finished coupons had less distinguished boundaries as the they did on the reasonably smooth surfaces. This is likely due to the fact that the grooves in the rougher surfaces may have acted in some form of capillary action to draw fluid along the grooves, making the edges appear less distinct.

Table 3-10 organizes all of the *E. coli* growth tests by substrate roughness.

Table 3-10. Growth Tests with the Same Substrate Surface Roughness

Same Roughnesses						
Roughness	**Test #**	**Coupons**				
0.25 µm	1	All				
0.25 µm	2	All				
0.25 µm	3	All				
0.02 µm	4	All				
0.02 µm	5	All				
0.02 µm	6	1	x	3	x	
0.02 µm	7	1	x	3	x	
0.02 µm	8	1	x	3	x	
0.02 µm	9	1	x	3	x	
7 µm	6	x	2	x	4	
41 µm	7	x	2	x	4	
41 µm	8	x	2	x	4	

Color Key (Material Types) for Tables 3-6 to 3-10	
	= 304SS
	= AgSSA
	= CuSSA
	= test ran both AgSS and CuSS coupons, in separate channels

Figures 3-41 through 3-43 show the presence of the droplet-like lines observed on the 41 µm polished samples. These darker regions which look like spread fluid could either be nutrient broth and/or collections of cells which were unable to be resolved at higher magnitudes due to background contrast problems associated with increased roughness.

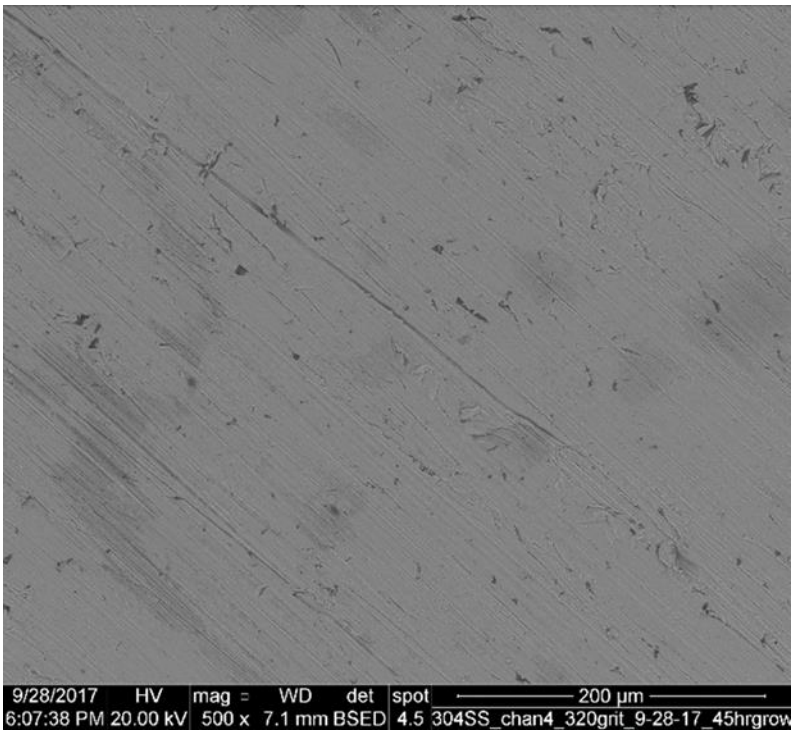

Figure 3-41. 500× BSD E-SEM Image of Biofilm on 41 µm Finish 304SS, Coupon 4 in Test #7. Darker regions which look like spread fluid could either be nutrient broth and/or collections of cells unable to be resolved at higher magnitudes due to background contrast problems associated with increased roughness.

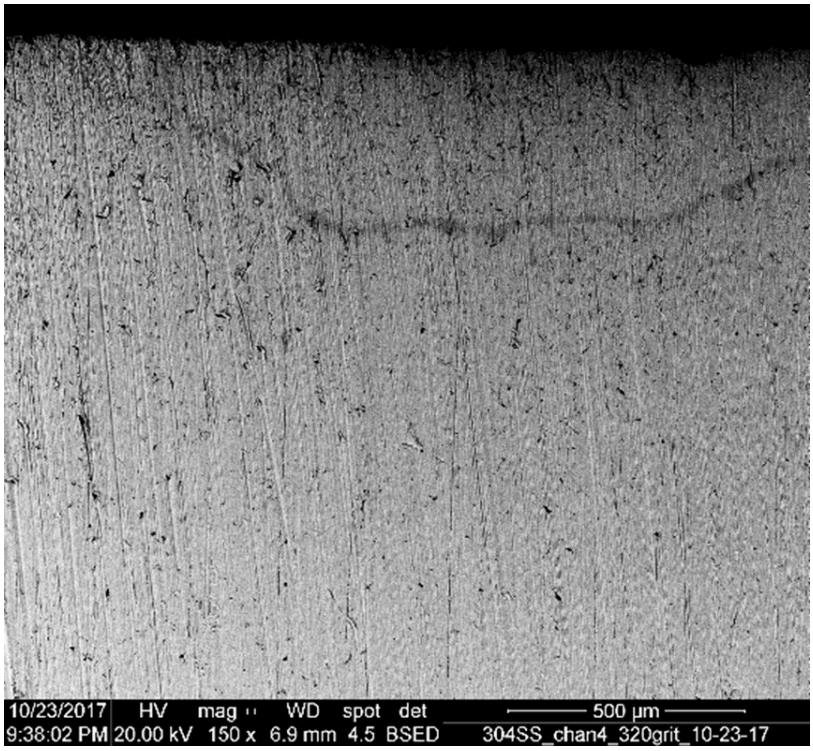

Figure 3-42. 150× BSD E-SEM Image of Biofilm on 41 µm Finish 304SS, Coupon 4 in Test #8. Darker ring-like region could either be nutrient broth and/or collections of cells which were unable to be resolved at higher magnitudes, due to background contrast problems associated with increased roughness.

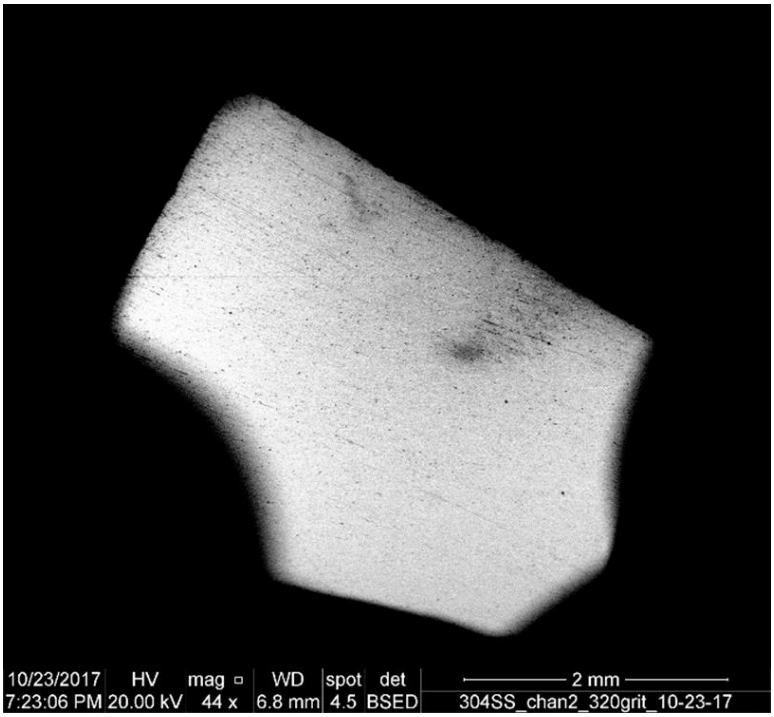

Figure 3-43. 44× BSD E-SEM Image of Biofilm on 41 µm Finish 304SS, Coupon 2 in Test #8. Darker regions which look like spread fluid could either be nutrient broth and/or collections of cells unable to be resolved at higher magnitudes due to background contrast problems associated with increased roughness.

Figure 3-44a-b demonstrate the difficulty in resolving the 41 µm surfaces to detect bacterial cells. Figure 3-44a and Figure 3-44b are of the exact same location with different detector imaging. When the magnification of the dark droplet-like regions were increased, the location and detection of any cells could not be confirmed.

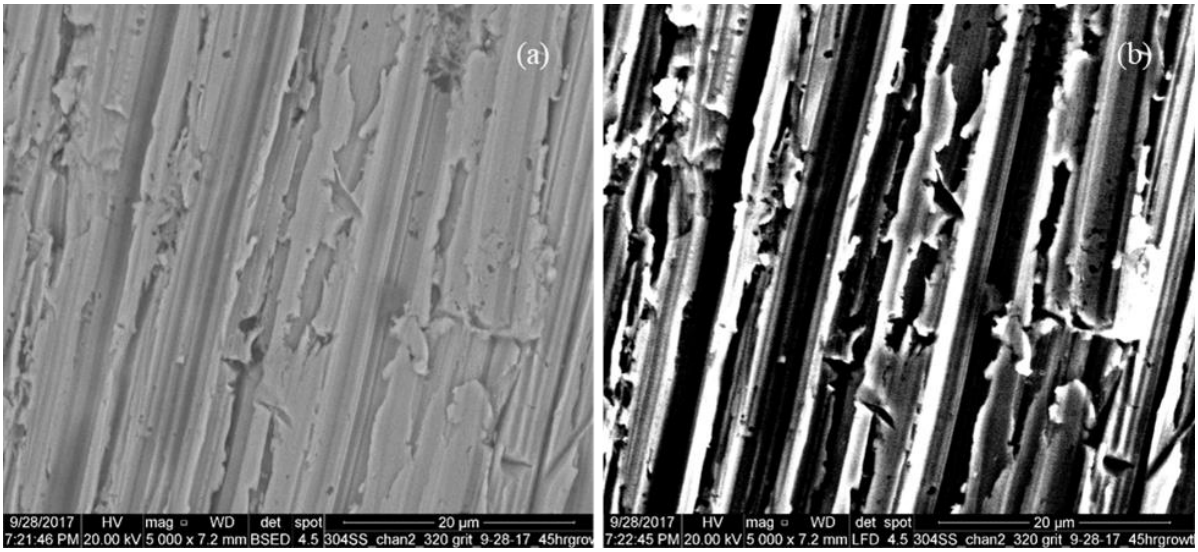

Figure 3-44a-b. E-SEM Imaging Taken from the Same Region on 304SS with 41 µm Finish. Taken from Coupon 2 in Growth Test# 7. Both BSD and SED imaging had too much background contrast from the roughness to adequately identify the presence of cells. (a) 5000× BSD E-SEM Image. (b) 5000× SED E-SEM Image

3.2.3. Influence of Pre-wash and Post-wash on *E. coli* Growth

There were few differences between the different types of pre-washes and post-washes on the observed biofilm growth. The main difference between the PBS and DI H_2O washes was that nearly all of the coupons which were post-washed with 5mL or more of PBS had the presence of salts on their surface. Coupons pre-washed with PBS but not post-washed generally had less salts on their surface than the coupons post-washed with PBS. Also, coupons washed with DI H_2O did not have salts deposited on their surface. The BSD images of coupons rinsed with PBS indicate that the salts present have a higher atomic mass than the bacteria observed but a lower atomic mass than the stainless steels. PBS is composed of inorganic salts such as NaCl, KCl, Na_2HPO_4, and KH_2PO_4. The building blocks of most organisms are carbon, hydrogen, nitrogen and oxygen, which are all lighter than the potential salts within PBS. Given this, it is very likely that salts observed were from the PBS washing solution.

As mentioned in section 3.3.1, the rinsing of the coupons with aqueous media after sterilization but before inoculation and after harvesting coupons may have had an effect on the shapes of the biofilms observed. Biofilm Shape 1 was most frequently found on coupons that did not undergo a post-wash. Biofilm shape 2 was most frequently found on coupons that underwent a pre-wash but not a post-wash. Biofilm shape 3 was most frequently found on coupons that underwent a post-wash. However, these were not definitive rules and these trends did not hold in every instance.

It should also be noted that the post-washing of the material coupons frequently pushed cells around on the material surfaces, either all but completely washing the cells from the surface or leaving behind a residue of cells shaped like a broth droplet. There was no significant observed difference in how the cells were pushed around between the 0.02, 0.25 and 7 μm surfaces. When the coupons were rinsed with DI water after harvesting, they were more likely to leave a residue of cells from where droplets once were. When the coupons were rinsed with 5 - 15mL of PBS after harvesting, there were more likely to be nearly entirely rinsed off the surfaces. However, this was not always true. Additionally, when coupons from the same growth test were post-washed with the same volume of fluid sometimes the cells were completely washed away and sometimes a residue was left behind.

It may also be significant to consider what effect the sterilization method of the coupons may have had on the surface conditioning of the substrates. It is likely that all of the fluids the coupons came in contact with had a role in the initial conditioning film that formed on the coupons surfaces when they were placed in the bioreactor. This includes the isopropanol used for sterilization, any DI H_2O or PBS washings, and the influent medium. However, it would be nearly impossible to speculate the effect each fluid had on either the passivation layer of the stainless steel or the initial conditioning film prior to biofilm formation at this point in time.

Table 3-11 organizes all of the growth tests by the pre-wash the substrates were exposed to. Table 3-12 organizes all of the growth tests by the post-wash the *E. coli*/SS coupons were exposed to after harvesting.

Table 3-11. Growth Tests with the Same Substrate Wash Prior to Insertion in the Bioreactor

Same Pre-Washes		
Wash	**Test #**	**Coupons**
None	1	All
None	8	All
None	9	All
PBS	2	All
PBS	3	All
PBS	4	All
PBS	5	All
PBS	7	All
DI H2O	4	All
DI H2O	6	All

Table 3-12. Growth Tests with the Same Coupon Wash After Harvesting

Same Post-Washes			
Wash	**Test #**	**Coupons**	**Volume/Wash (mL)**
None	1	All	0
None	2	x 2 x 4	0
None	3	1 x x x	0
None	4	1 x x x	0
None	7	All	0
None	8	All	0
None	9	All	0
PBS	2	1 x 3 x	1 to 2
PBS	3	x 2 3 4	5, 10, 15 (2,3,4 respectively)
PBS	4	x 2 3 4	5, 10, 15 (2,3,4 respectively)
DI H2O	5	All	5
DI H2O	6	All	3

Color Key (Material Types) for Tables 3-6 to 3-10	
	= 304SS
	= AgSSA
	= CuSSA
	= test ran both AgSS and CuSS coupons, in separate channels

Figures 3-45a-b, 3-46a-b, 3-47, and 3-48 all demonstrate the presence of the salts observed on the surfaces of coupons which were pre-washed with PBS and post-washed with 5mL of PBS. A mentioned above, these salts were likely deposited on the surface from the PBS rinsing solution.

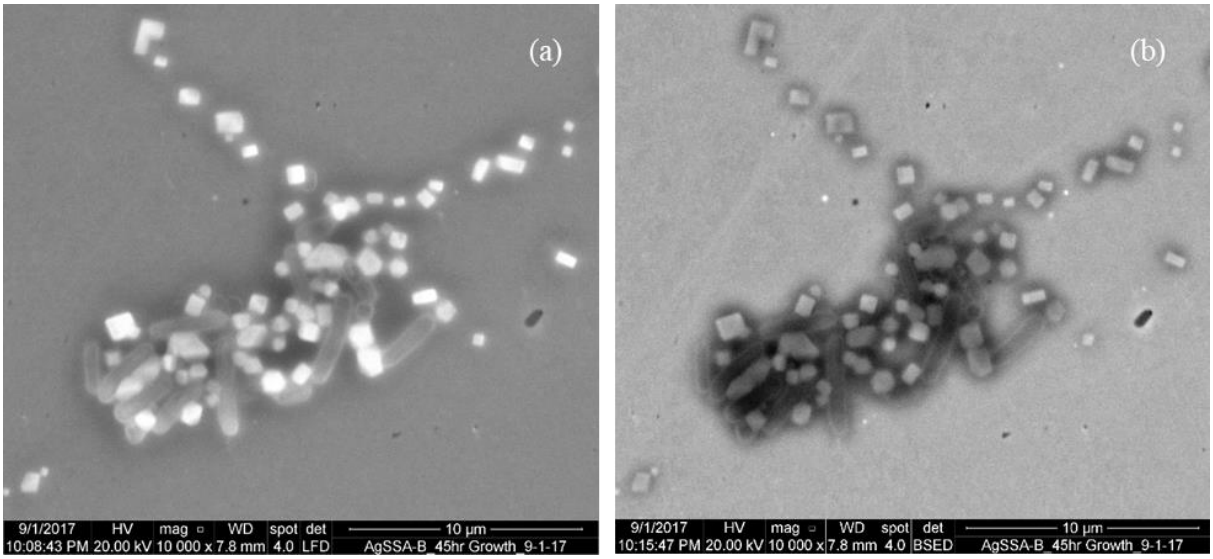

Figure 3-45a-b. E-SEM Imaging of Bacteria with Salts in Same Region of Coupon 2 in Test #4. The BSD image suggests that the salts are of higher atomic mass than the bacteria but lower atomic mass than the steel, suggestive that they are from PBS. (a) 10,000× SED E-SEM Image of Bacteria with Small Salts on AgSS. (b) 10,000× BSD E-SEM Image of Bacteria with Small Salts on AgSS

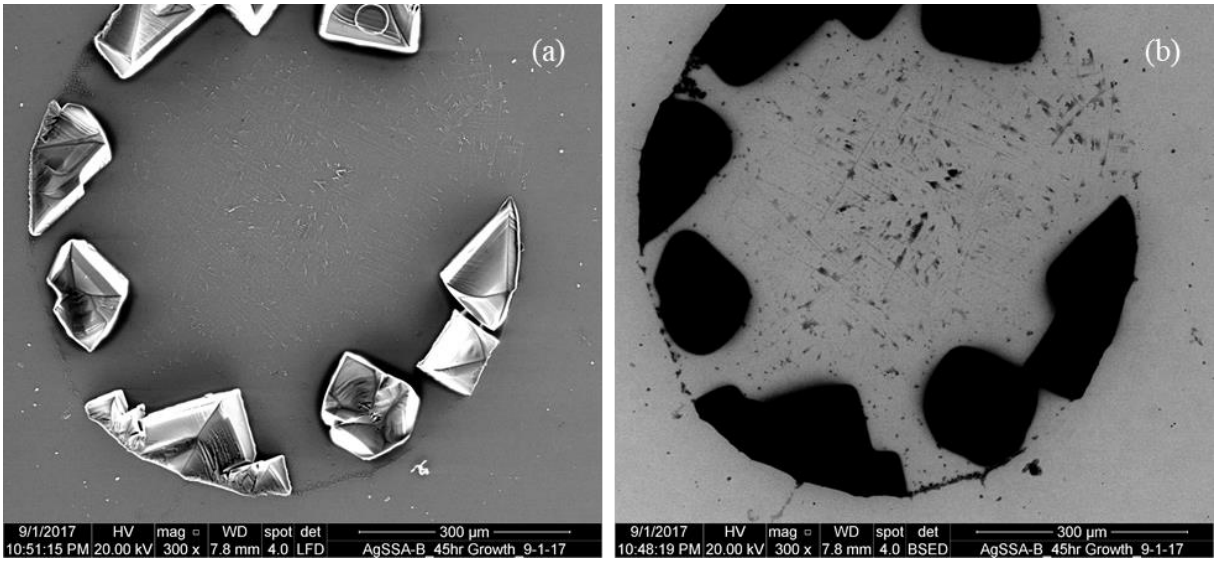

Figure 3-46a-b. E-SEM Images of Large Salts, Taken from the Same region on Coupon 2 in Test #4. The BSD image suggests the salts are of significantly lower atomic mass than the steel, which is suggestive that they are from PBS. (a) 300× SED E-SEM Image of Salts on AgSS. (b) 300× BSD E-SEM Image of Salts on AgSS

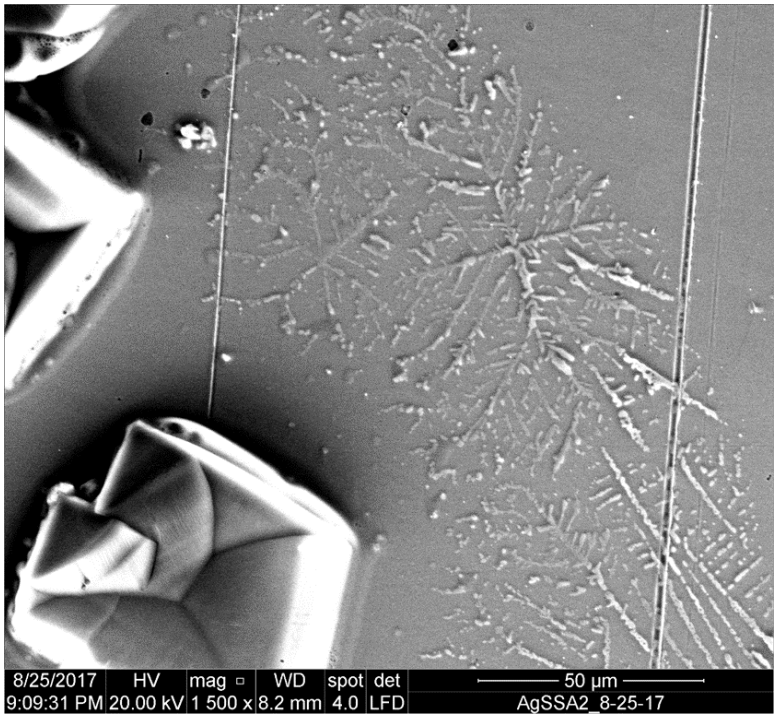

Figure 3-47. 1500× SED E-SEM Image of Small and Large Salts on AgSS, Coupon 2 in Test #3

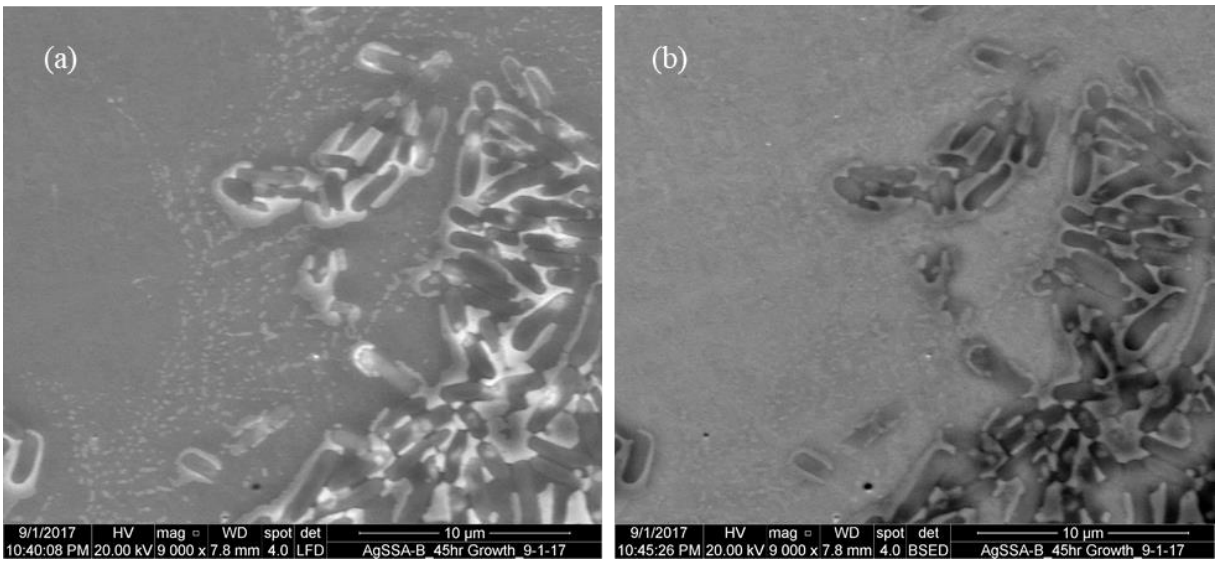

Figure 3-48a-b. E-SEM Images of Bacteria with Small Salts in Same Region on Coupon 2 in Test #4. The BSD image suggests that the salts are of higher atomic mass than the bacteria but are of lower atomic mass than the steel, which likely means they were from the PBS washing. (a). 9000× SED E-SEM Image of Bacteria with Salts on AgSS. (b) 9000× BSD E-SEM Image of Bacteria with Salts on AgSS

Figures 3-49 through 3-53 demonstrate some of the effects of post-washing on the observed biofilms. Figures 3-49 through 3-52 shown some of the ring-like residues observed. Figure 3-53 is representative of what a surface looked like when most of the bacteria were rinsed away with the post-wash.

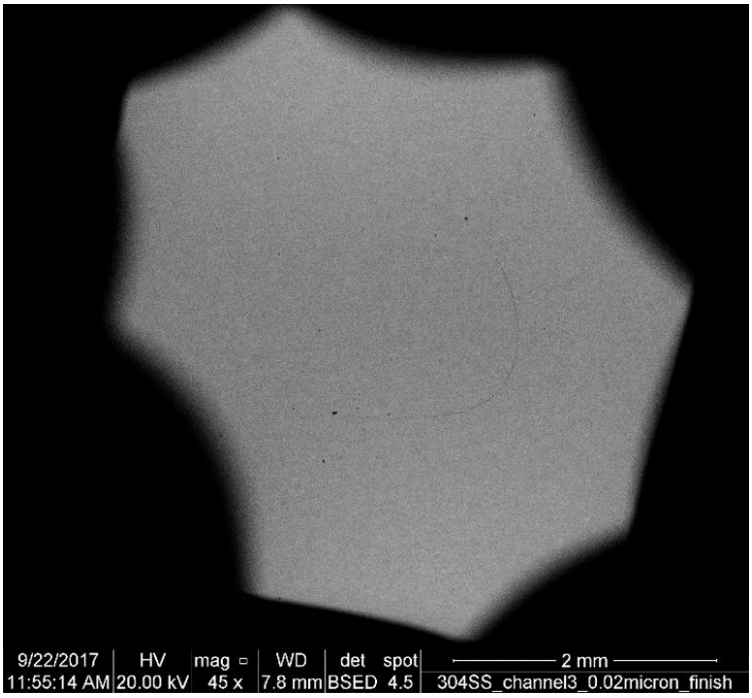

Figure 3-49. 45× BSD E-SEM Image of Bacteria Residue After 3mL DI H2O Post-Wash on 304SS, Coupon 3 in Test #6

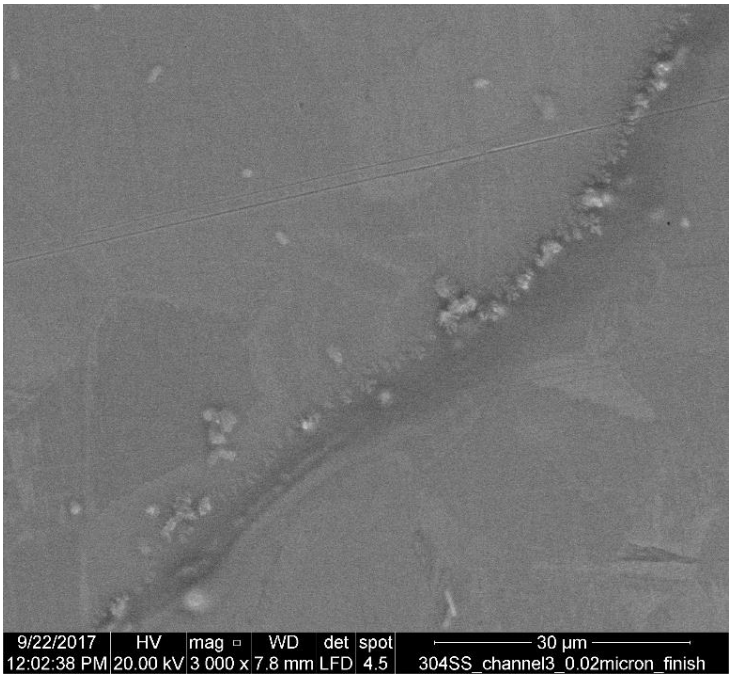

Figure 3-50. 3000 × SED E-SEM Image of Ring Residue Shown in Figure 3-49, from Coupon 3 in Test# 6. The salts present are likely due to contamination from autoclaving the coupons within the bioreactor, not the DI H_2O. This was the only test where the coupons were sterilized this way. It caused contamination problems on the surface. See Figure 4-1a-b. There were no other instances of salts present when washing the surfaces with DI water apart from Test #6.

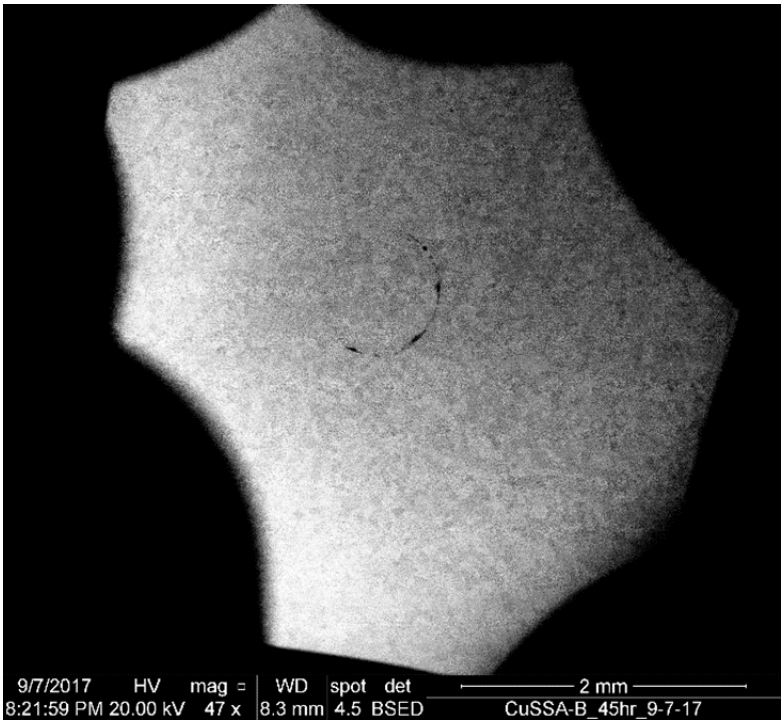

Figure 3-51. 47× BSD E-SEM Image of Bacteria Residue Ring After 5mL DI H_2O Post-Wash on CuSS, Coupon 2 in Test #5

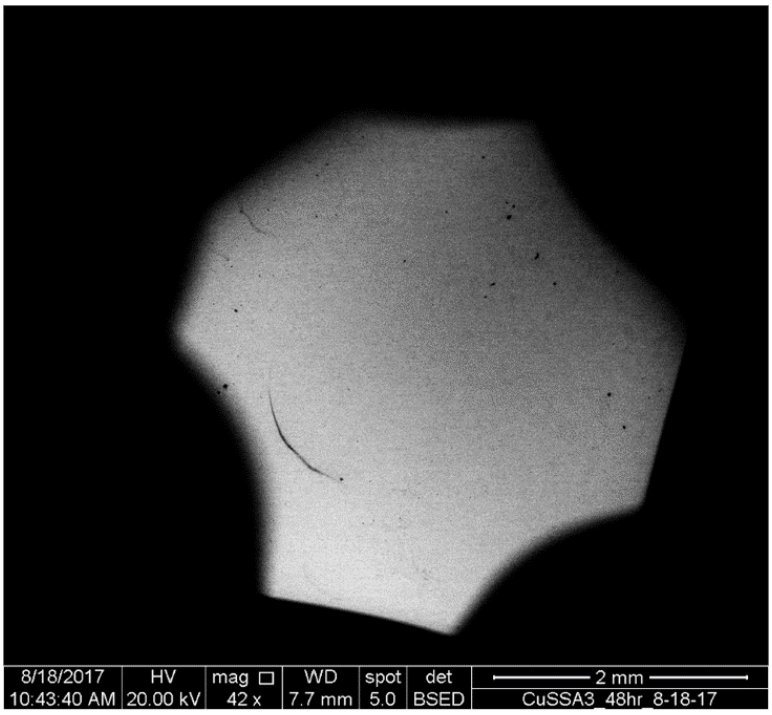

Figure 3-52. 42× BSD E-SEM Image of Bacteria Residue Ring After 1-2mL PBS Post-Wash on CuSS, Coupon 3 in Test #2

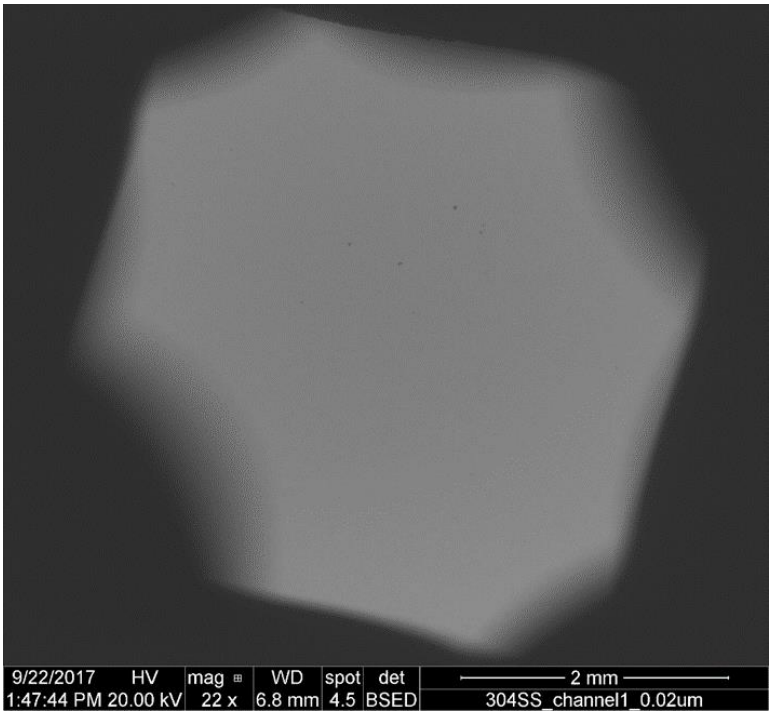

Figure 3-53. Typical Image of what a coupon surface looked like when all or most of the bacteria were washed away by the post-wash. 22× BSD E-SEM Image of 304SS, Coupon 1 in Test #6. There may also be contaminates from the autoclave in this sample, as mentioned in Figure 3-50.

3.2.4. Influence of Longer Growth Duration and Elevated Temperature on *E. coli* Growth

Almost all of the tests were run for 48 hours at room temperature. The two tests which were run for 96 hours were run at 37 ± 3°C in an attempt to optimize growth conditions to obtain more mature biofilms. 37 °C is the optimal growth temperature for *E coli*. Allowing for a longer duration of time for growth allows for more growth to occur. Significantly more mature biofilms did not result, but the biofilms which resulted appeared to have had a higher concentration of cells compared to the biofilms grown for 48hr at room temperature (approximately 20 °C). Table 3-13 organizes all of the growth tests by the duration of their continuous phase growth.

Table 3-13. Growth Tests with the Same Growth Durations

Same Continuous Phase Growth Durations	
Duration (hr)	**Test #**
48	1
48.42	2
48	3
45	4
45	5
46	6
45.75	7
96.33	8
94.66	9

Color Key (Material Types) for Tables 3-6 to 3-10	
	= 304SS
	= AgSSA
	= CuSSA
	= test ran both AgSS and CuSS coupons, in separate channels

Figures 3-54a-b through 3-59a-b compare the biofilms grown on each material type for 48 hours at room temperature versus 96 hours at 37°C. All of the coupons in Figures 3-54

through 3-59 were not post-washed after harvesting. Consistently, the biofilms grown on the same material at 37°C for 96hr have significantly more cells present along the biofilm droplet edge than the biofilms grown at room temperature for 48hr. Additionally, the biofilms grown at 37°C for 96hr tended to have dense regions with multiple layers of cells present whereas many of the biofilms grown at room temperature for 48hr appear to have many regions with on single layers of cells. Figures 3-54a-b and 3-55a-b compare biofilms grown on 304SS at the different time and temperature conditions. Figures 3-56a-b and 3-57a-b compare biofilms grown on CuSS at the different time and temperature conditions. Figures 3-58a-b and 3-59a-b compare biofilms grown on AgSS at the different time and temperature conditions.

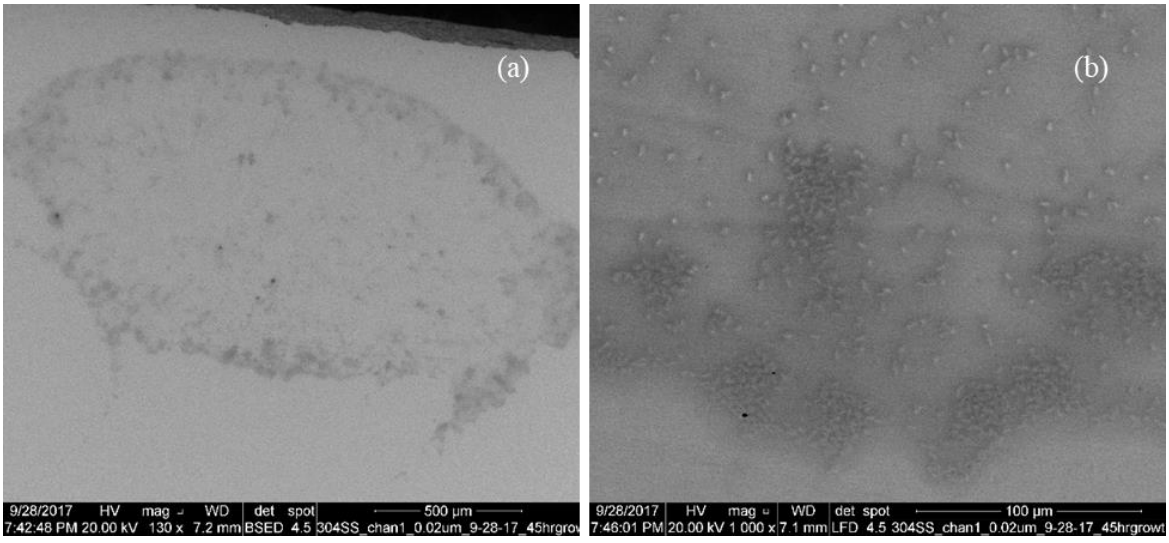

Figure 3-54a-b. Low Magnification and High Magnification of 48 hr RT Biofilm Grown on 304SS. Coupon 1 in Test #7. (a) 130× BSD E-SEM Image (b) 1,000 × SED E-SEM Image

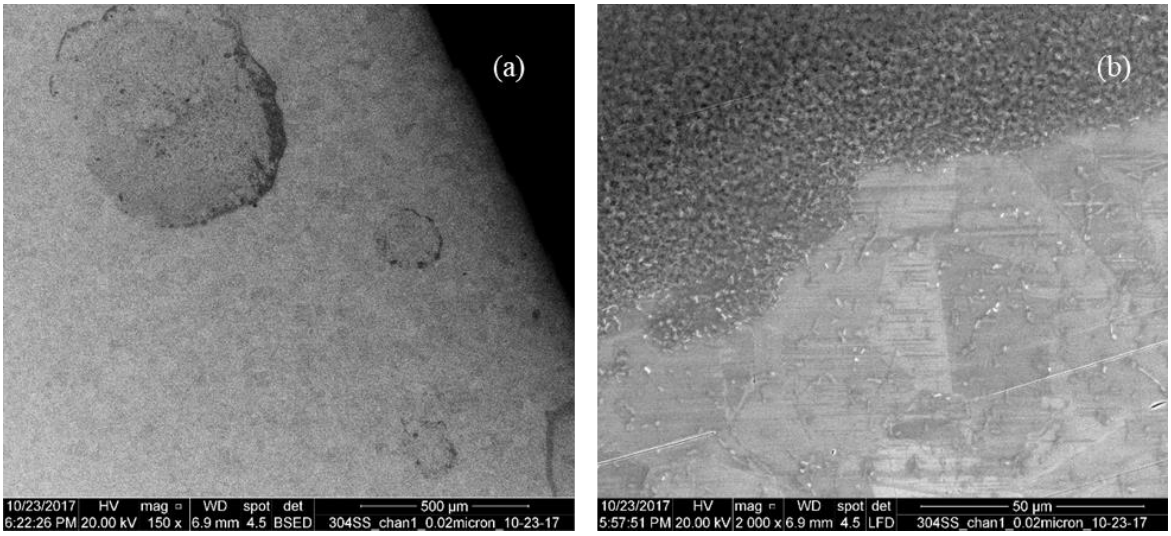

Figure 3-55a-b. Low Magnification and High Magnification of 96 hr 37ºC Biofilm Grown on 304SS. Coupon 1 in Test #8. (a) 150 × BSD E-SEM Image. (b) 2,000× SED E-SEM Image.

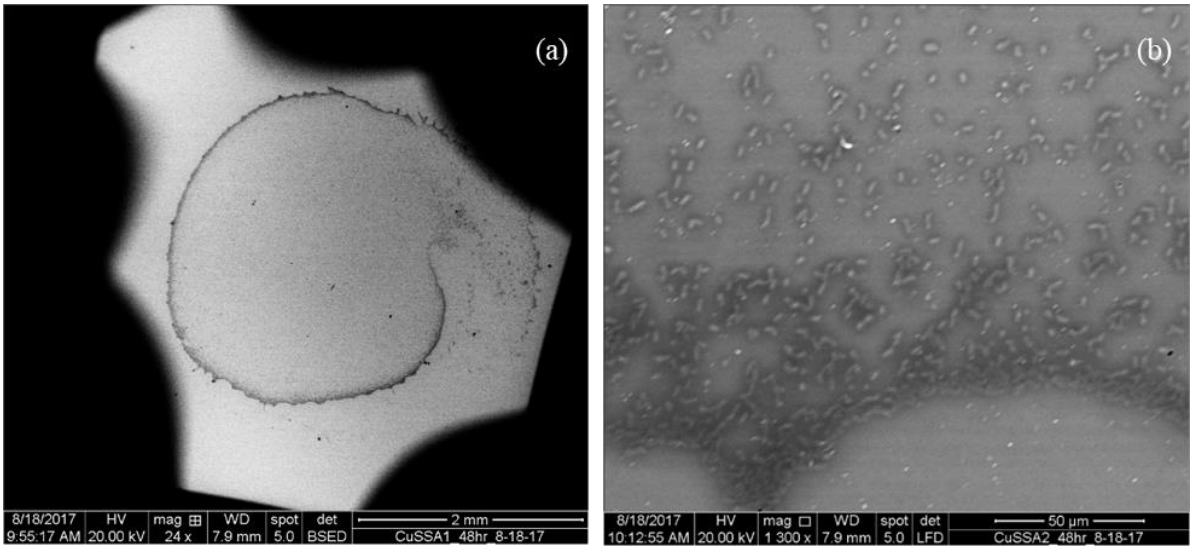

Figure 3-56a-b. Low Magnification and High Magnification of 48 hr RT Biofilm Grown on CuSS. Coupon 1 in Test #2. (a). 24× BSD E-SEM Image. (b) 1,300× SED E-SEM Image

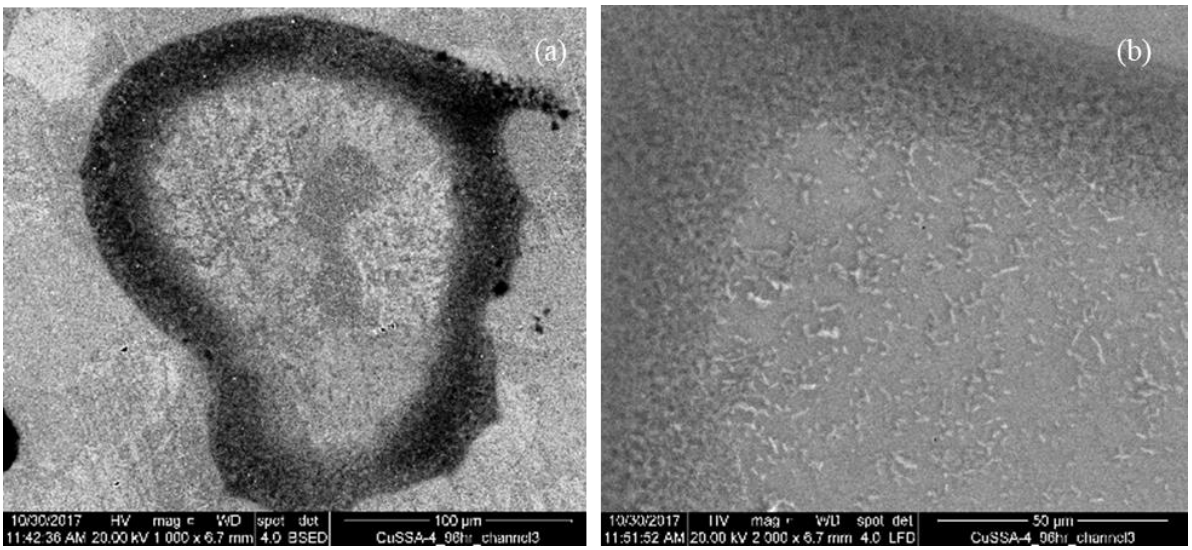

Figure 3-57a-b. Low Magnification and High Magnification of 96 hr 37ºC Biofilm Grown on CuSS. Coupon 4 in Test #9 (a) 1000× BSD E-SEM Image (b) 2000× BSD E-SEM Image

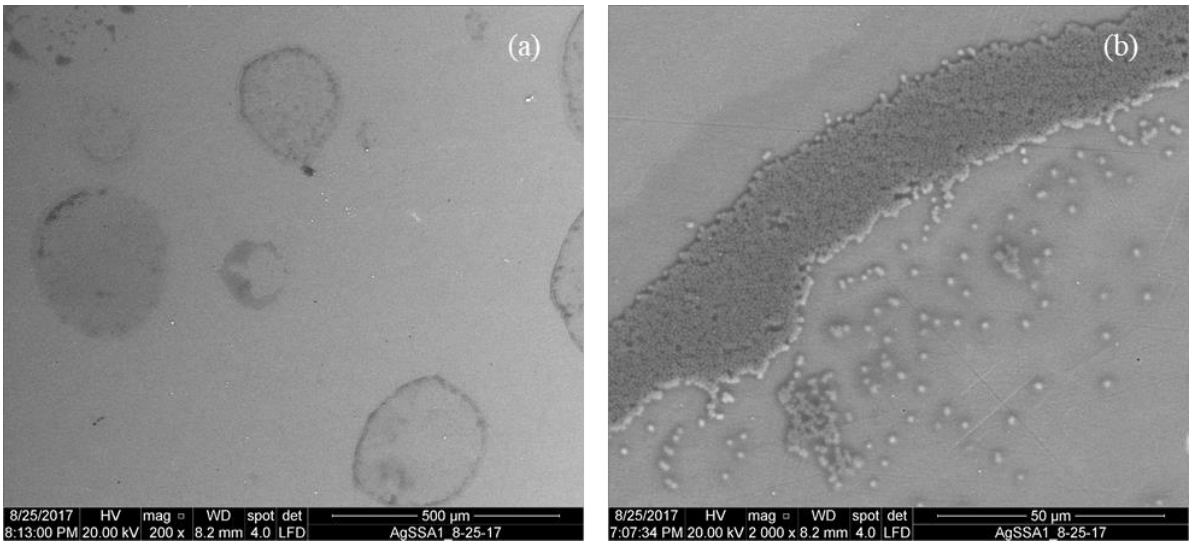

Figure 3-58a-b. Low Magnification and High Magnification of 48 hr RT Biofilm Grown on AgSS. Coupon 1 in Test #3. (a) 200× SED E-SEM Image (b) 2000× SED E-SEM Image

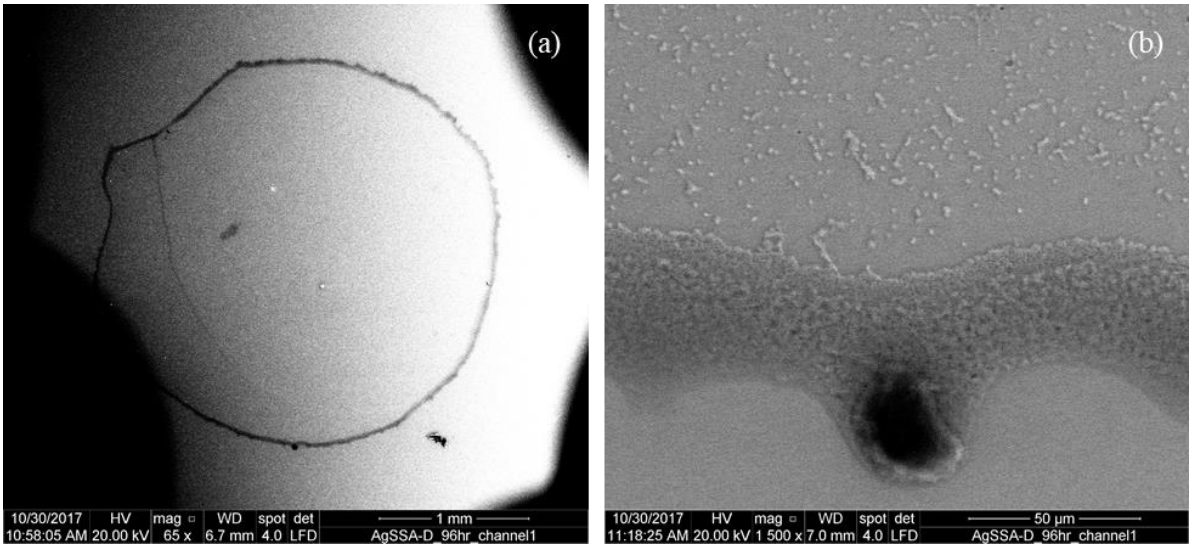

Figure 3-59a-b. Low Magnification and High Magnification of 96 hr 37ºC Biofilm Grown on AgSS. Coupon 3 in Test #9. (Coupon labeled improperly in image, should be C not D) (a) 65× SED E-SEM Image. (b) 1500× SED E-SEM Image

Chapter 4 Discussion

4.1. Biofilm Structure and Stage of Formation

All of the *E. coli* biofilms formed on reasonably smooth surfaces had similar features in regard to their shape and structure. All of the observed biofilms existed in droplet-like shapes on the coupon surfaces, typically with the majority of cells aggregated along the droplet edges and cells either collected in the center of the droplet or scattered throughout the center of the droplet. Multiple biofilm droplets were also frequently observed on a single coupon surface.

The formation of the biofilms into droplet-like shapes could have been due to the influence of the surface forces at play. Water and aqueous solutions tend to bead in spherical shapes to minimize the surface tension of the fluid. The fact the all of the biofilms formed in droplet-like configurations suggests that the surfaces had reasonable wettability to grow biofilms on the surfaces but were also slightly hydrophobic, causing the biofilms to grow primarily in roughly spherical and ovular rings. These observations also suggest that the biofilms only grew in regions where there was permanent or semi-permanent wetting of the coupon surface.

All of the biofilms observed had no evidence of significant EPS production. When they were rinsed after harvesting, the cells were easily pushed around on the surface. In many regions of the biofilms, there was only single-layers of cells attached to the surface, even on the biofilms grown at optimal temperature for twice the amount of time in continuous phase. These three observations suggest that all of the observed biofilms had only reached the reversible attachment phase of growth. This suggests that *E. coli* ATCC 8739 was unable to reach maturity on these three stainless steel surfaces within a 2 to 4-day timeframe under the environmental growth conditions of influent nutrient level, temperature, flow rate, and pH used within this study. The fact that there was little difference between the baseline stainless steel and the copper- and silver-containing stainless steels suggests that longer durations of time would be needed to achieve mature ATCC 8739 biofilms within the current reactor set-up, independent of the potential biocidal effects of the copper- and silver-alloyed stainless steels.

4.2. Influence of Material Type – Surface Chemistry and Alloy Microstructure

Material type appeared to have little effect on the biofilms observed. There was no observed correlation between bacterial attachment and a material's surface chemistry and microstructural features. Bacteria attachment appeared to be completely random and based entirely on where the coupon surfaces were consistently wetted during growth. This was interesting, since the copper- and silver-alloyed stainless steels used are well documented within literature as having an antimicrobial affect over a 24-hour time frame, as commonly determined through the Japanese standard JIS-Z-2801(2010).

The majority of the material coupons were polished to a submicron finish (an order of magnitude smaller than most bacterial cells) in an attempt to eliminate the effect of surface roughness in preferential bacterial attachment, leaving any preferential bacterial attachment to be based on material surface chemistry and microstructural features. The fact that there was little difference between the biofilms grown on the copper- and silver-alloyed stainless steels and the baseline 304 stainless steel may suggest a few things:

1) The size scale of the surface chemistry and surface features of the steels was either too small or too large to influence preferential bacterial attachment with those specific regions of the surface. The grain structures of the steels are quite macroscopic when compared to the size of a single *E. coli* cell. Similarly, the EDS detection of the bare metal surfaces indicated that the majority of the biocidal elements were either fairly uniformly spread throughout the bulk or concentrated within precipitates that were orders of magnitude smaller that the size of a single *E. coli* cell. The size scale of the roughness on the submicron stainless steels was also too small to

influence bacterial attachment. The literature suggests that bacteria interact the most with surface features on size scales that are approximately the same size as a single cell [17].

2) The lack of difference in the observed biofilms between material types may also suggest that on submicron polished stainless steel surfaces, *E. coli* interacts with stainless steel surfaces in essentially the same way, especially when the heterogeneous microstructural features of the steel are on size scales drastically different than size of a bacterial cell. The extremely smooth surfaces on the submicron polished steels may have also eliminated any topographical differences of steel surface pits, dents, or small cracks, thus also eliminating any preferential attachment to those locations. The steel surfaces were also not electropolished or otherwise etched, so there was no preferential etching of the steel grain boundaries, and thus no observed effects on attachment at the grain boundaries or defects within the steels.

3) Perhaps the formation of the surface conditioning film generated from exposure to in a nutrient broth medium, or excess carbon from isopropanol and acetone, or from rinsing with DI H_2O or PBS, effectively inhibited the "antimicrobial" steels' ability to elute the biocidal metal ions effectively from their surfaces. Surface roughness may also influence the formation of the conditioning film on the surfaces of the steels, by possibly effecting the wettability of the steels and/or how ions are eluted from the steel surface. However, since the 41 µm polished surfaces could not be imaged properly and the majority of the analysis was performed on submicron polished surfaces, there were no conclusions which could be drawn on this effect within this study.

4) Perhaps even within a low-flow, low-shear environment, the presumed eluted copper or silver ions were washed away from the surfaces into the effluent before they could impart any antimicrobial effect to the *E. coli*. Conversely, perhaps the low flow environment gave any eluted ions more time to interact with the conditioning film and perhaps be trapped within this layer by chemically bonding with it. Bonded metallic copper and silver likely have less of a biocidal effect than ionic copper and silver. The concentration of the eluted biocidal ions could have also simply not been in sufficiently high concentrations to impart a biocidal effect on the E coli.

It should also be noted, that by E-SEM analysis alone, it was impossible to definitively and directly assess whether the observed cells were alive or dead. However, none of the observed cells appeared to be damaged; most appeared to be fully hydrated with their cell membranes intact. Additionally, though there is also the factor of increased temperature to consider, the biofilms appeared to have grown denser over the 96-hour continuous phase than they did in the 48-hour continuous phase. This could suggest that the cells on the surfaces were still primarily alive after the 48-hour timeframe of continuous phase growth.

The best way to better assess whether or not the copper-alloyed and silver-alloyed stainless steels imparted a biocidal effect on the *E. coli* grown in comparison to the baseline 304 stainless steel would be to incorporate some type of cell viability testing between material types in the future. The reason biofilm resistant surface testing was not performed as outlined in ASTM E2467-13 was due to the fact that the biofilms grown appeared to not have passed the

reversible stage of attachment, and thus there was concern there would not be enough cells present on the surface to carry out the cell viability assessments with statistical confidence. Additionally, the method outlined within ASTM E2647-13 requires the entire biofilm to be sacrificed, which would have limited the amount of the samples which could be analyzed by E-SEM.

Live-dead cell staining and florescent microscopy could also have been used to assess the location and quantity of live cells on the coupon surfaces. However, florescence microscopy would not have allowed for any insight into location of the cells in relation to the stainless steel microstructures. Also this technique was outside of our budget due to the high cost of the dyes required.

It would also be useful to try to better understand the mechanism of biological inhibition on the copper- and silver-containing stainless steel surfaces. This could be done by measuring the amount of copper or silver ions eluted into broth media over a given period of time, potentially using Inductively Coupled Plasma Mass Spectrometry or Atomic Absorption Spectroscopy. The effect of surface conditioning from the nutrient broth medium and sterilization via soaking in isopropanol on the elution mechanism of the antimicrobial metals would also be significant to better understand. This perhaps could be done using x-ray photoelectron spectroscopy and/or secondary ion mass spectrometry.

4.3. Influence of Roughness

There was little observed difference between the 0.02 µm, 0.25 µm and 7 µm surface finished coupons. This suggests that reasonably smooth surfaces likely have similar surface interactions with the *E. coli* cells. The 41 µm finished surfaces analyzed had too much background contrast to adequately visualize within the E-SEM. However, low magnification images of the 41 µm polished surfaces showed similar droplet-like regions using the BSD detector. These regions could have just shown where the surfaces were wetted with high concentrations of broth, or they may have been regions which contained cell growth.

Literature suggests that bacterial cells prefer attachment to rougher surfaces over smoother surfaces[25]. As so it is likely that the 41 µm polished samples did contain cells on their surfaces despite being unable to image the cells. Rough surfaces provide a larger surface area for bacteria to attach to as well as an evacuation space which can provide protection against shearing forces in a flow environment [25]. Other studies have shown that bacteria will align themselves longitudinally within the grooves on a rough steel surface when the size of the grooves are on a size scale similar to single bacterial cells. When the grooves are much larger or smaller than the size scale of a bacterial cell, attachment is generally much more random [17].

Additionally, the contrast problems associated with the imaging of the rougher samples may had something to do with them being visualized in E-SEM (at low vacuum with water vapor) rather than standard high-vacuum SEM. Other studies[17] have been able to visualize bacteria on rougher stainless steel surfaces with standard SEM. However, biological samples in standard SEM must be dried, fixed, and coated in order to be imaged (at the very least, coated). The surfaces of the rough coupons were wet when analyzed. Perhaps the instance of liquid

caught in the grooves of the rougher surface caused charging which caused the contrast problems.

It should also be noted that industrial and commercial steel surfaces are typically quite rough; they are generally polished between a 180 – 320 grit (106 µm - 41 µm diameter media) finish. The smooth submicron finished surfaces in this study allowed for assessment of the effect the microstructural and surface chemistry features of the steels on bacterial attachment. However, practically speaking, surfaces in current industrial systems and processes would likely not be polished to a submicron level. It is extremely difficult and costly to manufacture and maintain very smooth steel surfaces for industrial and commercial applications. These larger roughness finishes have grooves which are large enough to harbor bacteria. A 180-grit finish is generally considered sanitary for dairy, food, and pharmaceutical applications, but maintaining sufficiently sterile surfaces in food industry and pharmaceutical settings requires frequent high pressure washing, scrubbing, and/or the use of disinfectants [25].

4.4. Influence of Pre-wash and Post-wash

The pre-washing of the coupons did not appear to have a direct effect on the biofilm growth. Prewashing was expected to potentially have an effect on growth, since it could have influenced the conditioning of the stainless steel surfaces. However, there was little observed difference between the coupons of the same material which were pre-washed or not pre-washed. Since all of the substrates were cleaned and sterilized in the same way, and then exposed to the liquid broth media for essentially the same amounts of time, perhaps the brief rinsing of the coupons before growth had little overall effect on the conditioning film of the steel surfaces.

The sterilization method of soaking the coupons in isopropanol may have had a larger effect on the conditioning film than rinsing the coupons with DI H_2O or PBS before growth. Hedberg et al. found that low molecular weight carbon contamination played the largest role on the wettability of stainless steels. Such contamination could come from solvents such as acetone and isopropanol. They were unable to detect trend between the contact angle and the oxide layer on the steels[23]. Mantel et al. also suggest that as a surface contamination layer on stainless steel increases, the surface free energy decreases, making it more hydrophobic[55].

Prewashing of the coupons with PBS also deposited salts onto the coupon surfaces rinsed with it. Coupons which were post-washed with PBs tended to have more salts present.

Post-washing had little observed effect apart from pushing cells around on the surface or leaving a ring-like residue on the surface. There was no significant observed difference in how the cells were pushed around between the 0.02, 0.25 and 7 µm surfaces. Post-washing the surfaces primarily gave insight that the bacteria were still loosely adhered to the surfaces, which suggested that all of the bacteria grown with a 48-hour continuous phase at room temperature likely only reached the reversible attachment phase of growth.

4.5. Influence of Temperature and Time

The 96-hour continuous growth tests grown at 37°C were designed to optimize growth conditions over a longer time frame in an attempt to develop more mature *E. coli* biofilms on the

material surfaces. This had limited success. Qualitatively, the coupons grown with a 96-hour continuous phase at 37°C did appear to have denser cell aggregations than the biofilms grown under 48-hour continuous phase at room temperature. As touched on already in the previous discussion sections, the optimization of the *E coli* growth within the limits of the reactor system was not able to produce biofilms which demonstrated EPS production or other hallmarks of a more mature biofilm.

Additionally, the fact that the biofilms grown at optimal temperature for twice the duration of continuous phase growth demonstrated increased growth suggests that the majority of the cells visualized on the surfaces of the coupons grown with a 48-hour continuous phase growth at room temperature were likely mostly alive at the time of visualization.

It could have been interesting to have rinsed some of the 96-hour, 37°C test coupons after harvesting to see if more cells remained attached to the surface compared to the coupon samples grown for 48-hour at room temperature. If more cells remain attached to the surface after rinsing, it could be indicative of a more mature biofilm structure having been formed in the 96-hour tests than in the 48-hour tests.

4.6. Potential Contamination and Cell Morphology

There were two main concerns which arose with potential contamination issues. The first contamination concern regarded deposits potentially made on surfaces inside the bioreactor channels via autoclaving. The second concern was the potential for bacterial contamination of the pure strain of *E. coli* ATCC 8739 within the bioreactor system and subsequently the biofilms.

In regard to the first concern, it was decidedly a good decision to sterilize the stainless steel coupons within isopropanol rather than within the bioreactor chambers via autoclave. The coupons in Test # 6 were sterilization via autoclave inside the bioreactor with the glass slide coupon holders. This resulted with a large amount of contaminates to be deposited on all of the test coupons. This was not too surprising, as the cleanliness level of the water source used during steam sterilization within the autoclave is uncertain. The autoclaves in VT Kelly Hall are used for the sterilization of a wide variety of materials, including biowaste. Due to the contaminates size and shape they appear to have been some kind of salt. This also may have given some insight to the presence of random salts and organic “fuzzies” throughout all of the test samples. Figure 4-1a-b gives an example of this contamination observed in Test #6.

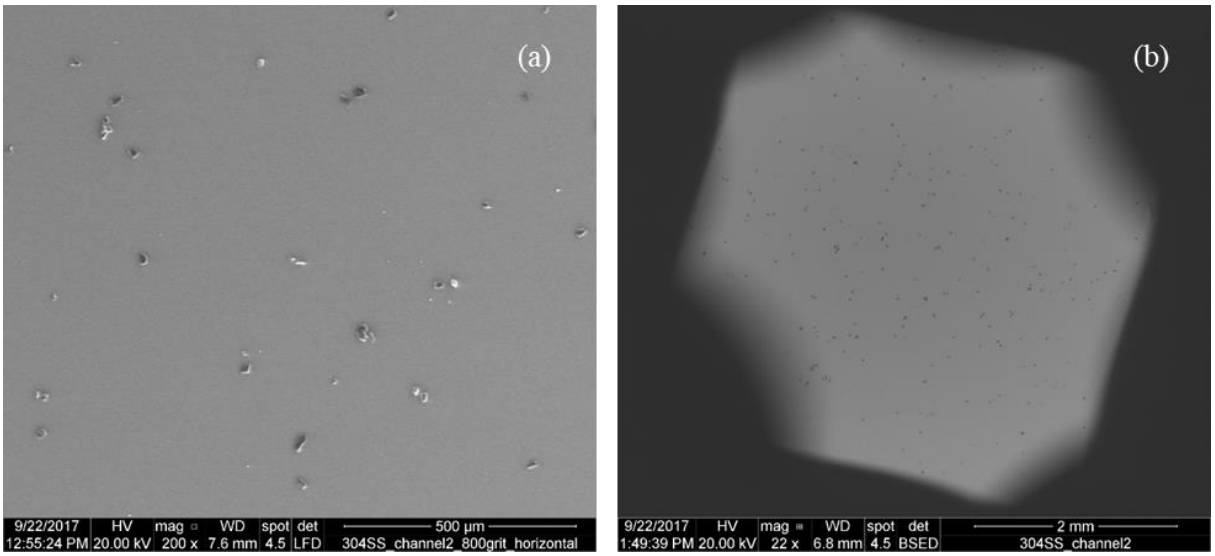

Figure 4-1a-b. Autoclave Contamination on 304SS Surface, Coupon 2 in Test# 7. (a) 200× SED E-SEM Image. (b) 22× BSD E-SEM Image. The BSD image suggests the autoclave contamination is of a lower atomic mass than the steel, so it is likely some type of organic or small inorganic salts, both of which are commonly sent through autoclave sterilization and are found in low-purity water.

If the same type of contaminates were consistently deposited inside the bioreactor chambers during sterilization, it is likely that they may have been washed onto the coupon surfaces at some point during the continuous growth phase. Autoclaving the bioreactor with its test coupons inserted in it is part of the standard ASTM-E2647-13. Depending on how much the autoclave steam could influence the surface conditioning of the test coupons in a study, this could potentially be one drawback of the drip flow reactor system or an area which could produce inconsistencies between lab groups.

In regard to the second contamination concern, it should be noted that nutrient broth and nutrient agar are non-selective growth mediums, meaning they have the potential of growing a wide variety of organisms, not just ATCC 8739. There are many points of access during the bacteria manipulation in which bacteria from the lab environment or the natural human flora could contaminate the pure strain used within the bioreactor. This is why proper aseptic technique and managing a sterile environment is so important. The bioreactor system itself also has many components which could expose the reactor to the open air if they are not properly sealed. As so, it would not hard to imagine the potential for bacterial contamination within the biofilm samples. However, by E-SEM analysis alone, it is difficult to assess the exact bacteria present on the observed surfaces. More refined methods such as genetic analysis of the bacteria present and less refine methods such as gram-staining could better identify the exact strain or type of bacteria present.

Almost all of the observed cells on the test coupons fit the description for the typical morphology of *E. coli* bacteria, a rod-like bacterium with a length of approximately 1 – 2 microns and width of approximately 0.5 – 1 microns. However, there were slight noticeable differences in the cells observed and one particular instance where there appeared to be two distinct cell types in close proximity to each other on the same coupon surface. This occurred on

a AgSS sample, Coupon 1 in Test #3, where there was a cluster of cells which appeared more spherical and a collection of cells which appeared more rod-like. Figure 4-2 shows this observation through a SED imaging. The image was post-processed in ImageJ to measure the length and width of the two shapes of observed cells. The measurements are labeled on Figure 4-2 and are tabulated in Table A-1 in Appendix A. Figure 4-3a shows the same region in Figure 4-2 except through BSD imaging. The two features have approximately the same level of grayscale associated with them in this image, suggesting they both are likely cells, and that one of them isn't a collection of something other than cells. Figure 4-3b shows the same region in Figure 4-2 at a lower magnification. The approximate region in Figure 4-2 is outlined with a blue box.

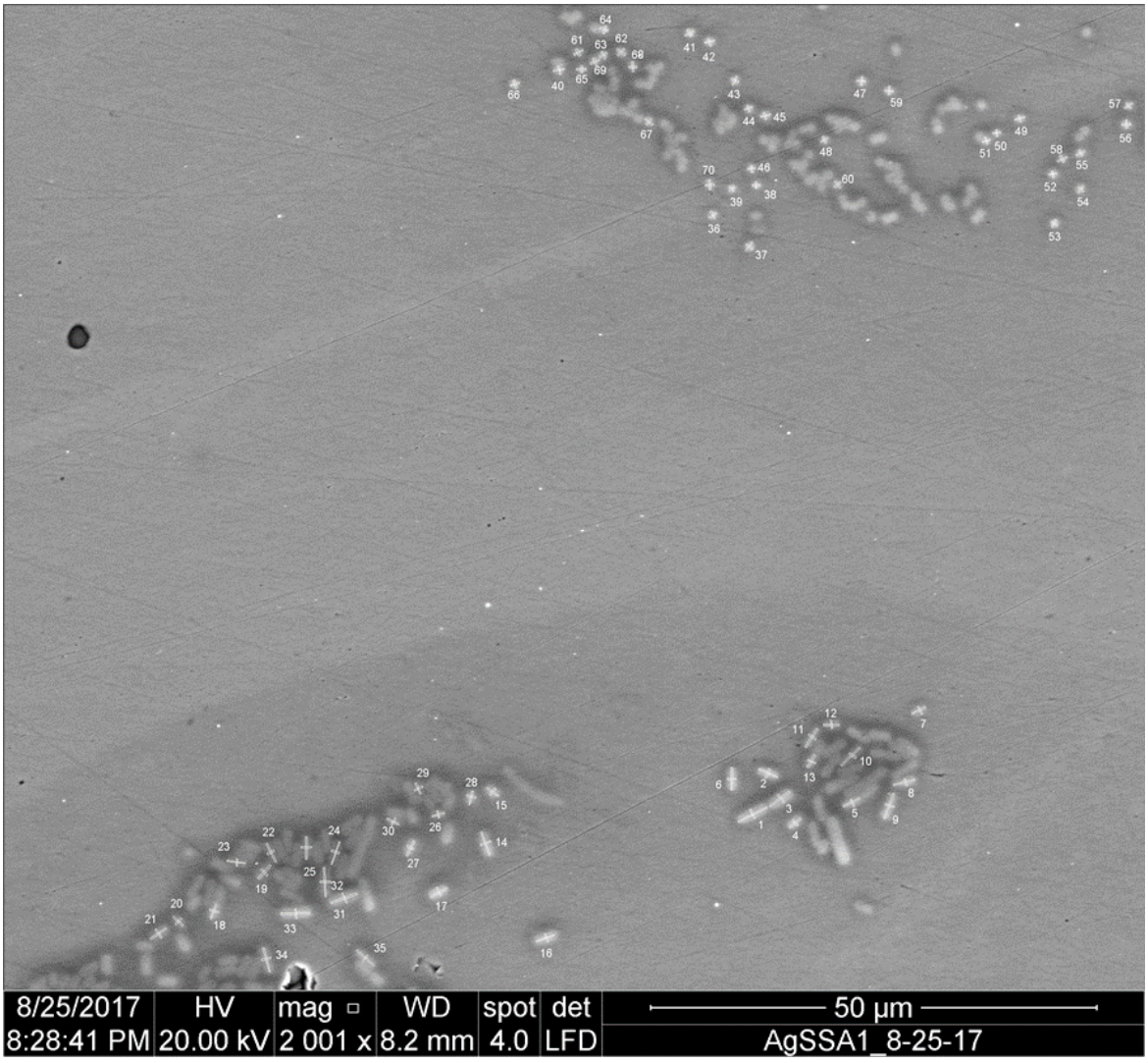

Figure 4-2. 2,001× SED E-SEM Image of Different Bacteria Shapes Found on AgSS, Coupon 1 in Test #3. The image was post-processed in ImageJ for length and width measurements of the bacteria. This image shows the length and width measurements made in ImageJ and which are presented in Table A-1. The image was zoomed in as much as possible while processing in ImageJ in order to make as accurate of measurements as possible.

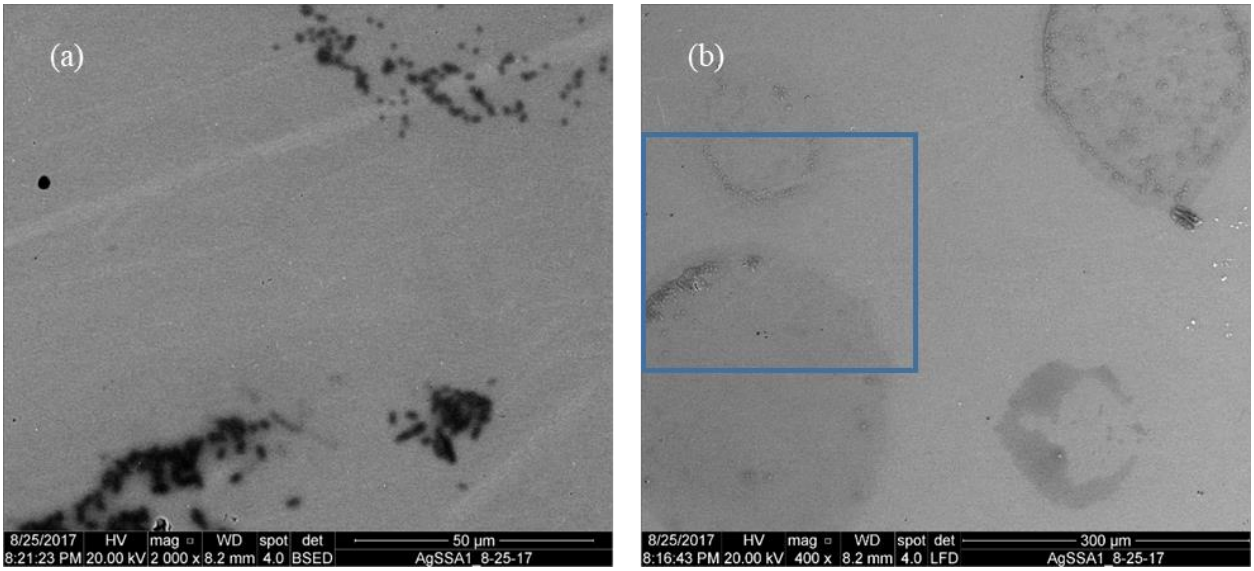

Figure 4-3a-b. (a). 2,000 × BSD E-SEM Image of Same Region Imaged by SED in Figure 3-45. Both features are likely bacteria since they have the same contrast in BSD against the steel surface. (b) 400 × SED E-SEM Image, shows a higher magnification of the region imaged in Figure 4-2. The specific region of the bacteria imaged in Figure 4-2 is outlined in the blue box. Both (a) and (b) are of AgSS Coupon 1 in Test# 3, as in Figure 4-2.

The average length of the more rod-like bacteria was 2.23 ± 0.69 µm and the average width of the more rod-like bacteria was 0.95 ± 0.07 µm. The average length of the more spherical bacteria was 0.96 ± 0.06 µm and the average width was 0.85 ± 0.09 µm. With consideration of the standard deviations associated with the measurements, both cell clusters objectively fall within what is considered a typical morphology for *E. coli*.

However, there was also speculation that perhaps some of the differences in cell shapes may have been due to *E. coli* expressing a different morphology. No EPS production was observed within the biofilms grown in this study, and as so there was no observed complex matrix structures. However, Serra et al. assessed that *E. coli* bacteria had different cell morphologies at distinct locations within biofilms which were grown on solid agar surfaces and imaged in standard SEM (dehydration and fixation of samples). They also assessed that the different cell morphologies were related to the production of either curli or flagella, the primary structural components to the *E coli* EPS matrix[56]. It was assessed that "In the outer edge zone of the macrocolony, and in the lower areas nearer to the agar surface, the rod-shaped cells are in a state of post-exponential growth and are still dividing, and are also still able to produce flagella. In the upper, central zones of the biofilms the cells have entered stationary phase due to nutrient limitation, causing them to stop producing flagella, and instead become smaller ovoid cells that produce curli."[57] This could suggest that perhaps the differences in the cells shapes seen in Figure 4-2 are due to a different morphology being expressed. Perhaps the more rod-shaped cells are merely undergoing reproduction whereas the sphere-shaped ones are not.

However, if that is not the case, and the sphere-like cells are a bacterial contaminate, a good candidate would be *Staphylococcus aureus* which is spherical and typically up to 1 µm

diameter in size. *S. aureus* is also a part of the natural human skin flora, making it easy to spread from human hands onto other surfaces.

With the question of potential bacterial contamination, the morphology of the bacterial between the three material types was called into question. As so, a few choice images were selected to take length and width measurements of the bacteria cells observed on AgSS, CuSS and 304SS. All of the measurements were made through post-processing in ImageJ, just as in Figure 4-2.

Figure 4-4 is an image taken from a different region on the same coupon in 4-2. The length and width measurements are tabulated in Table A-2 in Appendix A.

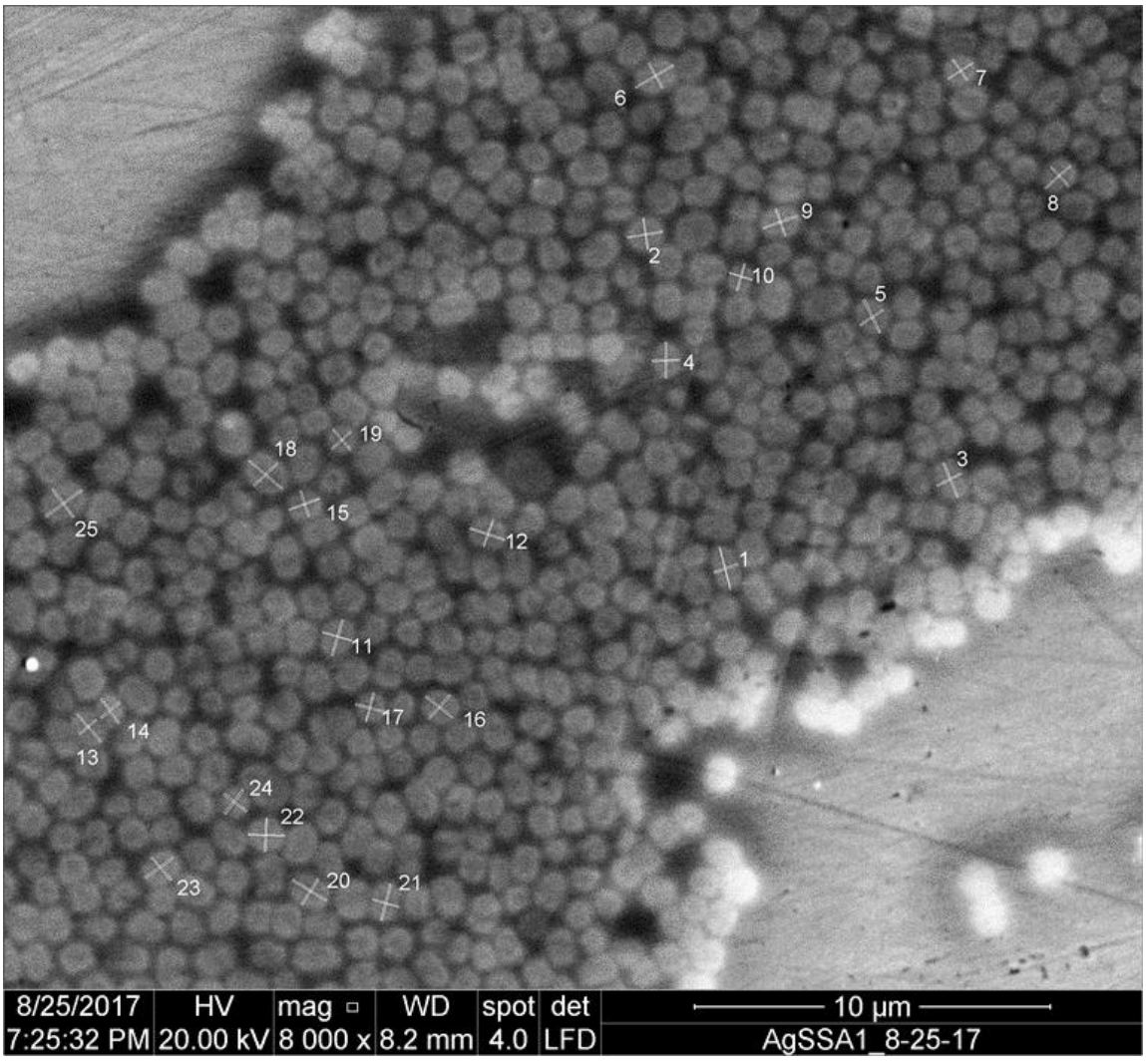

Figure 4-4. 8000× SED E-SEM Image of bacteria found within a different region of the same sample as in Figure 4-2. AgSS Coupon 1 in Test # 3. The image was post-processed in ImageJ for length and width measurements of the bacteria. This image shows the length and width measurements made in ImageJ and which are presented in Table A-2

Figure 4-5 is an image taken from a different region on 304SS from Coupon 1 in Test #1. The length and width measurements are tabulated in Table A-3 in Appendix A.

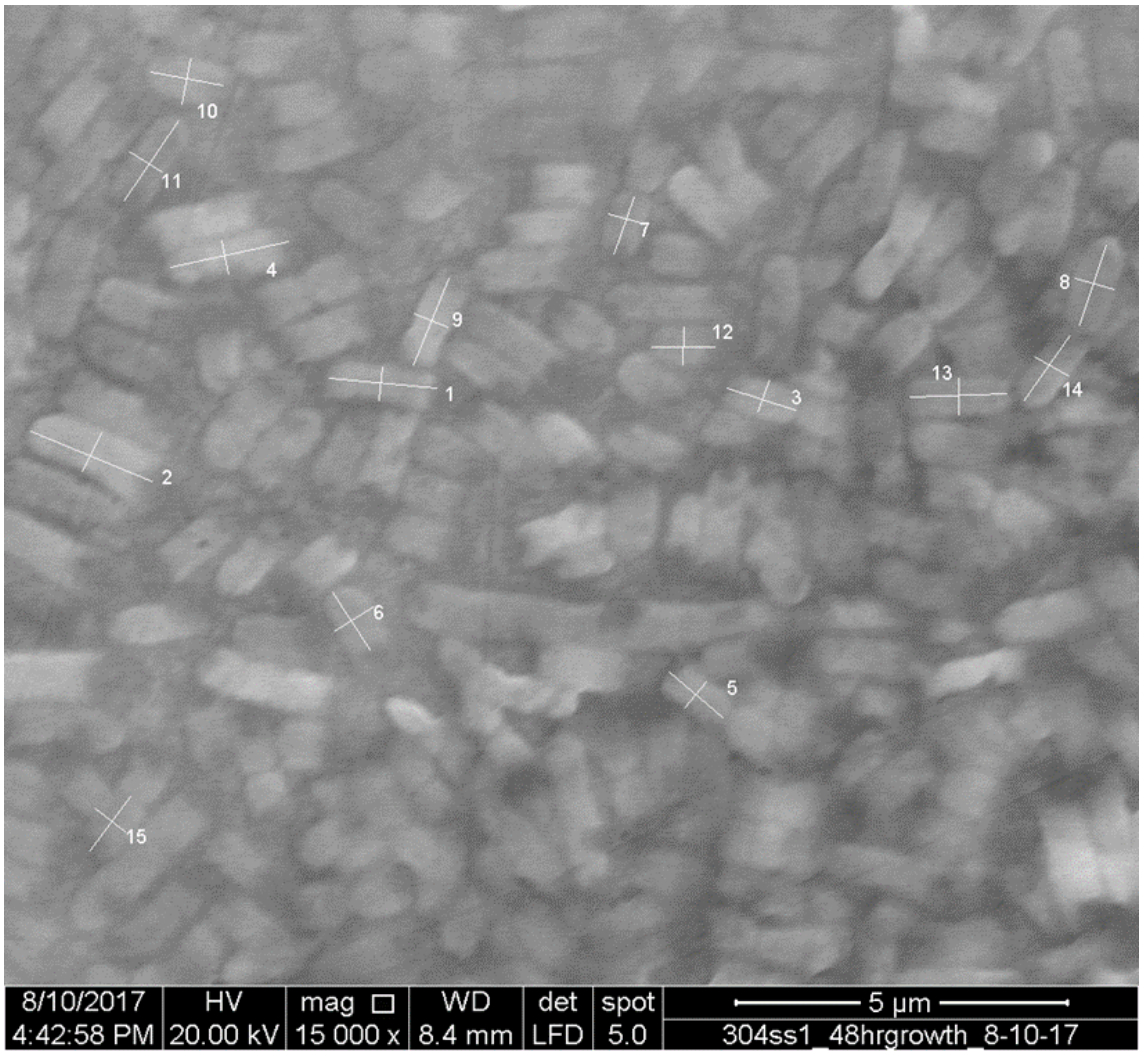

Figure 4-5. 15,000× SED E-SEM Image of Bacteria on 304SS, Coupon 1 Test #1. The image was post-processed in ImageJ for length and width measurements of the bacteria. This image shows the length and width measurements made in ImageJ and which are presented in Table A-3.

Figure 4-6 is an image taken from a different region on 304SS from Coupon 2 in Test #1. The length and width measurements are tabulated in Table A-4 in Appendix A.

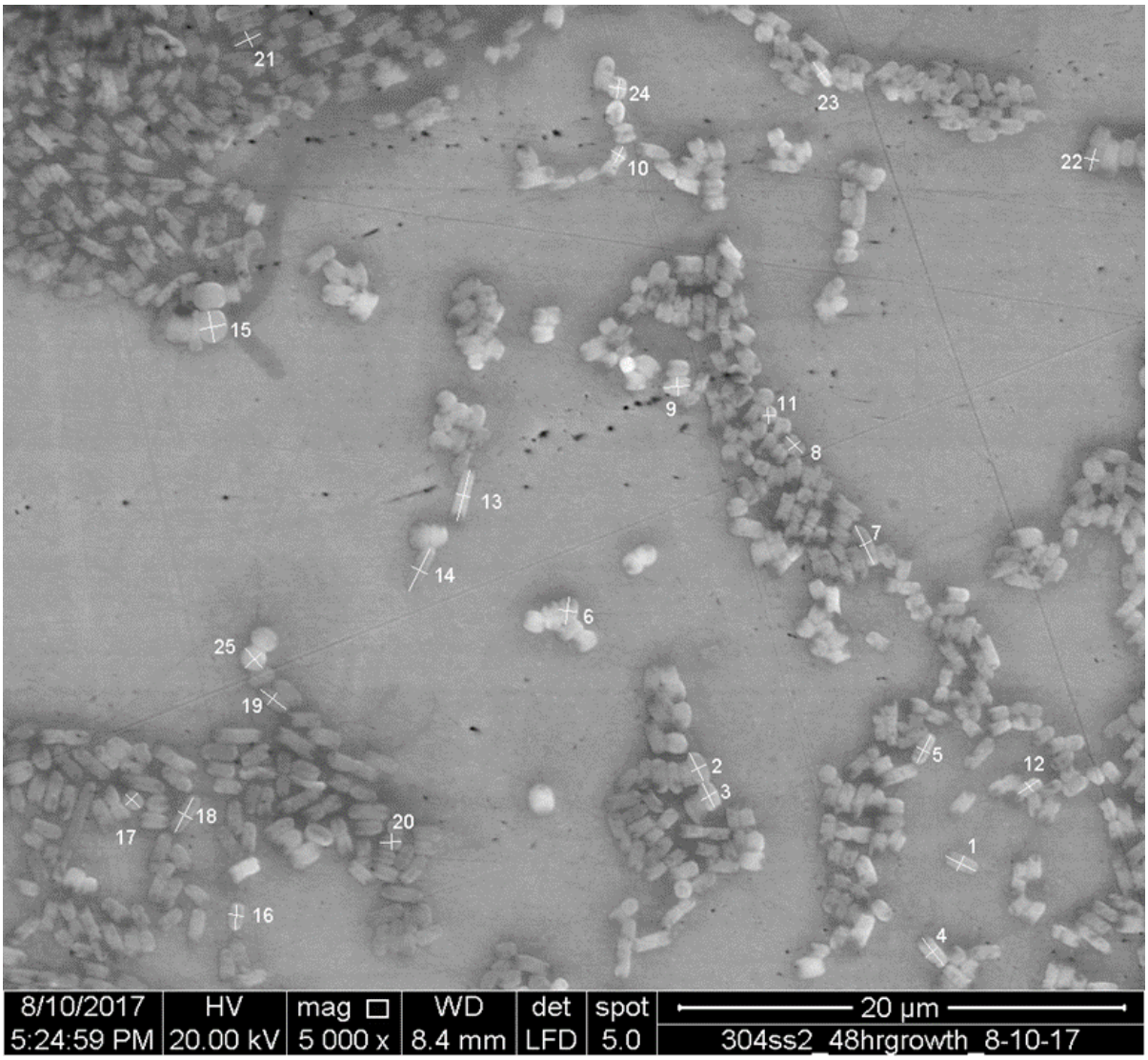

Figure 4-6. 5,000× SED E-SEM Image of Bacteria on 304SS, Coupon 2 Test #1. The image was post-processed in ImageJ for length and width measurements of the bacteria. This image shows the length and width measurements made in ImageJ and which are presented in Table A-4.

Figure 4-7 is an image taken from a different region on 304SS from Coupon 3 in Test #7. The length and width measurements are tabulated in Table A-5 in Appendix A.

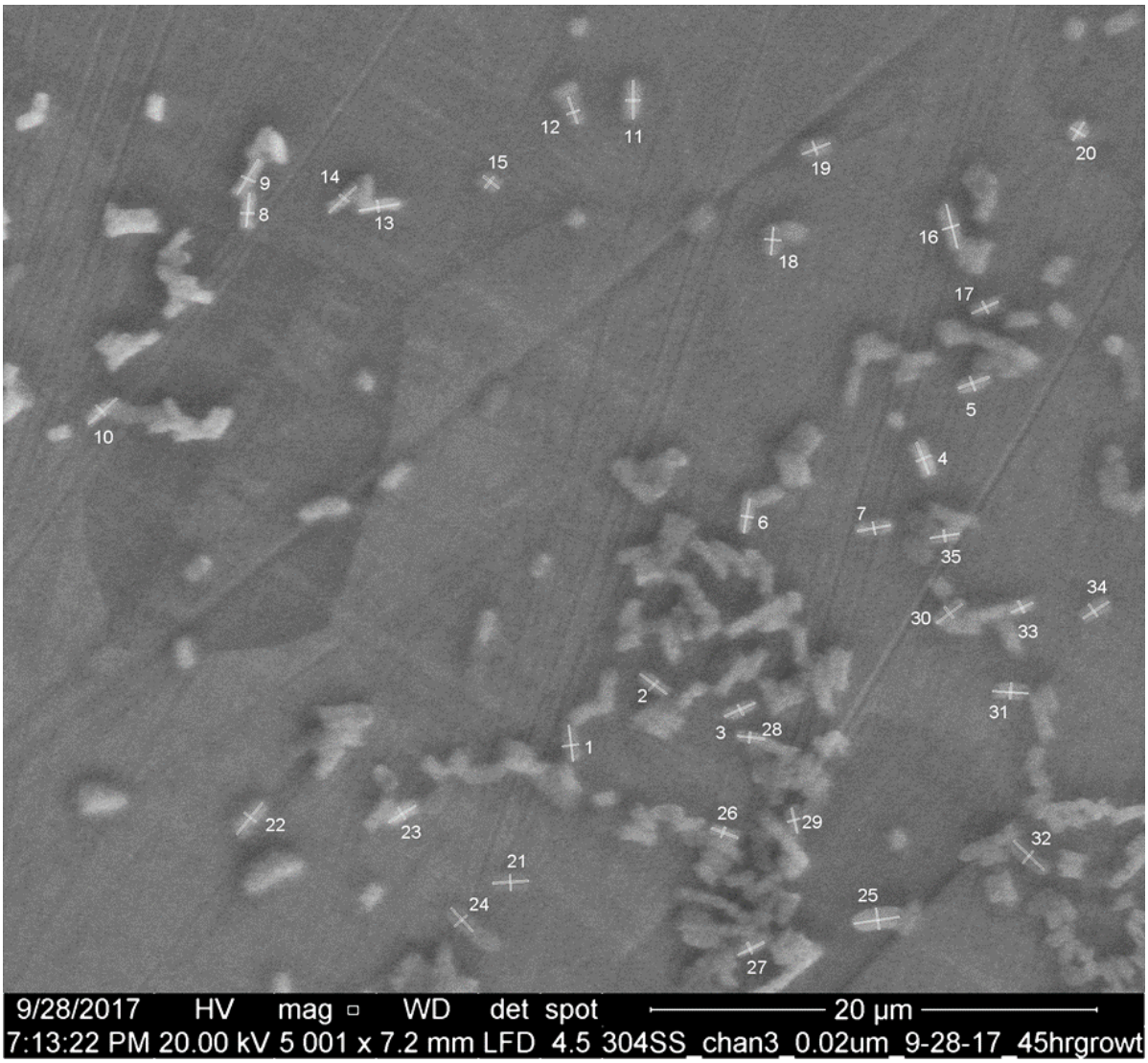

Figure 4-7. 9,000× SED E-SEM Image of Bacteria on 304SS, Coupon 3 Test #7. The image was post-processed in ImageJ for length and width measurements of the bacteria. This image shows the length and width measurements made in ImageJ and which are presented in Table A-5.

Figure 4-8 is an image taken from a different region on CuSS from Coupon 3 in Test #2. The length and width measurements are tabulated in Table A-6 in Appendix A.

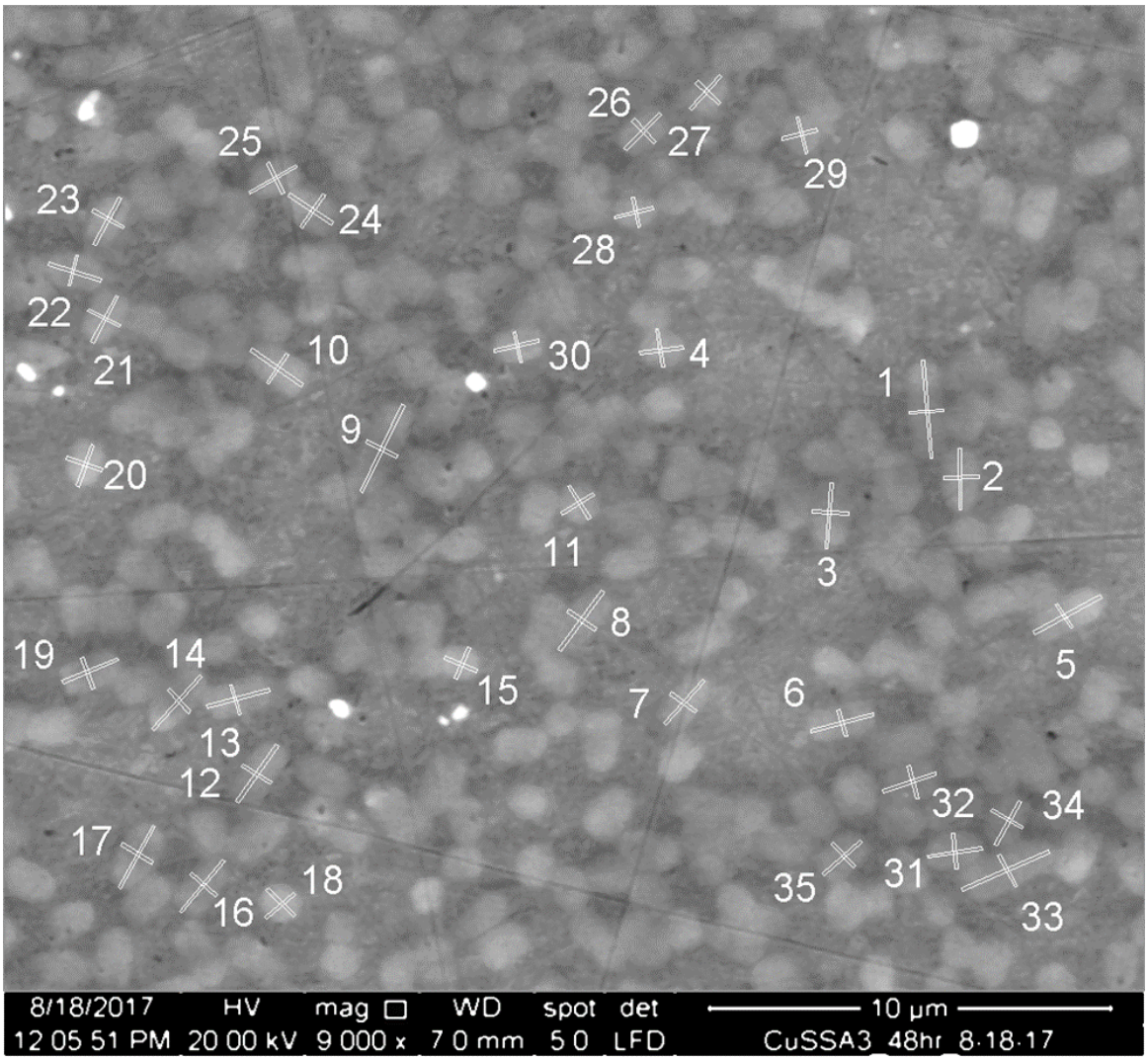

Figure 4-8. 9,000 × SED E-SEM Image of Bacteria on CuSS, Coupon# 3 from Test# 2. The image was post-processed in ImageJ for length and width measurements of the bacteria. This image shows the length and width measurements made in ImageJ and which are presented in Table A-6.

Table 4-1 summarizes the bacterial length and width measurements from Figures 4-2, and 4-4 to 4-8 and Tables A-1 to A-6. Despite the slight differences in how the cells appear visually in the imaging, overall the measured observed cells on a sampling of the coupon surfaces were fairly similar to each other when the standard deviations to the averages were taken into account. As so, it cannot be said with confidence that the *E. coli* cells expressed different morphologies between the different substrate surfaces. Similarly, the presence of bacterial contamination within the observed biofilms cannot be adequately discerned.

Table 4-1. Summary of the Averages and Standard Deviations of the Length and Width Measurements of Bacteria from Figures 4-2,4-4 to 4-8 and Tables A-1 to A-6.

Figure	Material Type	Length (µm)	Width (µm)
4-2. rod	AgSS	2.23 ± 0.69	0.95 ± 0.07
4-2. sphere	AgSS	0.96 ± 0.06	0.85 ± 0.09
4-4.	AgSS	0.94 ± 0.08	0.79 ± 0.09
4-5.	304SS	1.19 ± 0.42	0.57 ± 0.06
4-6.	304SS	1.15 ± 0.44	0.70 ± 0.12
4-7.	304SS	1.45 ± 0.51	0.64 ± 0.10
4-8.	CuSS	1.39 ± 0.51	0.84 ± 0.07

Chapter 5 Conclusion

All of the *E. coli* ATCC 8739 biofilms grown appeared to have not passed the reversible attachment growth stage of biofilm formation and did not display a matured biofilm architecture. This was indicated by the lack of observed EPS production, the ease in which the cells were pushed around on the surface by liquids, and the frequency of the biofilms having regions of single-layers of cells.

The growth conditions could perhaps be modified for longer durations of time, beyond the 96-hour continuous phase timeframe, on order to obtain more mature biofilms in the future. The growth tests rat at optimal temperature for 96-hour continuous phase growth did demonstrate the development of denser collections of cells than were observed within the 48-hour continuous phase growth tests run at room temperature.

On submicron polished surfaces, the stainless steel material type appeared to have little to no effect on the biofilms observed. There was no observed correlation between bacterial attachment and a material's surface chemistry and microstructural features. Bacteria attachment appeared to be completely random and based entirely on where the coupon surfaces were consistently wetted during growth. There was also no biocidal effect of the copper- and silver-alloyed stainless steels in comparison to the baseline stainless steel which was observable by E-SEM alone. This could have been due to: 1) the size of the surface chemistry and surface features of the steels were on orders of magnitude too different in comparison to the size of the bacterial cells for the bacterial cells to preferentially interact with said features. 2) On submicron polished stainless steel surfaces, *E. coli* interacts with the surfaces in essentially the same way, especially when the heterogeneous surface features of the steel are on size scales drastically different than size of a bacterial cell. 3). The eluted copper and silver ions were washed away from the surfaces into the effluent before they could impart any antimicrobial effect to the *E. coli*. The concentration of the eluted biocidal ions could have also simply not been sufficiently high concentrations to impart a biocidal effect on the E coli. 4) The formation of a conditioning film on the "antimicrobial" stainless steels inhibited the elution of the biocidal copper and silver ions from the steels surfaces.

The biofilms grown on the rougher surfaces were unfortunately unable to be effectively visualized via E-SEM, so there is no comparison available of the growth between material types

on a rougher surface. Since the literature suggests that bacterial preferentially attach to rougher surfaces over smoother surfaces, it is likely that these samples did contain cells on their surfaces despite the difficulties with imaging.

Pre-washing the coupons had little effect on the resulting biofilms. However, the sterilization method of soaking the coupons in isopropanol may have had a significant effect on the surface conditioning of the biofilms, as indicated in the literature. Post-washing of the coupons after harvesting primarily had no effect apart from pushing cells around on the surface or leaving a ring-like residue on the surface. There was no significant observed difference in how the cells were pushed around between the 0.02, 0.25 and 7 μm surfaces. Post-washing the surfaces primarily gave insight that the bacteria were still loosely adhered to the surfaces, which suggested that all of the bacteria grown with a 48-hour continuous phase at room temperature likely only reached the reversible attachment phase of growth. It could have been interesting to have rinsed some of the 96-hour, 37°C test coupons after harvesting, to see if more cells remained attached to the surface compared to the coupon samples grown for 48-hour at room temperature. If more cells remain attached to the surface after rinsing, it could be indicative of a more mature biofilm structure having been formed in the 96 hour tests than in the 48-hour tests. Rinsing of the surfaces with PBS all resulted in the deposit of salts onto the surface.

Overall, E-SEM characterization offered good insight into monitoring the growth which occurred on each material coupon under a variety of conditions. However, using this technique alone also had many limitations. This study could be further improved with additional analysis methods such as viable cell quantification through live-dead staining or plating, XPS to assess surface conditioning, and ICPMS to measure the amount of silver and copper ions eluted into solution over a given time frame. This could allow more detailed information to be gathered on the effect of *E coli* growth on what has been documented within literature and marketed by steel companies as being antimicrobial stainless steels. It would be valuable to continue gathering information on the bioresistant properties of these materials within the scope of bacterial biofilms over longer time durations than the conditions outlined within JIS-Z-2801 (2010).

Thus, this type of bioreactor set-up has been proven to be implementable within our lab group. Along with some of the proposed suggestions for more thorough characterization, this system could also easily be modified to accommodate the assessment of a wide variety of bacterial biofilms on an equally wide variety of surfaces in the future.

References

[1] K. Sauer, A.K. Camper, G.D. Ehrlich, J.W. Costerton, D.G. Davies, J Bacteriol 184 (2002) 1140-1154.
[2] P. Stoodley, K. Sauer, D. Davies, J.W. Costerton, Annual Reviews in Microbiology 56 (2002) 187-209.
[3] W.M. de Vos, Npj Biofilms And Microbiomes 1 (2015) 15005.
[4] J.W. Costerton, K.J. Cheng, G.G. Geesey, T.I. Ladd, J.C. Nickel, M. Dasgupta, T.J. Marrie, Annual Review of Microbiology 41 (1987) 435-464.
[5] The Role of Biofilms in Device-Related Infections, Springer 2009.
[6] J.D. Bryers, Biotechnology and bioengineering 100 (2008) 1-18.
[7] H.-C. Flemming, Microbial Biofouling: Unsolved Problems, Insufficient Approaches, and Possible Solutions, in: H.-C. Flemming, J. Wingender, U. Szewzyk (Eds.), Biofilm Highlights, Springer Berlin Heidelberg, Berlin, Heidelberg, 2011, pp. 81-109.
[8] J. Wingender, H.-C. Flemming, International Journal of Hygiene and Environmental Health 214 (2011) 417-423.
[9] B.J. Little, J.S. Lee, International Materials Reviews 59 (2014) 384-393.
[10] J.V. G. Koch, N. Thompson, O. Moghissi, M. Gould, J. payer, International Measures of Prevention, Application, and Economics of Corrosion Technologies Study, in: G. Jacobson (Ed.) NACE International, Houston, TX, 2016, pp. 1-216.
[11] J.S.L. B.J. Little, Microbiologically Influenced Corrosion, John Wiley & Sons, Inc, Hoboken, NJ, 2007.
[12] S.K. Hood, E.A. Zottola, Food Control 6 (1995) 9-18.
[13] H.-C. Flemming, J. Wingender, U. Szewzyk, P. Steinberg, S.A. Rice, S. Kjelleberg, Nat Rev Micro 14 (2016) 563-575.
[14] J. van Gestel, H. Vlamakis, R. Kolter, Microbiology Spectrum 3 (2015).
[15] H.B. Z. Lewandowski, Fundametals of Biofilm Research CRC Press New York, 2007.
[16] W.M. Dunne, Clin Microbiol Rev 15 (2002) 155-166.
[17] M.J. M Hocevar, M. Godec, Damjana Drobne3, Materials and technology 48 (2014) 609-617.
[18] M. Hermansson, Colloids and Surfaces B - Biointerfaces 14 (1999) 105-119.
[19] T.R.L. Y. Yuan, Contact angle and wetting properties, in: B.H. G. Bracco (Ed.) Surface Science Techniques, Springer Series in Surface Sciences, vol 51, Springer, Berlin, GE, 2013, pp. 3–34.
[20] M.P.H. Y. Yuan, P.R. Hardwidgeb, J. Kim, Royal Society of Chemistry Advances 7 (2017) 14254-14261.
[21] G.S. Lorite, C.M. Rodrigues, A.A. de Souza, C. Kranz, B. Mizaikoff, M.A. Cotta, Journal of Colloid and Interface Science 359 (2011) 289-295.
[22] X. Zhang, L. Wang, E. Levänen, RSC Advances 3 (2013) 12003-12020.
[23] Y. Hedberg, M.-E. Karlsson, E. Blomberg, I. Odnevall Wallinder, J. Hedberg, Colloids and Surfaces B: Biointerfaces 122 (2014) 216-222.
[24] T.F. Tadros, Interfacial Phenomena and Colloid Stability - Basic Principles, Volume 1, Walter de Gruyter GmbH, Boston, 2015.
[25] Biofilm: The Key to Understanding and Controlling Bacterial Growth in Automated Animal Drinking Water Systems, Edstrom Industries, 2003, pp. 1-19.

[26] J. Ingraham, 97. Effect of Temperature, Water Activity, and Pressure on Growth, in: F.C. Neidhardt (Ed.) Esherichia coli and Samonella Typhimurium Cellular and Molecular Biology, vol 2, Library of Congress Cataloging-in-Publication Data, USA, 1987, pp. 1543-1554.
[27] D. Sun, M. Babar Shahzad, M. Li, G. Wang, D. Xu, Materials Technology 30 (2015) B90-B95.
[28] A. Ewald, S.K. Glückermann, R. Thull, U. Gbureck, BioMedical Engineering OnLine 5 (2006) 22-22.
[29] N. Tran, M.N. Kelley, P.A. Tran, D.R. Garcia, J.D. Jarrell, R.A. Hayda, C.T. Born, Materials Science and Engineering: C 49 (2015) 201-209.
[30] M.T. T. Yokota, M. Ohta, Silver Dispersed Stainless Steel with Antibacterial Property, vol Technical Report 46, Kawasaki Steel, 2002, pp. 37-41.
[31] N.O. S. Nakamura, K. Miyakusu, M. Hasegawa, Y. Munesue, Antimicrobial activity and basic properties of "NSSAM-1" antimicrobial ferritic stainless steel, Nisshin Steel Technical Reports, vol 76, Nisshin USA, Inc., 1997, pp. 48-55.
[32] J.R. Davis, ASM Specialty Handbook - Stainless Steels, ASM International.
[33] Q.L. Feng, J. Wu, G.Q. Chen, F.Z. Cui, T.N. Kim, J.O. Kim, Journal of Biomedical Materials Research 52 (2000) 662-668.
[34] C.R. G. Grass, M. Solioz, Applied and Environmental Microbiology 77 (2011) 1541–1547.
[35] G. Borkow, J. Gabbay, Copper, An Ancient Remedy Returning to Fight Microbial, Fungal and Viral Infections, 2009, p. 272-278.
[36] U.D.o.H.a.H. Services, Toxicological Profile for Copper, in: U.S.D.o.H.a.H. Services (Ed.) Atlanta, Georgia, 2004.
[37] P.L. Drake, K.J. Hazelwood, The Annals of Occupational Hygiene 49 (2005) 575-585.
[38] B.S.S. Association, The Suitability and Use of Stainless Steel for Plumbing Applications, Special BSSA Report, British Stainless Steel Association, Sheffield, England, 2003, pp. 1-4.
[39] K.R. Sreekumari, Y. Sato, Y. Kikuchi, Materials transactions 46 (2005) 1636-1645.
[40] S. Zhang, C. Yang, G. Ren, L. Ren, Materials Technology 30 (2015) B126-B132.
[41] S. Suzuki, K. Miyakusu, Y. Sato, Y. Kikuchi, H. Kawakami, Tetsu to Hagane-Journal of the Iron and Steel Institute of Japan 100 (2014) 1021-1028.
[42] S. Wang, C. Yang, M. Shen, K. Yang, Materials Technology 29 (2014) 257-261.
[43] L. Ren, K. Yang, L. Guo, H.-w. Chai, Materials Science and Engineering: C 32 (2012) 1204-1209.
[44] I. Hong, C.H. Koo, Materials Science and Engineering: A 393 (2005) 213-222.
[45] J. Kielemoes, W. Verstraete, Letters in applied microbiology 33 (2001) 148-152.
[46] Y. Xuan, C. Zhang, N. Fan, Z. Yang, Acta Metallurgica Sinica (English Letters) 27 (2014) 539-545.
[47] K.-H. Liao, K.-L. Ou, H.-C. Cheng, C.-T. Lin, P.-W. Peng, Applied Surface Science 256 (2010) 3642-3646.
[48] W.-C. Chiang, I.S. Tseng, P. Møller, L.R. Hilbert, T. Tolker-Nielsen, J.-K. Wu, Materials Chemistry and Physics 119 (2010) 123-130.
[49] K.R. Sreekumari, K. Nandakumar, K. Takao, Y. Kikuchi, ISIJ international 43 (2003) 1799-1806.
[50] J.S. Association, JIS Z 2801: 2010 (E): Antibacterial products -- Test for antibacterial activity and efficacy, Japanese Standards Association Tokyo, Japan, 2010, pp. 1-27.
[51] D.M. Goeres, M.A. Hamilton, N.A. Beck, K. Buckingham-Meyer, J.D. Hilyard, L.R. Loetterle, L.A. Lorenz, D.K. Walker, P.S. Stewart, Nature protocols 4 (2009) 783-788.

[52] R.P. Carlson, R. Taffs, W.M. Davison, P.S. Stewart, Journal of Biomaterials Science, Polymer Edition 19 (2008) 1035-1046.
[53] A. International, ASTM E2647-13: Standard Test Method for Quantification of Pseudomonas aeruginosa Biofilm Grown Using Drip Flow Biofilm Reactor with Low Shear and Continuous Flow, ASTM International, West Conshohocken, PA, 2013, pp. 1-6.
[54] D.E.N. J.D. Goldstein, P. Echlin, D.C. Joy, A.D. Romig, C.E. Lyman, C. Fiori, E. Lifshin, Scanning Electron Microscopy and X-Ray Microanalysis, Plenum Press, New York, 1992.
[55] M. Mantel, J.P. Wightman, Surface and Interface Analysis 21 (1994) 595-605.
[56] R.A. Serra DO, Klauck G, Mika F, Hengge R, mBio 4 (2013) 1-12.
[57] L. Hobley, C. Harkins, C.E. MacPhee, N.R. Stanley-Wall, FEMS Microbiology Reviews 39 (2015) 649-669.

Appendix A. Tables Containing All Length and Width Measurements of Bacteria Made Within Figures 4-2 and 4-4 through 4-8.

Table A-1. Bacteria Length and Width Measurements of Bacteria in Figure 4-1.

Rod			Sphere		
Bacteria	**Length (μm)**	**Width (μm)**	**Bacteria**	**Length (μm)**	**Width (μm)**
1	4.00	1.00	36	0.95	0.91
2	2.00	1.00	37	1.00	0.98
3	3.00	1.00	38	0.87	0.72
4	2.00	0.91	39	0.75	0.71
5	2.00	0.91	40	1.00	0.96
6	2.00	1.00	41	1.00	0.86
7	2.00	0.99	42	1.00	0.82
8	2.00	0.79	43	1.00	0.85
9	3.00	1.00	44	0.93	0.72
10	3.00	0.92	45	1.00	0.80
11	2.00	1.00	46	0.81	0.81
12	2.00	0.92	47	0.94	0.97
13	2.00	0.95	48	0.95	0.79
14	3.00	1.00	49	1.00	0.75
15	2.00	0.95	50	0.88	0.78
16	2.00	1.00	51	0.91	0.79
17	2.00	1.00	52	0.88	0.76
18	2.00	1.00	53	0.95	0.80
19	2.00	0.99	54	0.97	0.71
20	1.00	0.93	55	1.00	0.75
21	2.00	1.00	56	1.00	0.97
22	2.00	0.84	57	1.00	0.79
23	2.00	0.81	58	1.00	0.85
24	3.00	0.90	59	0.94	0.94
25	2.00	1.00	60	0.97	0.99
26	1.00	0.79	61	1.00	0.87
27	2.00	0.85	62	1.00	1.00
28	2.00	1.00	63	0.95	0.89
29	1.00	1.00	64	0.97	0.87
30	1.00	0.95	65	1.00	0.75
31	3.00	1.00	66	1.00	1.00
32	3.00	1.00	67	1.00	0.85
33	3.00	1.00	68	1.00	0.90
34	3.00	1.00	69	1.00	0.82
35	3.00	0.93	70	1.00	1.00
Average	**2.23**	**0.95**	**Average**	**0.96**	**0.85**
Standard Deviation	**0.69**	**0.07**	**Standard Deviation**	**0.06**	**0.09**

Table A-2. Length and Width Measurements of Bacteria in Figure 4-3

Bacteria	Length (µm)	Width (µm)
1	1.00	0.69
2	0.99	0.87
3	1.00	0.75
4	0.98	0.77
5	1.00	0.77
6	1.00	0.77
7	0.82	0.69
8	0.95	0.74
9	1.00	0.80
10	0.76	0.65
11	1.00	0.85
12	1.00	0.78
13	1.00	0.63
14	0.85	0.67
15	0.91	0.73
16	0.96	0.88
17	0.82	0.84
18	1.00	0.92
19	0.77	0.72
20	1.00	0.83
21	1.00	0.75
22	0.92	1.00
23	0.97	0.84
24	0.83	0.80
25	1.00	0.98
Average	**0.94**	**0.79**
Standard Deviation	**0.08**	**0.09**

Table A-3. Length and Width Measurements of Bacteria in Figure 4-4

Bacteria	Length (µm)	Width (µm)
1	2.00	0.49
2	2.00	0.64
3	1.00	0.50
4	2.00	0.52
5	1.00	0.49
6	1.00	0.68
7	0.89	0.58
8	1.00	0.60
9	1.00	0.53
10	1.00	0.70
11	1.00	0.58
12	0.95	0.56
13	1.00	0.55
14	1.00	0.57
15	1.00	0.57
Average	**1.19**	**0.57**
Standard Deviation	**0.42**	**0.06**

Table A-4. Length and Width Measurements of Bacteria in Figure 4-5

Bacteria	Length (µm)	Width (µm)
1	1.00	0.71
2	1.00	0.72
3	1.00	0.78
4	2.00	0.69
5	1.00	0.60
6	1.00	0.81
7	2.00	0.60
8	0.99	0.67
9	1.00	0.84
10	0.75	0.72
11	0.67	0.55
12	1.00	0.53
13	2.00	0.62
14	2.00	0.79
15	1.00	1.00
16	1.00	0.65
17	0.80	0.70
18	2.00	0.66
19	1.00	0.64
20	0.87	0.67
21	1.00	0.71
22	0.96	0.66
23	1.00	0.49
24	0.81	0.76
25	1.00	0.95
Average	**1.15**	**0.70**
Standard Deviation	**0.44**	**0.12**

Table A-5. Length and Width Measurements of Bacteria in Figure 4-6

Bacteria	Length (µm)	Width (µm)
1	2.00	0.74
2	2.00	0.61
3	1.00	0.54
4	2.00	0.71
5	1.00	0.67
6	2.00	0.56
7	1.00	0.59
8	2.00	0.60
9	2.00	0.68
10	2.00	0.62
11	2.00	0.65
12	1.00	0.58
13	2.00	0.51
14	2.00	0.52
15	0.88	0.62
16	2.00	0.78
17	1.00	0.63
18	1.00	0.73
19	1.00	0.64
20	0.94	0.75
21	2.00	0.73
22	2.00	0.68
23	1.00	0.62
24	1.00	0.76
25	2.00	0.96
26	1.00	0.49
27	1.00	0.55
28	1.00	0.50
29	1.00	0.55
30	1.00	0.65
31	2.00	0.72
32	2.00	0.72
33	1.00	0.57
34	1.00	0.68
35	1.00	0.54
Average	**1.45**	**0.64**
Standard Deviation	**0.51**	**0.10**

Table A-6. Length and Width Measurements of Bacteria in Figure 4-7

Bacteria	Length (µm)	Width (µm)
1	2.00	0.87
2	2.00	0.89
3	2.00	0.90
4	0.95	1.00
5	2.00	0.71
6	2.00	0.67
7	1.00	0.79
8	2.00	0.82
9	2.00	0.85
10	2.00	0.86
11	0.96	0.93
12	2.00	0.84
13	2.00	0.77
14	2.00	0.77
15	0.86	0.84
16	2.00	0.82
17	2.00	0.89
18	0.95	0.93
19	1.00	0.82
20	1.00	0.94
21	1.00	0.88
22	1.00	0.77
23	1.00	0.87
24	1.00	0.99
25	1.00	0.85
26	1.00	0.78
27	1.00	0.78
28	0.99	0.75
29	0.93	0.90
30	1.00	0.78
31	1.00	0.89
32	1.00	0.84
33	2.00	0.88
34	1.00	0.88
35	1.00	0.80
Average	**1.39**	**0.84**
Standard Deviation	**0.51**	**0.07**